AD-A206 756

NUMERICAL EVALUATION AND COMPARISON OF SUBCYCLING ALGORITHMS FOR STRUCTURAL DYNAMICS

G. M. Hulbert
T. J. R. Hughes
Stanford University
Division of Applied Mechanics
Department of Mechanical Engineering
Stanford, CA   94305

20 September 1988

Technical Report

Prepared for
    Director
    Defense Nuclear Agency
    Washington, DC 20305-1000

89 4 07 071

DISTRIBUTION LIST UPDATE

This mailer is provided to enable DNA to maintain current distribution lists for reports. We would appreciate your providing the requested information.

☐ Add the individual listed to your distribution list.

☐ Delete the cited organization/individual.

☐ Change of address.

NAME: _____

ORGANIZATION: _____

OLD ADDRESS	CURRENT ADDRESS
_____	_____
_____	_____
_____	_____

TELEPHONE NUMBER: ( ) _____

SUBJECT AREA(s) OF INTEREST:

_____	_____
_____	_____
_____	_____

DNA OR OTHER GOVERNMENT CONTRACT NUMBER: _____

CERTIFICATION OF NEED-TO-KNOW BY GOVERNMENT SPONSOR (if other than DNA):

SPONSORING ORGANIZATION: _____

CONTRACTING OFFICER OR REPRESENTATIVE: _____

SIGNATURE: _____

CUT HERE AND RETURN

Director
Defense Nuclear Agency
ATTN: TITL
Washington, DC 20305-1000

REPORT DOCUMENTATION PAGE

1a REPORT SECURITY CLASSIFICATION UNCLASSIFIED			1b RESTRICTIVE MARKINGS			
2a. SECURITY CLASSIFICATION AUTHORITY N/A since Unclassified			3 DISTRIBUTION / AVAILABILITY OF REPORT Approved for public release; distribution is unlimited.			
2b DECLASSIFICATION DOWNGRADING SCHEDULE N/A since Unclassified						
4 PERFORMING ORGANIZATION REPORT NUMBER(S)			5 MONITORING ORGANIZATION REPORT NUMBER(S) DNA-TR-88-8			
6a. NAME OF PERFORMING ORGANIZATION Stanford University	6b. OFFICE SYMBOL (If applicable)		7a. NAME OF MONITORING ORGANIZATION Director Defense Nuclear Agency			
6c. ADDRESS (City, State, and ZIP Code) Division of Applied Mechanics Department of Mechanical Engineering Stanford, CA 94305			7b ADDRESS (City, State, and ZIP Code) Washington, DC 20305-1000			
8a. NAME OF FUNDING / SPONSORING ORGANIZATION	8b OFFICE SYMBOL (If applicable) SPSD/Goering		9 PROCUREMENT INSTRUMENT IDENTIFICATION NUMBER DNA 001-84-C-0306			
8c. ADDRESS (City, State, and ZIP Code)			10 SOURCE OF FUNDING NUMBERS			
			PROGRAM ELEMENT NO 62715H	PROJECT NO S	TASK NO C	WORK UNIT ACCESSION NO DH251255

11 TITLE (Include Security Classification)

NUMERICAL EVALUATION AND COMPARISON OF SUBCYCLING ALGORITHMS FOR STRUCTURAL DYNAMICS

12. PERSONAL AUTHOR(S)
Hulbert, G.M. and Hughes, T.J.R.

13a. TYPE OF REPORT Technical	13b. TIME COVERED FROM 840927 TO 880129	14. DATE OF REPORT (Year, Month, Day) 880920	15. PAGE COUNT 76

16. SUPPLEMENTARY NOTATION
This work was sponsored by the Defense Nuclear Agency under RDT&E RMC Code X344084466 S C 00010 259040.

17. COSATI CODES			18. SUBJECT TERMS (Continue on reverse if necessary and identify by block number)
FIELD	GROUP	SUB-GROUP	Structural Dynamics Tranal Code
12	3		Algorithms
12	1		Numerical Analysis

19. ABSTRACT (Continue on reverse if necessary and identify by block number)

This report compares numerical results obtained from seven proposed subcycling algorithms which were used to solve three test problems. The numerical results show that three of the subcycling algorithms - TRANAL, and the linear and quadratic nodal interpolation schemes - produced accurate and stable solutions. The free element partition algorithm produced stable but significantly inaccurate results for two of the three test problems. Subsequently, the two best algorithms - TRANAL and the linear nodal interpolation algorithm - were used to solve a larger test problem.

20. DISTRIBUTION / AVAILABILITY OF ABSTRACT ☐ UNCLASSIFIED/UNLIMITED ☑ SAME AS RPT ☐ DTIC USERS	21 ABSTRACT SECURITY CLASSIFICATION UNCLASSIFIED	
22a. NAME OF RESPONSIBLE INDIVIDUAL Bennie F. Maddox	22b TELEPHONE (Include Area Code) (202) 325-1078	22c. OFFICE SYMBOL DNA/CSTI

DD Form 1473, JUN 86   Previous editions are obsolete.
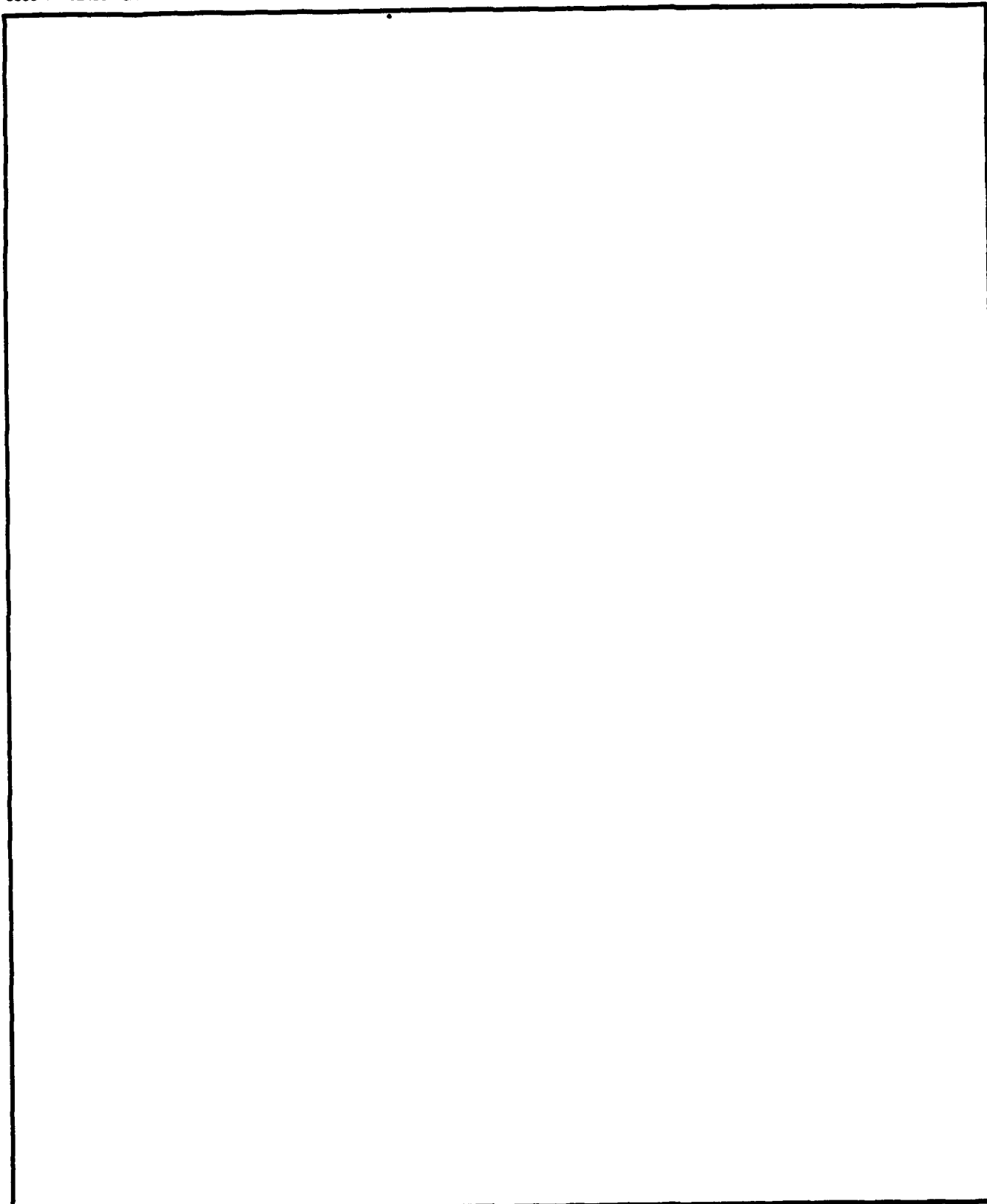
Preface

This report compares numerical results obtained from seven proposed subcycling algorithms used to solve three test problems. The numerical results show that three subcycling algorithms – TRANAL, and the linear and quadratic nodal interpolation schemes – produced accurate and stable results. While the subcycling algorithms achieved stability, the natural structure of the finite element assembly process was lost. To be competitive with fixed time-step explicit algorithms currently implemented on vector machines, a new subcycling algorithm will be needed.

iii

TABLE OF CONTENTS

LIST OF ILLUSTRATIONS

SECTION 1

INTRODUCTION

Numerous explicit subcycling algorithms for structural dynamics have been proposed and implemented in specialized finite element codes. While numerical evaluations of several subcycling algorithms have been published, no comparison of the various proposed algorithms has been reported. Nor does there exist a rigorous analysis of subcycling algorithms to prove stability and convergence for structural dynamics problems.

This report compares numerical results obtained from seven proposed subcycling algorithms which were used to solve three test problems. The numerical results show that three of the subcycling algorithms — TRANAL, and the linear and quadratic nodal interpolation schemes — produced accurate and stable solutions. The "free" element partition algorithm produced stable but significantly inaccurate results for two of the three test problems. Subsequently, the two best algorithms — TRANAL and the linear nodal interpolation algorithm — were used to solve a larger test problem.

The results presented in this study do not ensure that the algorithms are convergent for other structural dynamics problems. Even for the simple test problems studied, deviation from the "natural" subcycle-zone partitioning was required for stable solutions when using solution time steps equal to the critical subcycle-zone time steps. Thus, the subcycling algorithms achieved stability, but sacrificed exploiting the "natural" structure of the finite element assembly process. To be competitive with fixed time-step explicit algorithms currently implemented on vector machines, a new subcycling algorithm will need to be developed.

The next section describes the seven subcycling algorithms studied. Numerical results and discussion of the results are then presented. A brief summary of the performance of the subcycling algorithms concludes this report.

1

SECTION 2

DESCRIPTION OF SUBCYCLING ALGORITHMS

To facilitate description of the different subcycling algorithms, a simple one dimensional bar problem is presented. Figure 1 shows the bar which is composed of two different materials; the material on the right half of the bar has a modulus of elasticity four times that of the left half. Both materials have the same density. Thus, the minimum critical time step for the problem is governed by the stiffer material on the right.

A subcycle zone is defined as a group of elements or nodes for which a solution is to be calculated using the same time step. The elements or nodes in a given subcycle zone do not need to be contiguous. The example problem is divided into two subcycle zones. The major cycle zone is associated with the softer material while the minor cycle zone is associated with the stiffer material.

Time step values must be chosen for each subcycle zone. To minimize computation, it is desirable to select as large a time step as possible for each subcycle zone. As the subcycling algorithms studied in this report are adaptations of the central difference algorithm, critical time steps are imposed on each subcycle zone to maintain stability. An upper bound on a subcycle zone critical time step can de determined from the maximum element eigenvalue of the elements in the subcycle zone.

Subcycling algorithms may be classified as either nodal or element partition algorithms. In an element partition algorithm, different element groups are assigned to different subcycle zones. This partitions the global stiffness matrix into subcycle element groups which can be easily formed using the standard finite element assembly algorithms. In a nodal partition algorithm, different nodes are assigned to different subcycle zones. This approach partitions the global stiffness matrix into nodal blocks. Such a split of the global stiffness matrix requires additional assembly algorithms in a finite element code and thus nodal partition algorithms are somewhat more cumbersome than element partition algorithms.

2

2.1 Nodal Partition Algorithms.

Four nodal partition algorithms were evaluated. Three of these algorithms were first proposed by Belytshcko, Yen, and Mullen[1]. The fourth nodal partition algorithm was proposed by Liu and Belytschko[2]. These algorithms differ only in the method used to estimate the displacement of major cycle nodes during minor cycle updates. Displacement estimates are required only for the major cycle nodes which are connected to minor cycle nodes.

Let m denote the integer ratio of the major time step to minor time step ($m = 2$ in the example problem), k denotes the number of major cycle time steps processed and n denotes the number of minor cycle steps processed.

2.1.1 Nodal Partition Algorithm 1.

Figures 2 and 3 depict the calculation procedure for the first of the nodal partition algorithms. In Figure 2a, all nodal displacements and element stresses are known at time step $n = mk$. Nodal velocities for the minor cycle nodes are known at time step $n - 1/2$ while the major cycle nodal velocities are known at time step $m(k - 1/2)$. Note that the interface node, that is, the node which connects the major and minor cycle zone elements, is grouped with the minor cycle nodes. The interface node is associated with the minor cycle zone in all the subcycling algorithms to satisfy time step restrictions imposed by the central difference algorithm.

Using the known stresses, the equations of motion are solved for all nodal accelerations at time step $n = mk$. The nodal velocities are then updated; the minor cycle velocities are updated to time step $n + 1/2$ while the major cycle nodal velocities are updated to time step $m(k + 1/2)$. Nodal displacements are updated, with the minor cycle values updated to time step $n + 1$ while the major cycle displacements are updated to time step $m(k + 1)$.

Processing of only the minor cycle zone then occurs. As shown in Figure 2b, minor cycle stresses are calculated at time step $n + 1$. Note that calculation of these stresses also includes

3

calculating stresses in one element of the major cycle zone. To calculate stresses in this element requires a displacement value for a major cycle zone node. The first nodal partition algorithm assumes that the major cycle node displacement remains constant at the value calculated at time step mk. *This assumption is physically equivalent to fixing the bar at this major cycle node during the minor cycle updates.*

Once the minor cycle stresses are calculated, the minor cycle accelerations can be computed at time step $n + 1$ (Figure 3a). Subsequently, the minor cycle velocities are updated to time step $(n + 1) + 1/2$, and then the displacements are updated to time step $n + 2$. As $n + 2 = m(k + 1)$, all nodal displacements are known at time step $m(k + 1)$ and thus all stresses can be calculated (Figure 3b). The entire process is then repeated until the entire transient response is calculated.

2.1.2 Nodal Partition Algorithm 2.

In the second nodal partition algorithm (Figures 4 and 5), the same procedure is performed as in the first algorithm with the exception of the major cycle node displacement assumption. In the second method, this displacement value is assumed to vary linearly with time between time steps mk and $m(k + 1)$. This is equivalent to a constant velocity assumption during the minor cycle updates. While the second nodal partition, called the linear nodal interpolation partition, requires nominally more computation than the first algorithm, it might be expected to provide a better solution as the linear variation assumption should more closely approximate the actual displacement variation than the constant displacement assumption. The improved performance of the linear nodal interpolation algorithm is clearly evident from the test problem solutions.

2.1.3 Nodal Partition Algorithm 3.

The third nodal partition algorithm (Figures 6 and 7), called the extrapolated nodal partition algorithm, is identical to the first algorithm except that the constant displacement

value of the major cycle node is the known value at time step $m(k+1)$ rather than the value at time step mk.

2.1.4 Nodal Partition Algorithm 4.

The final nodal partition algorithm assumes a quadratic variation of the major cycle node displacement between time steps mk and $m(k+1)$. A quadratic variation is the highest order variation with respect to time that can be assumed using only the known nodal displacement and acceleration values at time step mk and the nodal velocity value at time step $m(k+1/2)$. Since the major cycle node displacement and acceleration values are known at time step mk while its velocity value is known at time step $m(k+1/2)$, the quadratic displacement variation is calculated using:

$$d_{mk+i} \quad = \quad d_{mk} + (i\Delta t)\left\{v_{m(k+\frac{1}{2})} - \frac{1}{2}m\Delta t a_{mk}\right\} + \frac{1}{2}(i\Delta t)^2 a_{mk}, \quad i = 1, ..., m \quad (1)$$

where Δt is the time step used to update the minor cycle zone. This quadratic variation requires slightly more computation than the linear nodal interpolation algorithm, but it might also be expected to provide a better solution. However, the test problems show only a minor improvement in calculated response.

2.2 Element Partition Algorithms.

Three element partition algorithms were evaluated. The first element partition algorithm is an extension to the structural dynamics problem of an element partition algorithm proposed in Liu and Lin [3] for the heat conduction problem. This subcycling algorithm, applied to the heat conduction problem, is the only one for which stability and convergence proofs exist [4-5]. The second element partition algorithm was proposed by Key but not published due its poor behavior. The final element partition algorithm studied is the subcycling algorithm implemented in the TRANAL finite element code. This algorithm is also unpublished but was described by John Baylor and Joseph Wright at Weidlinger Associates during many helpful conversations.

5

2.2.1 Element Partition Algorithm 1.

Figures 8 and 9 depict the first element partition subcycling algorithm applied to the example problem. As with the nodal partition algorithms, all stresses and displacements are known at time step $n = mk$, while major cycle velocities are known at time step $m(k - 1/2)$ and minor cycle velocities are known at time step $n - 1/2$. The acceleration values are obtained by solving the equation of motion at time step n. The velocities and displacements are then updated for all nodes.

Processing of only the minor cycle zone then occurs. As with the nodal partition algorithms, the stresses in the major cycle element adjacent to the minor cycle zone must be estimated during the minor cycle updates. The element partition algorithms, however, do not require an estimate for the displacement of the major cycle node associated with this inteface element.

As shown in Figure 8b, the first element partition algorithm assumes that the stresses in the interface element are zero during the minor cycle updates. *This is physically equivalent to a free boundary condition on the left end of the minor cycle zone.* The remaining minor cycle stresses are computed at time step $n + 1$ in the standard manner.

Once the stresses are known, the minor cycle acceleration values at time step $n + 1$ are computed. Next, as shown in Figure 9a, the minor cycle velocities are updated to time step $(n + 1) + 1/2$ and the minor cycle displacements are updated to time step $(n + 2)$. As $n + 2 = m(k + 1)$, all nodal displacements are known at time step $m(k + 1)$ and thus all stresses can be calculated (Figure 9b). The entire process is then repeated until the entire transient response is calculated.

2.2.2 Element Partition Algorithm 2.

The second element partition algorithm (Figures 10 and 11), is identical to the first except that the interface element stresses are assumed to remain constant at the values computed at the previous major cycle time step $n = mk$ during the minor cycle updates (Figure 10b). This

6

is physically equivalent to a constant force being applied to the left end of the minor cycle zone elements. The second element partition algorithm, called the constant stress algorithm, can be considered as the element equivalent of the first nodal partition algorithm. However, it may be expected that the element partition version will result in poorer solutions because less information is being included during the minor cycle updates.

2.2.3 Element Partition Algorithm 3.

The third element partition algorithm — the TRANAL subcycling scheme — is implemented in a form different than the previously described subcycling schemes. Instead of displacements and stresses being brought to the same time level, the TRANAL algorithm brings the subcycle velocities to the same time level while the displacements and stresses are staggered in time. Figures 12 - 14 depict the TRANAL subcycling algorithm.

As shown in Figure 12a, all nodal velocities are known at time step $n = mk$. The minor cycle stresses and displacements are known at time step $(n - 1/2)$ while the major cycle stress and displacement values are known at time step $m(k - 1/2)$. The current displacement value associated with the interface node was last updated at time step $n - 1/2$, that is, it was updated with the minor cycle zone. Stresses in the major cycle zone element adjacent to the minor cycle zone are always updated with the major cycle time step.

The major cycle displacements are next updated to time step $m(k + 1/2)$, excluding the interface node displacement. Next, the major cycle stresses are updated to time step $m(k + 1/2)$ (Figure 12a). The updated stresses are obtained by adding to the old stress values the incremental stresses calculated by using the velocities at time step mk. That is,

$$\sigma_{m(k+\frac{1}{2})} = \sigma_{m(k-\frac{1}{2})} + \Delta t \mathbf{D} \mathbf{B} v_{mk} \tag{2}$$

where $\mathbf{D}$ is the constitutive matrix, $\mathbf{B}$ is the discrete gradient matrix, and Δt is the time step used to update the minor cycle zone. As shown in Figure 12b, the major cycle acceleration values are calculated at time step $m(k + 1/2)$ and the major cycle velocities are then updated to time step $m(k + 1)$. Note that the interface node kinematic quantities are not updated

7

with the major cycle zone.

Processing of only the minor cycle zone is now performed. The minor cycle displacements are updated to time step $n + 1/2$, including the interface node displacement. Next, the minor cycle stresses are updated to time step $n + 1/2$ (Figure 13a). The equation of motion is to be solved at time step $n + 1/2$, which requires specifying stresses in the major cycle element adjacent to the minor cycle zone. The TRANAL algorithm uses the most recently calculated stresses for this element. As shown in Figure 13b, these stresses were last updated to time step $m(k + 1/2)$, so for this minor cycle update, an advanced stress solution is being used in the interface element. After solving for the minor cycle accelerations at time step $n + 1/2$, the minor cycle velocities are updated to time step $n + 1$.

The next step in the TRANAL algorithm is to update the minor cycle displacements and stresses to time step $(n + 1) + 1/2$, as shown in Figure 14a. The equation of motion is to be solved for the minor cycle accelerations at time step $(n + 1) + 1/2$, which again requires specifying the stresses in the adjacent major cycle element. As with the previous minor cycle update, the most recently calculated stresses for this element are used. The calculated stresses in the interface element now lag the calculated stresses in the minor cycle zone. Once the acceleration values for the minor cycle zone are calculated at time step $(n + 1) + 1/2$, the minor cycle velocities are updated to time step $n + 2$. Thus, all velocities are specified at time step $n + 2 = m(k + 1)$. The process repeats until the entire transient response has been solved.

It is difficult to interpret the TRANAL algorithm physically. The method in which the interface element stresses are used in the minor cycle calculations seems somewhat similar to using an average stress solution, which might imply relatively good solutions when using the algorithm. Good results from the TRANAL algorithm are observed in the test problems .

SECTION 3

NUMERICAL RESULTS AND DISCUSSION

To study the behavior of the seven proposed subcycling algorithms, three one dimensional test problems were analyzed. The test problems are shown in Figure 15. The bar was divided into two subcycle zones, each zone containing three elements. A unit value Heaviside step force was applied to the right end of the bar. The only difference between the test problems was specification of the elastic moduli for the two element groups. The transient response calculated using the various subcycling algorithms is compared to the transient response calculated using the standard central difference explicit algorithm with a time step equal to 0.495 of the critical time step in problem 1 and 0.496 of the critical time step in problems 2 and 3.

Not shown are results from the quadratic nodal interpolation algorithm as the solutions obtained were virtually identical to the linear nodal interpolation algorithm solutions.

a. Test Problem 1.

In the first test problem, the elastic moduli for the two element groups are equal. While subcycling is not beneficial for this problem, it was felt that the problem would be a fair comparison of the subcycling algorithms because the interface between the two element groups transmits the elastic wave with no reflections. Thus, the interface condition does not favor any particular subcycling algorithm.

An exact solution for this problem can be obtained using the standard central difference method with a time step equal to the critical time step. The exact solution is shown in Figure 17a.i. Also shown in Figure 17a are results from the central difference algorithm with a time step of 0.990 of the critical time step (Figure 17a.ii) and 0.495 of the critical value (Figure 17a.iii). As can be seen, the error in the calculated response increases as the time step is reduced, due to resolving the response of the undesirable high frequency modes.

For comparison with the subcycling algorithm solutions, it is appropriate to use Figure 17a.iii because the minor cycle time step used in the subcycling calculations was 0.495 of

9

the critical time step, while the major cycle time step was 0.990 of the critical value. Thus, $m = 2$ for problem 1. The group 1 elements were selected as the minor cycle elements.

Figure 17b presents results from three of the nodal partition algorithms. As can be seen from Figures 17b.ii and 17b.iv, the constant displacement algorithms produced unstable solutions. The observed instability is not the typical explosive growth associated with violating the critical time step criterion for explicit algorithms. Instead, the instability more closely resembles linear growth. Linear instability is the typical mode of instability observed in the subcycling algorithms, once the central difference algorithm time step restrictions are satisfied.

The linear nodal interpolation algorithm produced excellent results (Figure 17b.iii) when compared to the central difference algorithm (Figure 17b.i).

Figure 17c compares results from the central difference and the element partition algorithms. The "free" element partition algorithm (Figure 17c.ii) produced a stable solution but very poor accuracy as the free boundary condition during the minor cycle updates results in a significantly softer response exhibited by elongation of the period of vibration and increased displacement. Figure 17c.iii shows that the constant stress algorithm is unstable for this problem. Note that the magnitude of instability is much larger than observed in its nodal partition counterpart (Figure 17b.ii). This is the result of including less information in the minor cycle zone updates. Finally, the TRANAL algorithm results, shown in Figure 17c.iv, are in excellent agreement with the central difference algorithm solution.

It can be concluded from the first test problem that only the linear and quadratic nodal interpolation and the TRANAL element partition algorithms produced results of equal quality compared to the central difference algorithm.

b. Test Problem 2.

In the second test problem, the elastic modulus of the left element group was 64 times greater than that of the right element group. This problem is a more realistic application of the subcycling schemes and is representative of a soft structure mounted on a stiff foundation. The critical time step for group 1 is 8 times smaller than the critical time step for group 2, thus element group 1 is the minor cycle element group.

To determine how well the algorithms responded to different degrees of problem difficulty, the time step ratio, m, was varied. Typically the problem difficulty increased as m increased. The most difficult condition for the subcycling algorithms is when the solution time steps are equal to the critical subcycle zone time steps. With the minor cycle time step chosen as 0.992 times the critical minor zone time step, the major cycle time step was varied such that m equaled 2, 4, and 8. With the minor cycle time step chosen as 0.496 times the critical value, the major cycle time step was varied such that m equaled 4, 8, and 16.

For notational convenience, Δt_c represents a time step of 0.992 times the critical minor zone time step.

Figure 18a compares results from the central difference algorithm and nodal partition subcycling algorithms for $m = 2$ and $\Delta t_c = 1.0$. All the algorithms produced excellent results.

Figure 18b compares results from the element partition algorithms for $m = 2$ and $\Delta t_c = 1.0$. Again, all algorithms show excellent agreement with the central difference solution. The interface condition in this problem is similar to a free boundary condition, hence good results were obtained by the "free" element partition algorithm.

Figure 18c compares results from the nodal partition algorithms for $m = 4$ and $\Delta t_c = 1.0$. General comparisions are quite good, although some deviation in response is noted. Similar results are observed in the element partition algorithms as shown in Figure 18d.

By halving both major and minor cycle time steps, while keeping $m = 4$ (thus $\Delta t_c = 1/2$), Figures 18e and 18f show the results from the subcycling algorithms are nearly identical to

11

the central difference algorithm response.

Figure 18g shows results from the nodal partition algorithms when both subcycle zones were run at nearly critical time steps ($m = 8$, $\Delta t_c = 1.0$). Figure 18g.i shows results obtained by using the central difference algorithm with a time step equal to the minor cycle zone critical time step. While the first several cycles of response are in general agreement with the central difference solution, there is noticeable oscillation in the displacements of several nodes by the fifth vibration cycle. The solutions were continued and all of the subcycling algorithms exhibited unstable solutions, although the linear and quadratic nodal interpolation algorithms required more cycles to reach the same level of instability compared to the constant displacement nodal partition algorithm.

During the first several vibration cycles before the instabilities corrupted the solutions, the subcycling algorithms produced results which are closer to the expected exact solution of the partial differential equation than the central difference algorithm. The exact solution is expected to appear as step or triangular waves as seen in the exact solution to problem 1 with some perturbations due to reflections from the material discontinuity interface. The central difference algorithm allows optimal selection of the time step for the minor cycle zone, but also arouses the undesirable higher frequency modes of the system.

Figure 18h shows results for the element partition algorithms for the same parameter values ($m = 8$, $\Delta t_c = 1.0$). Figure 18h.i shows results obtained by using the central difference algorithm with a time step equal to the minor cycle zone critical time step. The "free" element partition algorithm solution, Figure 18h.ii, is in general agreement with the central difference solution and appears to more accurately portray the exact solution to the problem. Continuation of the solution showed the "free" element partition algorithm remained stable. The constant stress and TRANAL algorithms, Figures 18h.iii and 18h.iv, respectively, resulted in unstable solutions. The TRANAL algorithm shows particularly large instability by the end of the fifth vibration cycle.

This instability in the TRANAL algorithm has been noted by Wright and Baylor. In

the results shown so far, the TRANAL algorithm was implemented by splitting the subcycle zones directly at the material discontinuity. As described by Baylor, the following procedure is used in all subcycle calculations at Weidlinger Associates using the TRANAL algorithm. At each subcycle-zone interface, at least one element from the less critical element group is included in the more critical time step group. Thus, the subcycle-zone splits are not at the "natural" splits which result from the material discontinuities. Baylor also noted that for linear problems, the TRANAL code automatically selects a time step for a subcycle zone equal to 0.8 times the minimum critical time step for the elements in the zone.

Figure 18i compares results from the central difference algorithm using the critical minor zone time step (Figure 18i.i), TRANAL with the natural element split (Figure 18i.ii), and TRANAL with the recommended element split (Figure 18i.iii). Clearly, the solution is greatly improved by including one of the softer elements into the minor cycle zone. Extended calculations show that the TRANAL algorithm was stable when the element shift was performed.

With $m = 8$ and $\Delta t_c = 1/2$, results from the nodal and element partition subcycling algorithms, shown in Figures 18j and 18k, respectively, are again in good agreement with the central difference algorithm solution. These results are virtually identical to those shown in Figures 18c and 18d. The major time step value is the same in both sets of results. These results, coupled with the instabilities observed when $m = 8$ and $\Delta t_c = 1.0$, imply that the critical time step in subcycling algorithms, once the minor time time has been chosen properly, may be the major time step.

To substantiate this idea, the subcycling algorithms were run with $\Delta t_c = 1/2$ and $m = 16$. Thus, the major cycle time step was again nearly equal to the critical major zone time step. The results are shown in Figures 18l and 18m for the nodal and element partition algorithms, respectively. The central difference algorithm solution was obtained using the minor cycle zone critical time step. With the exception of the "free" element partition algorithm, the subcycling algorithms exhibit linear instability. In this case, the TRANAL algorithm was

13

run using the "natural" element split. Thus, the linear instability seems to be attributable to the choice of major zone time step while explosive instability is attributable primarily to the minor zone time step.

Figure 18n compares results obtained from the TRANAL algorithm, for $m = 16$ and $\Delta t_c = 1/2$, when using the different element split criteria. The recommended element split, (Figure 18n.iii) compares favorably with the central difference algorithm solution obtained using the critical minor cycle zone time step (Figure 18n.i), while the natural element split solution (Figure 18n.ii) exhibits linear instability.

Additional calculations were performed by selecting $m = 8$ and reducing the ratio of the solution time step to subcycle-zone critical time step. Stable solutions were obtained when a time step ratio of 0.96 was used for the quadratic interpolation nodal algorithm, 0.95 for the linear nodal interpolation algorithm, 0.94 for the TRANAL algorithm, and 0.90 for the remaining algorithms. These values are certainly problem dependent and emphasize the uncertainty in selecting subcycle time steps to obtain accurate and stable solutions.

It can be concluded from the problem 2 results that only the "free" element partition algorithm produced stable results in all cases tested. For this problem, unlike problem 1, the "free" element partition algorithm also produced accurate results. The remaining algorithms produced good solutions unless the major time step was chosen to be nearly equal to the major zone critical time step. Linear instability resulted when the major time step value was chosen to be equal to 0.992 times its critical time step value. For the TRANAL algorithm, however, by following the more restrictive Weidlinger Associates recommendations, a stable solution was obtained.

c. Test Problem 3.

In the third test problem, the elastic modulus of the right element group was 64 times greater than that of the left element group. This problem is representative of a stiff structure mounted on a soft foundation. The critical time step for group 2 elements is 8 times smaller

14

than the critical time step for group 1 elements, thus element group 2 is the minor cycle element group.

Figure 19a compares results obtained from the central difference algorithm and the nodal partition algorithms for $m = 2$ and $\Delta t_c = 1.0$. The first constant displacement algorithm, Figure 19a.ii, seemingly exhibits dissipative properties. However, continued solution of the problem showed linear instability. The linear nodal interpolation algorithm, Figure 19a.iii, is in excellent agreement with the central difference algorithm solution. The extrapolated displacement nodal algorithm solution, Figure 19a.iv, shows linear growth. The solution was continued and was observed to increase without bound.

Figure 19b shows results obtained from the element partition algorithms for the same parameter values ($m = 2$, $\Delta t_c = 1.0$). The "free" element partition algorithm, Figure 19b.ii, produced a stable solution but, like problem 1, the period and amplitude of response are very poor compared to the central difference algorithm solution. The constant stress algorithm, Figure 19b.iii, exhibits a linear growth in the displacement response which continued to increase as the solution was extended. Finally, the TRANAL algorithm, Figure 19b.iv, with a "natural" element split, is shown to be in excellent agreement with the central difference algorithm solution.

Since reducing the time step ratio to $\Delta t_c = 1/2$ in problem 2 greatly improved the subcycling algorithm solutions, provided that the major time step was not at its critical value, the same reduction was performed for problem 3 with $m = 2$. The results are shown in Figures 19c and 19d for the nodal and element partition algorithms, respectively. The linear nodal interpolation and TRANAL algorithms already provided excellent results for $\Delta t_c = 1.0$, and their solutions are equally good for $\Delta t_c = 1/2$ (Figures 19c.iii and 19d.iv, respectively). The dissipative behavior of the constant displacement algorithm, Figure 19c.ii, is less than observed for $\Delta t_c = 1.0$, but an extension of the solution showed that the algorithm was still unstable. As would be expected, the magnitude of the instability was less at the same time value when $\Delta t_c = 1/2$. Similarly, the solution growth observed for the extrapolated

15

displacement algorithm was less when $\Delta t_c = 1/2$, but also continued to increase without bound as the solution was extended.

The "free" element algorithm response, Figure 19d.ii, did not improve greatly by using $\Delta t_c = 1/2$ rather than $\Delta t_c = 1.0$. The constant stress algorithm, Figure 19d.iii, like the extrapolated displacement algorithm, showed improved response, but continued its linear growth with time. Thus, the reduction in the time step ratio did not appreciably improve the behavior of the subcycling algorithms for problem 3.

Figure 19e shows results obtained for $m = 4$, $\Delta t_c = 1.0$, when using the nodal partition algorithms. While the linear nodal interpolation algorithm, Figure 19e.iii, is in excellent agreement with the central difference algorithm, the onset of instability is easily seen in both constant displacement algorithms (Figures 19e.ii and 19e.iv).

Results obtained from the element partition algorithms for $m = 4$ and $\Delta t_c = 1.0$ are shown in Figure 19f. The "free" element algorithm solution, Figure 19f.ii, while stable, is greatly inaccurate. The onset of linear instability is clearly evident in the constant displacement algorithm solution, Figure 19f.iii. Like the linear nodalinterpolation algorithm, the TRANAL algorithm, with "natural" element split, Figure 19f.iv, agrees very well with the central difference algorithm.

The final set of results for problem 3 are shown in Figures 19g and 19h for $m = 8$ and $\Delta t_c = 1.0$. Linear instability is evident in the constant displacement algorithms, Figures 19g.ii and 19g.iv and also in the constant stress algorithm, Figure 19h.iii. The degradation of accuracy in the "free" element algorithm solution has continued, as shown in Figure 19h.ii. Only the linear nodal interpolation algorithm and the TRANAL algorithm, Figures 19g.iii and 19h.iv, respectively, are in agreement with the central difference algorithm.

It can be concluded from the problem 3 results that only the linear and quadratic nodal interpolation algorithms and the TRANAL algorithm produced stable and accurate results. The constant displacement and constant stress algorithms were not stable for any of the chosen parameter values. The "free" element algorithm , while stable, was not accurate.

16

d. Test Problem 4 .

The results from the first three test problems show that the most viable subcycling algorithms are the linear and quadratic nodal interpolation algorithms and the TRANAL algorithm. As noted above, the recommended implementation of the TRANAL algorithm is to include at least one element from the less critical time step zone into the more critical time step zone when partitioning a problem. Also, in the TRANAL finite element code, a time step of 0.8 times the critical element time step is used in each subcycle zone for linear problems. The shifted element split was used in problem 2 and was shown to stabilize the TRANAL algorithm compared to the "natural" element split. However, due to the small problem size, this element shift left only one node in the major cycle zone. To determine the effectiveness of the element shift procedure, a 20 element version of problem 2 was evaluated.

Figure 20a shows the problem mesh and parameter values. The critical time steps for both element groups are identical to problem 2.

Figure 20c compares results obtained from the central difference algorithm using the critical minor cycle zone time step (Figure 20c.i), and various TRANAL algorithm implementations. The results shown in Figure 20c.ii were calculated with $\Delta t_c = 0.8$, $m = 8$, and the "natural" element split. The instability is evident by the end of the third vibration cycle. Thus, it is not sufficient to only reduce the time step to 0.8 times the critical time step. The sensitivity of solution stability to the chosen subcycle time steps and problem specification is apparent when the results from this problem are compared to the problem 2 results. In problem 2 , the TRANAL algorithm was stable with time step ratios less than or equal to 0.94.

Next, the time step ratios were maintained in both subcycle zones at 0.8 times the critical values while one of the major cycle elements was shifted into the minor cycle zone. The results in Figure 20c.iii show that the element shift and the reduced time step ratio were sufficient to stabilize the algorithm. Finally, the time step ratios in both subcycle zones were set equal to their critical time steps and one of the major cycle elements was shifted to the

17

minor cycle zone. Figure 20c.iv shows that the element shift alone is sufficient to stabilize the algorithm. These results imply that the combination of reduced time step and element shift provides some margin of stability for the TRANAL algorithm. However, it is not possible to define a definite stability criterion based on the results of these simple test problems.

Since the element shift greatly improved the stability of the TRANAL algorithm, it is natural to apply the same technique to the linear interpolation nodal algorithm. Figure 20d compares results from the central difference algorithm using the critical minor cycle zone time step and two linear nodal interpolation algorithm implementations with $m = 8$. With the time step values equal to 0.8 times the critical values and the standard nodal split, Figure 20d.ii shows the linear nodal interpolation algorithm is in excellent agreement with the central difference algorithm. Unlike the TRANAL algorithm, this reduction in time step was sufficient to stabilize the algorithm. Thus, there was no need to run the linear nodal interpolation algorithm with the reduced time step and the element shift (hence, no Figure 20d.iii). With both time steps equal to their critical values and one major cycle zone element shifted into the minor cycle zone, the linear nodal interpolation algorithm is stable and agrees well with the central difference algorithm (Figure 20d.iv).

It can be concluded that the linear nodal interpolation algorithm is more stable than the TRANAL algorithm for problem 4. Stability in both algorithms was acheived by shifting one major cycle element into the minor cycle zone.

SECTION 4

CONCLUSIONS

Of the seven subcycling algorithms evaluated, only the TRANAL algorithm and the linear and quadratic nodal interpolation algorithms provided stable and accurate solutions for the problems studied. However, when partitioning the problem into subcycle zones by using "natural" material partitions, time step restrictions more severe than time step restrictions based on the minimum time step in a subcycle zone were observed. This time step restriction was eliminated by shifting one element from the major cycle zone in the minor cycle zone. However, the ability to implement the subcycling algorithms on vector and parallel computers is lost when the "natural" element split is not used.

The only other stable algorithm for all test problems was the "free" element algorithm. However, the loss of accuracy when using this algorithm was severe in two of the three test problems. It can not be considered a viable algorithm for general problems.

The results from this study are not sufficient to specify a definite set of stability criteria for subcycling algorithms. To define such a set of stability criteria requires a rigorous analysis of the subcycling algorithms. However, the algorithms evaluated in this study are not amenable to analysis using standard techniques.

The evaluation of the different proposed subcycling algorithms in this report has shown that these algorithms must be used with considerable caution. The reduction in the critical time step for stable solutions, without the element shift, introduces an undesirable variable in the subcycling algorithms, particularly when applying these algorithms to nonlinear problems where plasticity of the material may absorb energy produced by algorithmic instabilities. In such cases, the numerical solution would be stable but would exhibit excessive plasticity.

Further work is necessary to establish stability criteria for subcycling algorithms. The development of a new subcycling algorithm is also highly desirable. Such an algorithm should be amenable to stability and accuracy analysis. Effective implementation of any new subcycling algorithms should also be possible for vector and parallel computers. This is a *crucial* point.

19

It seems to us that current subcycling algorithms, due to restrictions on their use which are unnatural from a finite-element data-structure standpoint, will only perform in a superior way in a totally *sequential* computing environment. The state-of-the-art is already beyond this point. In fact, fully vectorized explicit schemes (as well as implicit) are in current use. Unless a new class of vectorizable/parallelizable subcycling schemes is developed, the current subcycling schemes will not be able to compete with existing vectorized explicit schemes.

SECTION 5

List of References

1. T. Belytschko, H.-J. Yen, and R. Mullen, "Mixed Methods for Time Integration," *Computer Methods in Applied Mechanics and Engineering*, **17/18**, 259–275, 1979, unclassified.

2. W. K. Liu, T. Belytschkc, and Y. F. Zhang, "Implementation and Accuracy of Mixed-Time Implicit-Explicit Methods for Structural Dynamics," *Computers & Structures*, **19**, 4, 521–530, 1984, unclassified.

3. W.K. Liu and J. Lin, "Stability of Mixed Time Integration Schemes for Transient Thermal Analysis," *Numerical Heat Transfer*, **5**, 211-222, 1982, unclassified.

4. T. Belytschko, P. Smolinski, and W. K. Liu, "Stability of Multi-Time Step Partitioned Integrators for First-Order Finite Element Systems," *Computer Methods in Applied Mechanics and Engineering*, **49** 281-297, 1985, unclassified.

5. T. J R. Hughes, T. Belytschko, and W. K. Liu, "Convergence of an Element-Partitioned Subcycling Algorithm for the Semidiscrete Heat Equation," *Numerical Methods for Partial Differential Equations*, **3**, 131–137, 1987, unclassified.
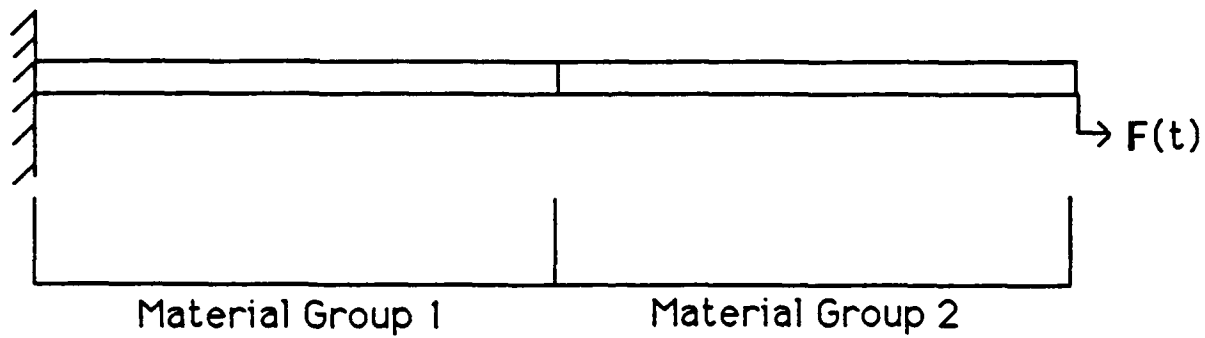
$$E_2 = 4 \, E_1$$

$$A_2 = A_1$$

$$\rho_2 = \rho_1$$

Figure 1. Example problem — one dimensional bar.
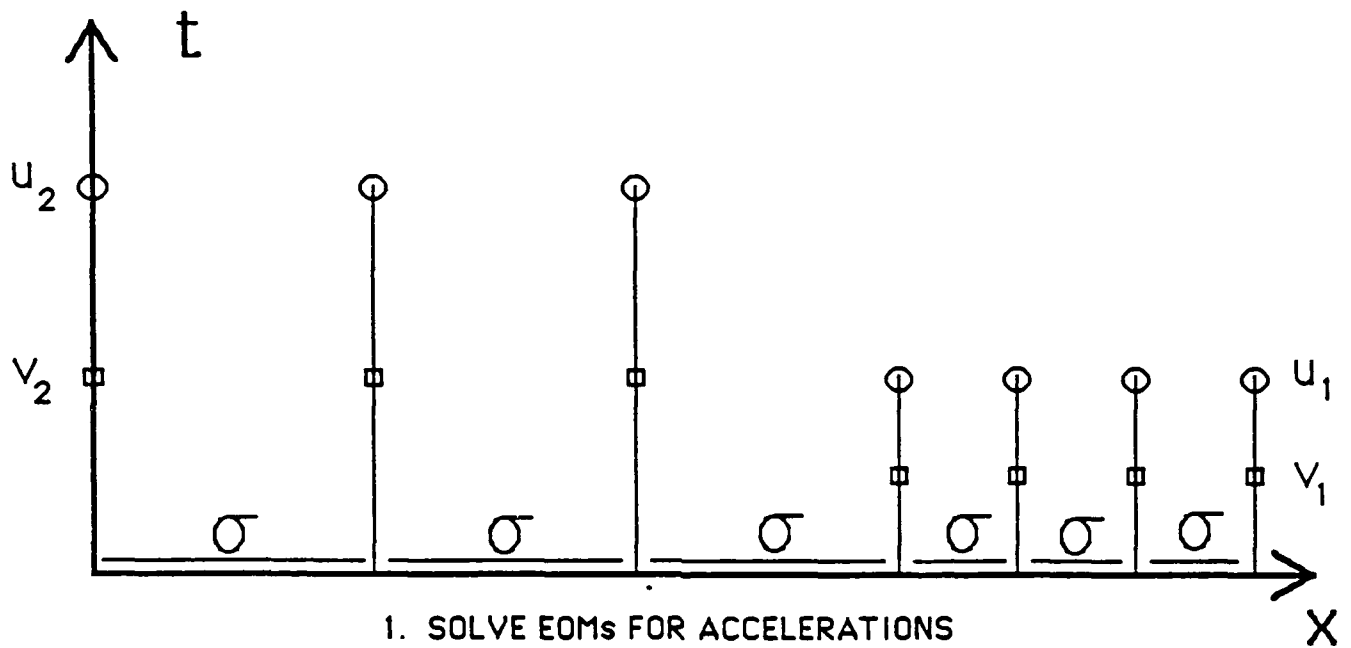
1. SOLVE EOMs FOR ACCELERATIONS
2. UPDATE VELOCITIES
3. UPDATE DISPLACEMENTS
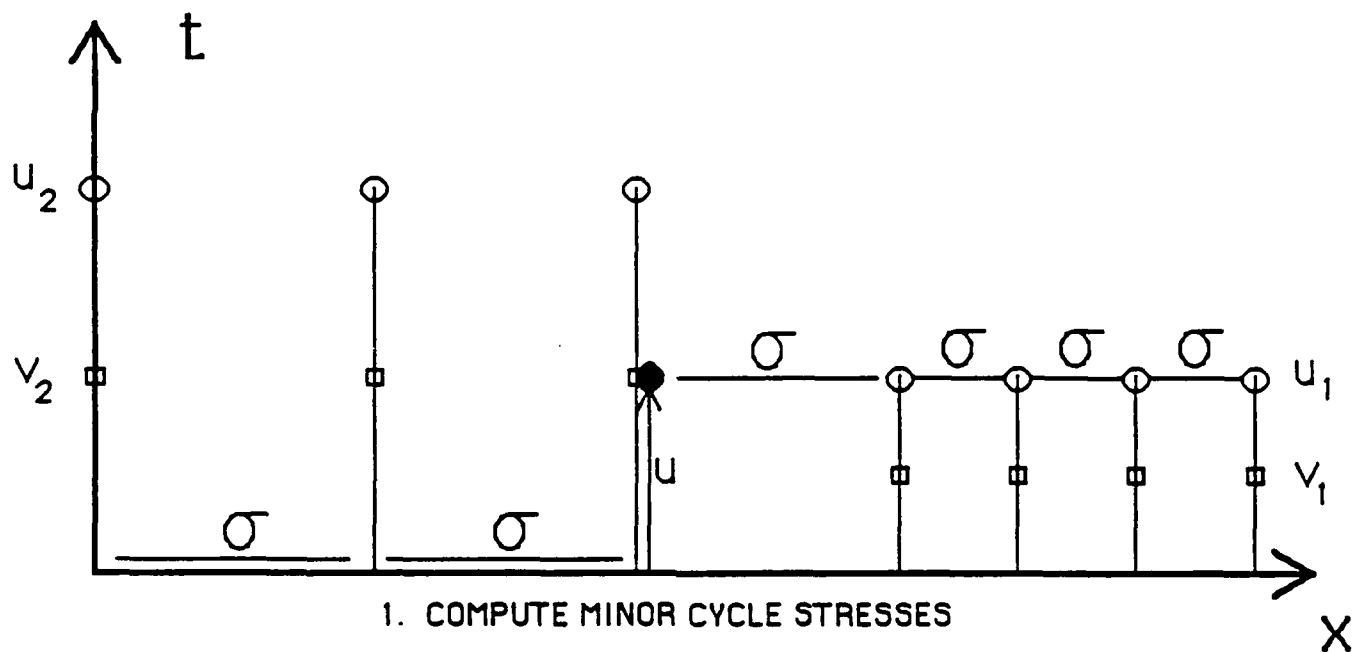
1. COMPUTE MINOR CYCLE STRESSES

NOTE: Interface node displacement constant
during minor cycle updates (zero velocity)

Figure 2. Timing diagrams for constant displacement nodal partition algorithm.

23

1. SOLVE EOMs FOR MINOR CYCLE ACCELERATIONS
2. UPDATE MINOR CYCLE VELOCITIES
3. UPDATE MINOR CYCLE DISPLACEMENTS

1. COMPUTE STRESSES FOR ALL ZONES
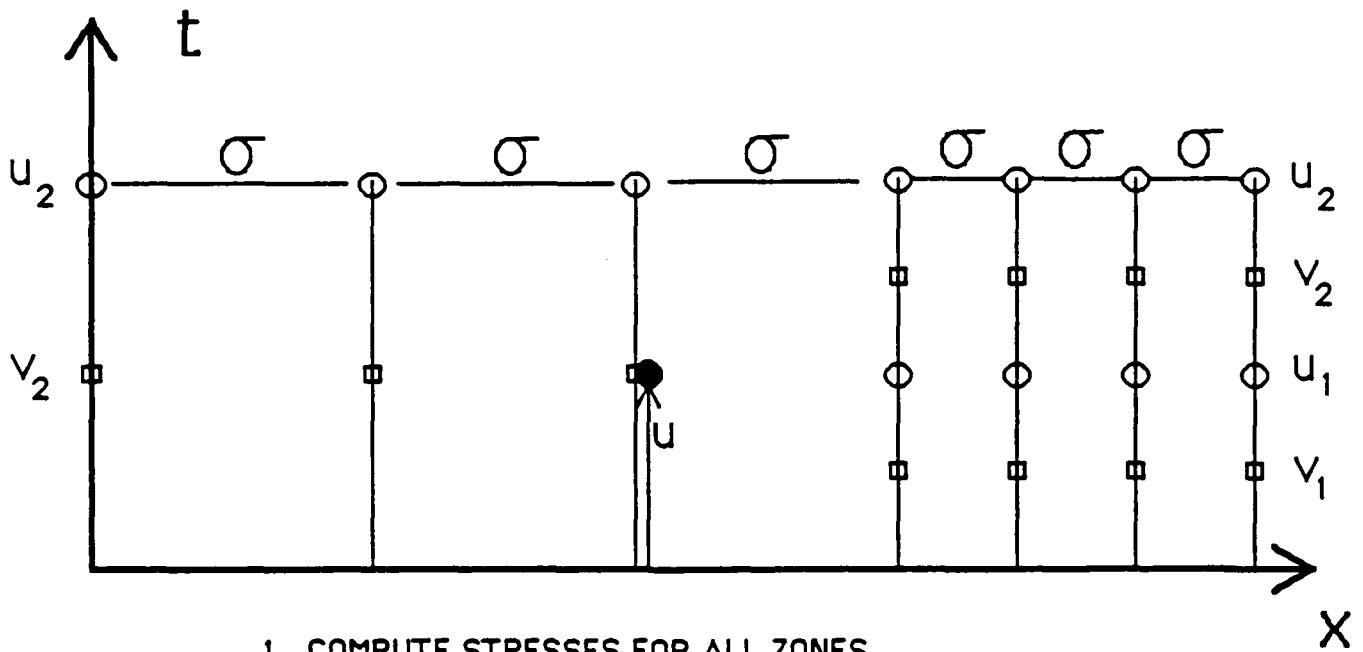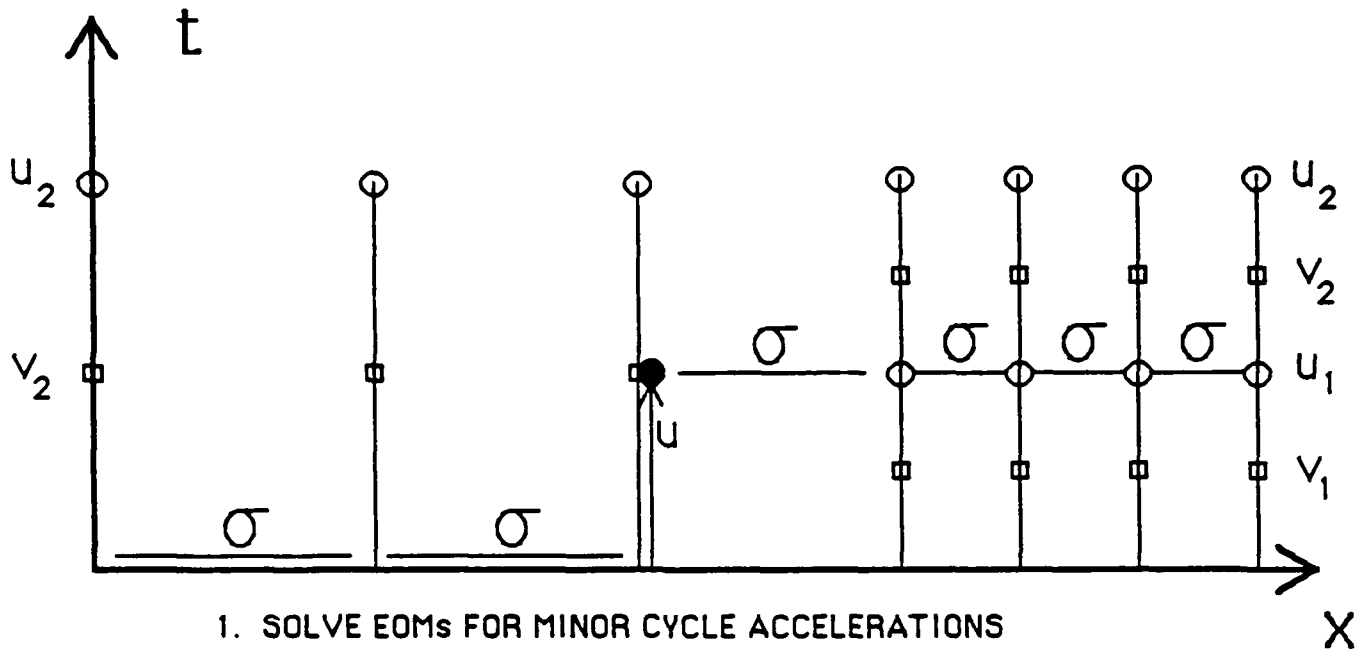
Figure 3. Timing diagrams for constant displacement nodal partition algorithm.
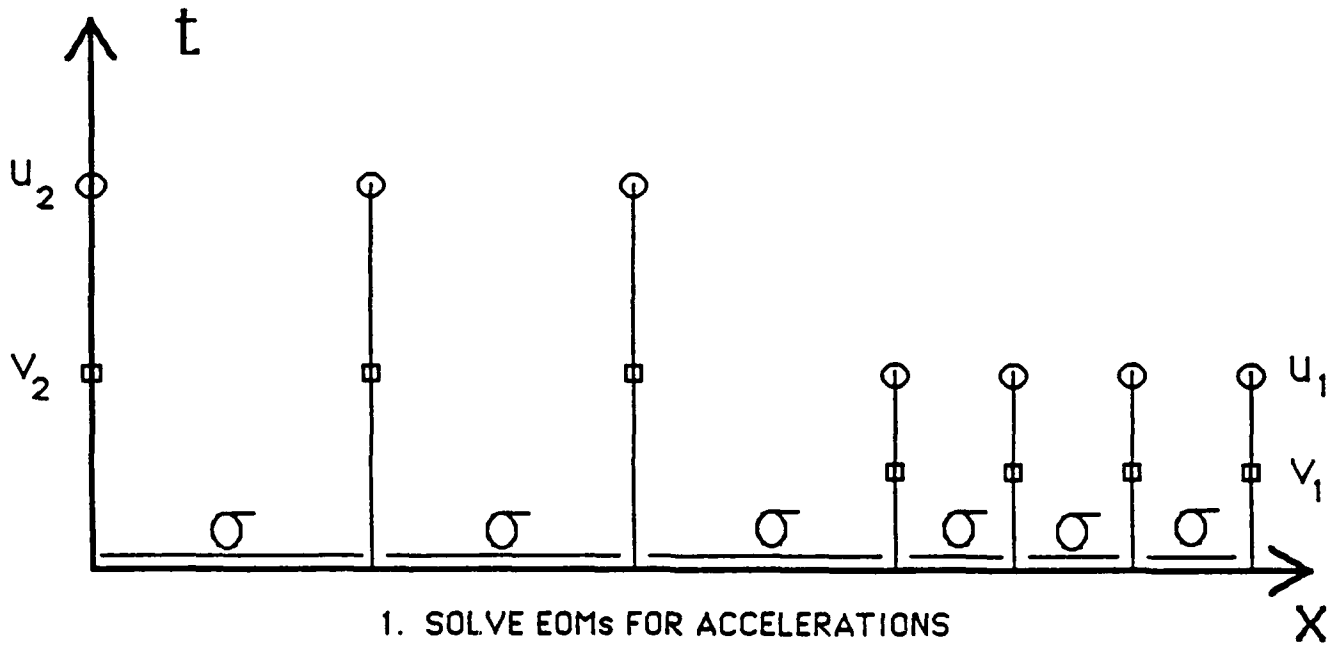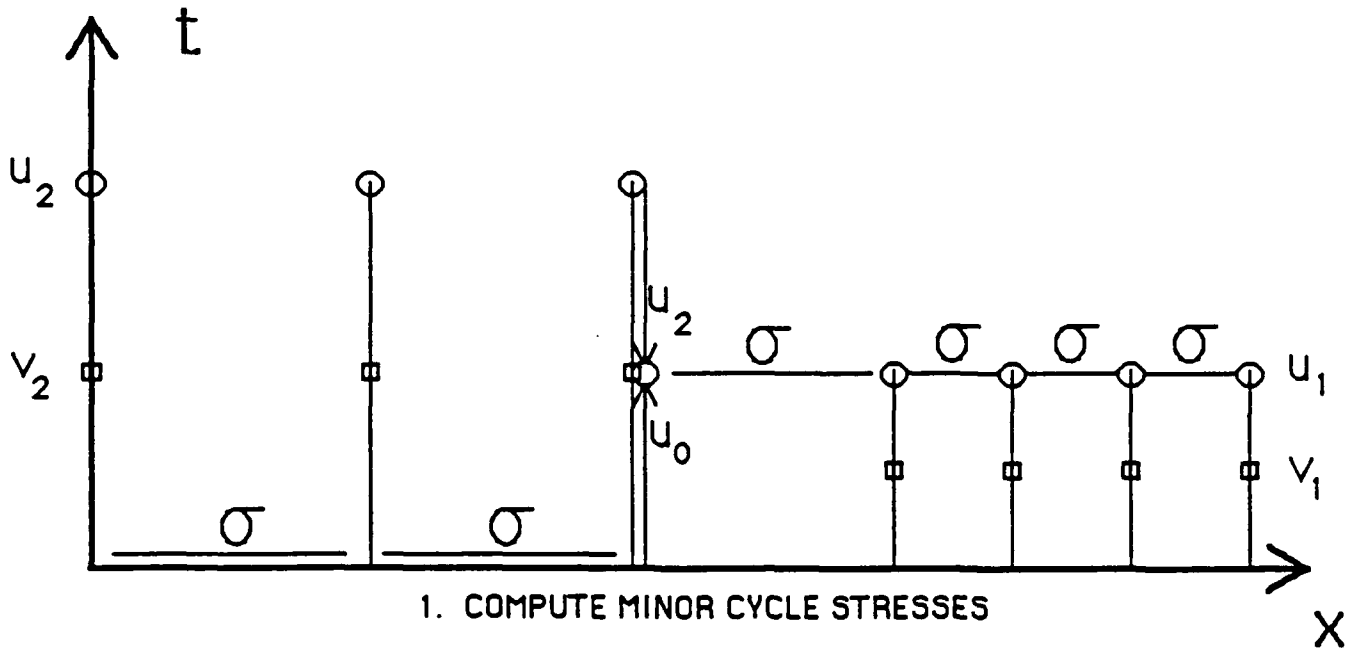
Figure 4. Timing diagrams for linear nodal interpolation algorithm.
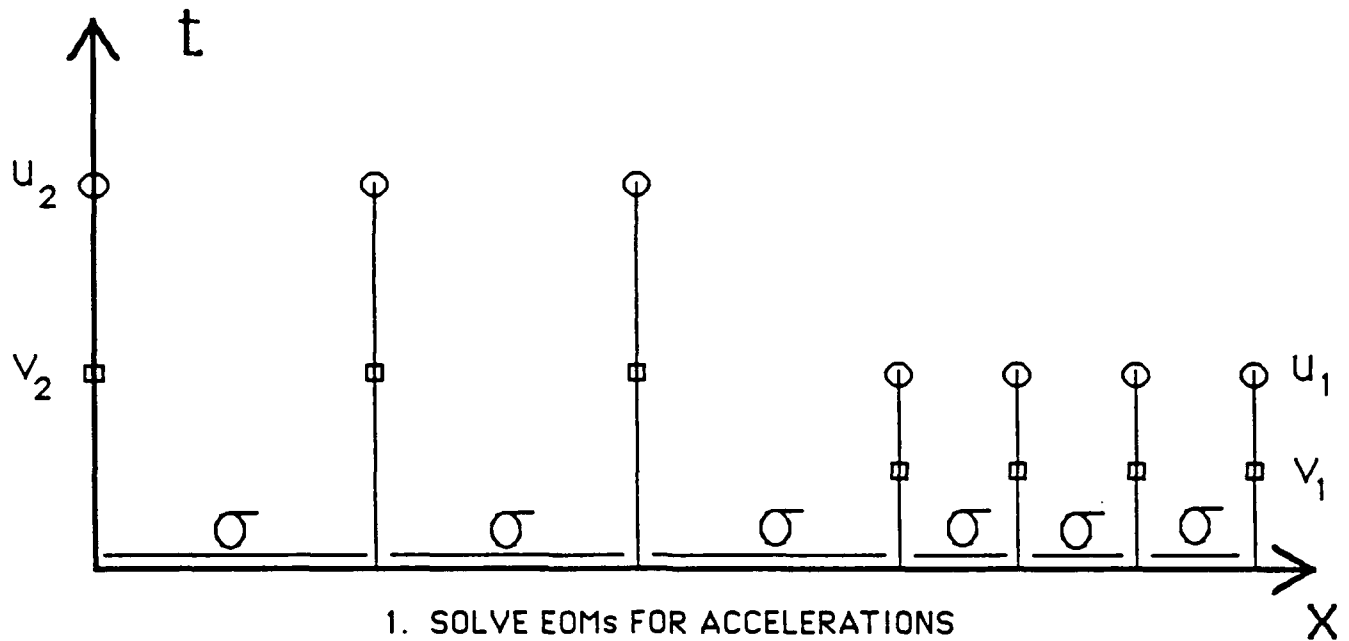
1. SOLVE EOMs FOR MINOR CYCLE ACCELERATIONS
2. UPDATE MINOR CYCLE VELOCITIES
3. UPDATE MINOR CYCLE DISPLACEMENTS

1. COMPUTE STRESSES FOR ALL ZONES

Figure 5. Timing diagrams for linear nodal interpolation algorithm.

1. SOLVE EOMs FOR ACCELERATIONS
2. UPDATE VELOCITIES
3. UPDATE DISPLACEMENTS

1. COMPUTE MINOR CYCLE STRESSES
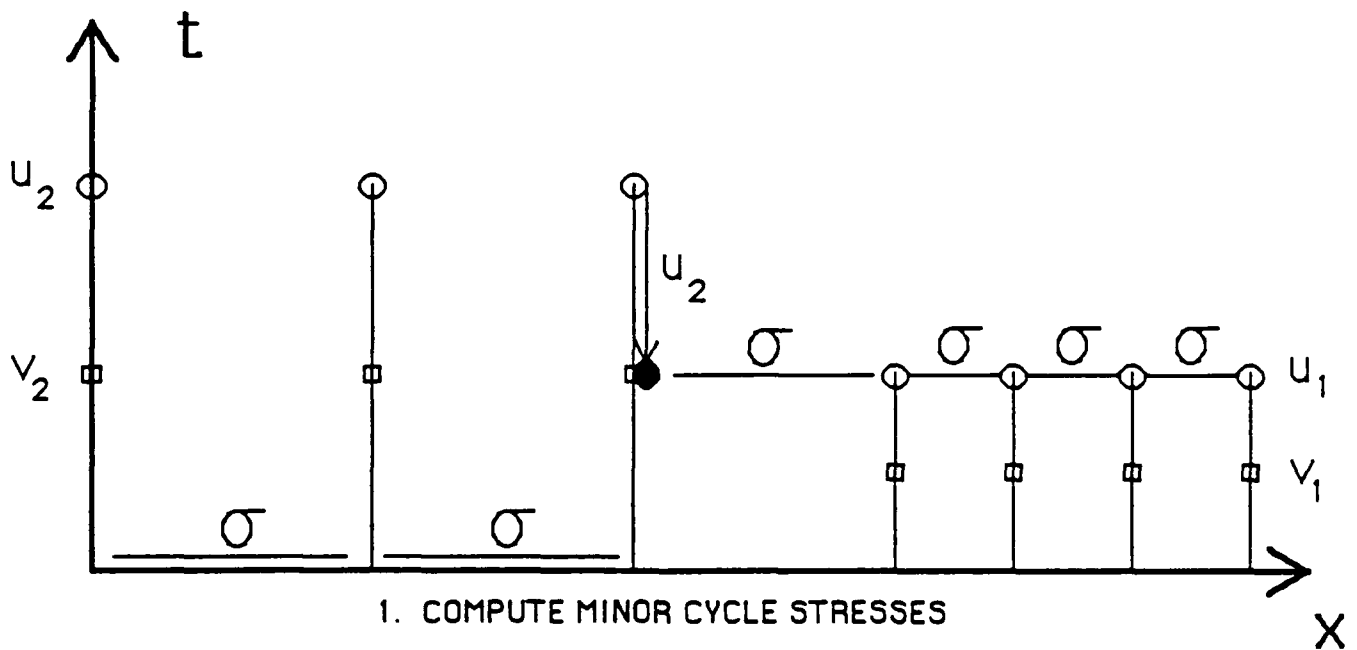
NOTE: Interface node displacement constant during minor cycle updates (extrapolated value)

Figure 6. Timing diagrams for extrapolated nodal partition algorithm.
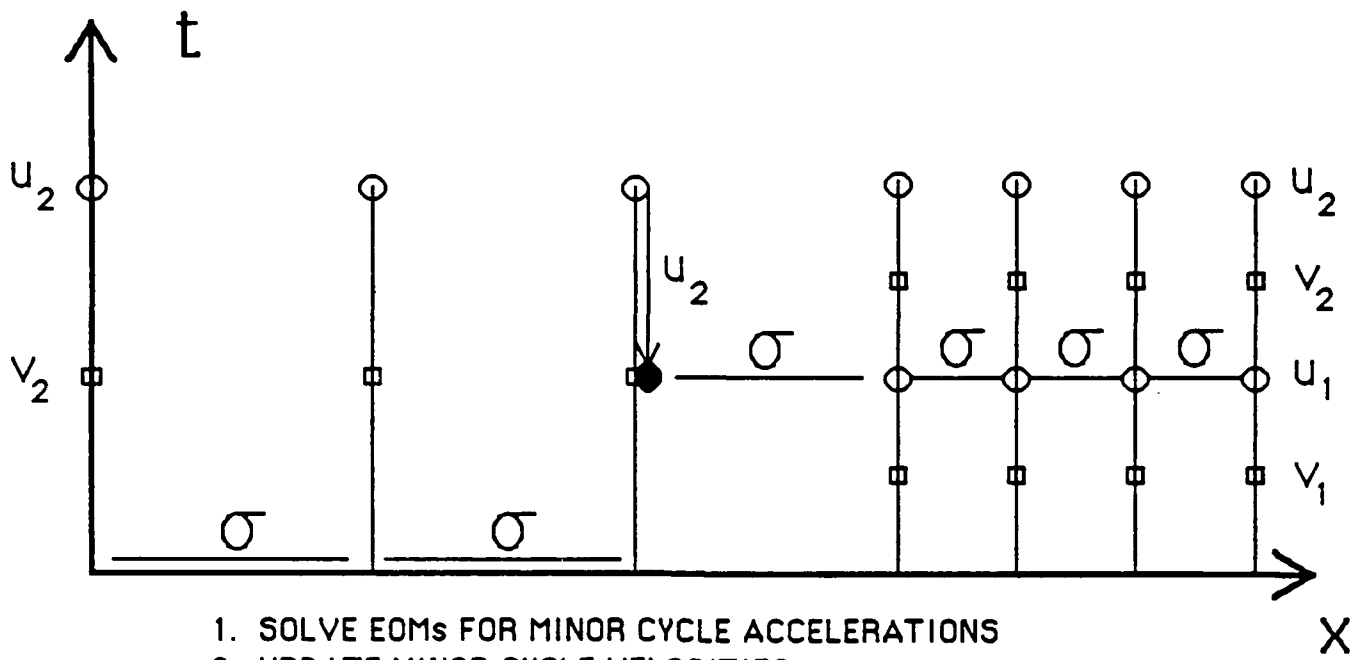
1. SOLVE EOMs FOR MINOR CYCLE ACCELERATIONS
2. UPDATE MINOR CYCLE VELOCITIES
3. UPDATE MINOR CYCLE DISPLACEMENTS
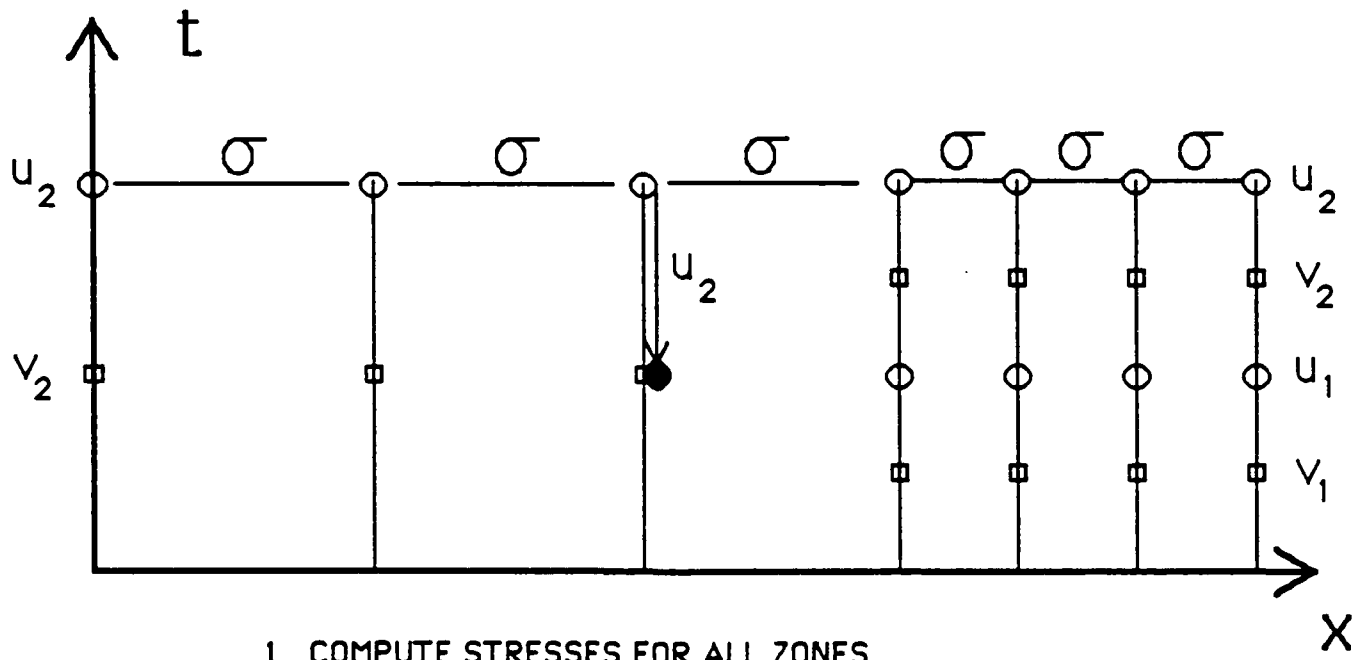
1. COMPUTE STRESSES FOR ALL ZONES

Figure 7. Timing diagrams for extrapolated nodal partition algorithm.
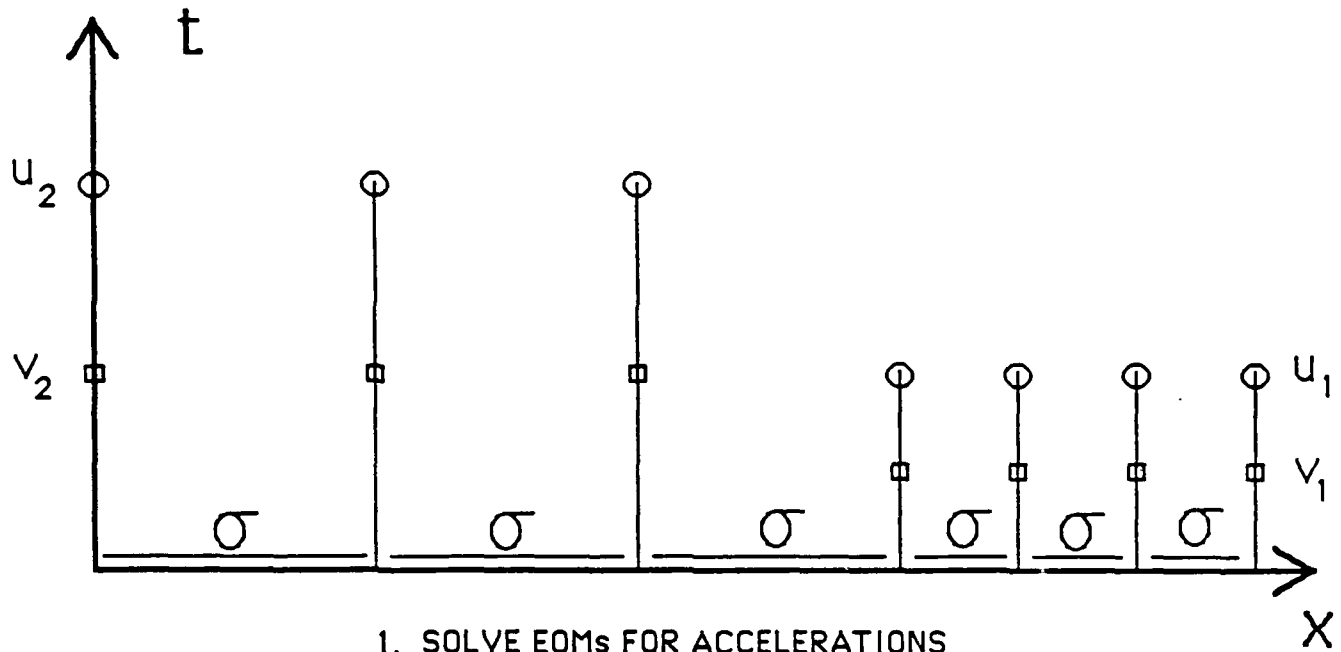
1. SOLVE EOMs FOR ACCELERATIONS
2. UPDATE VELOCITIES
3. UPDATE DISPLACEMENTS
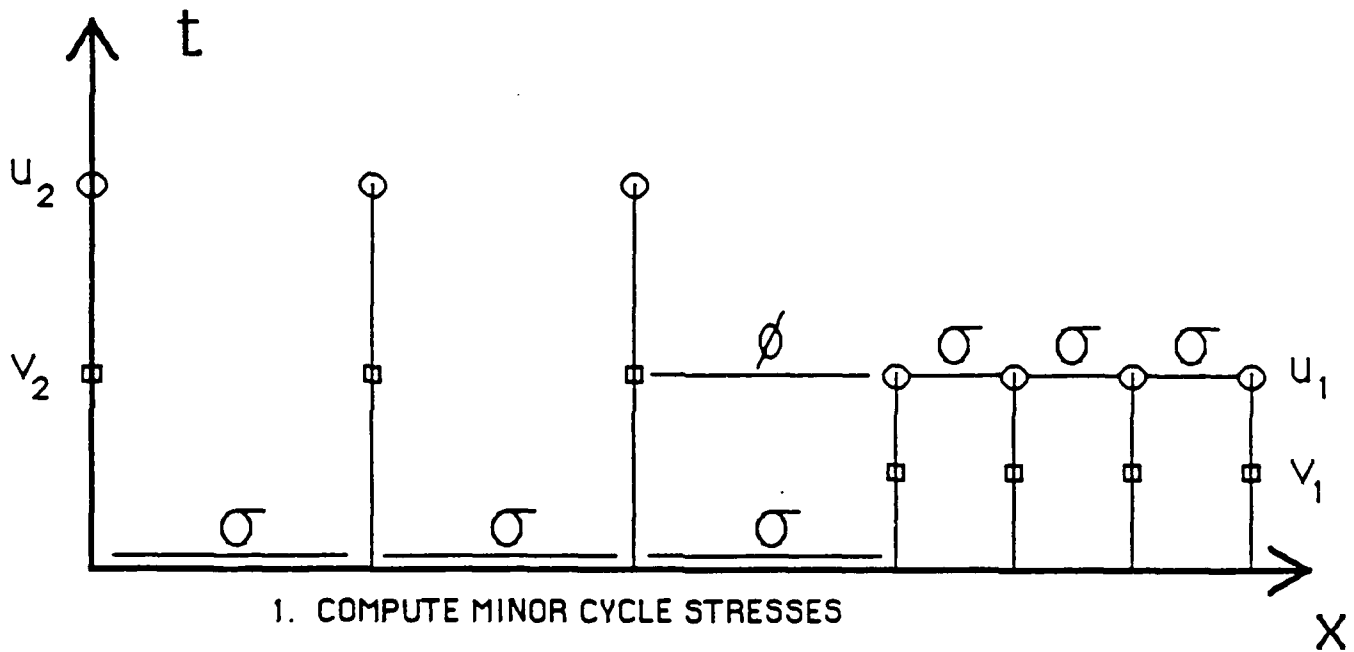
1. COMPUTE MINOR CYCLE STRESSES

NOTE: Subcycle zones disconnected during
minor cycle updates

Figure 8. Timing diagrams for "free" element partition algorithm.
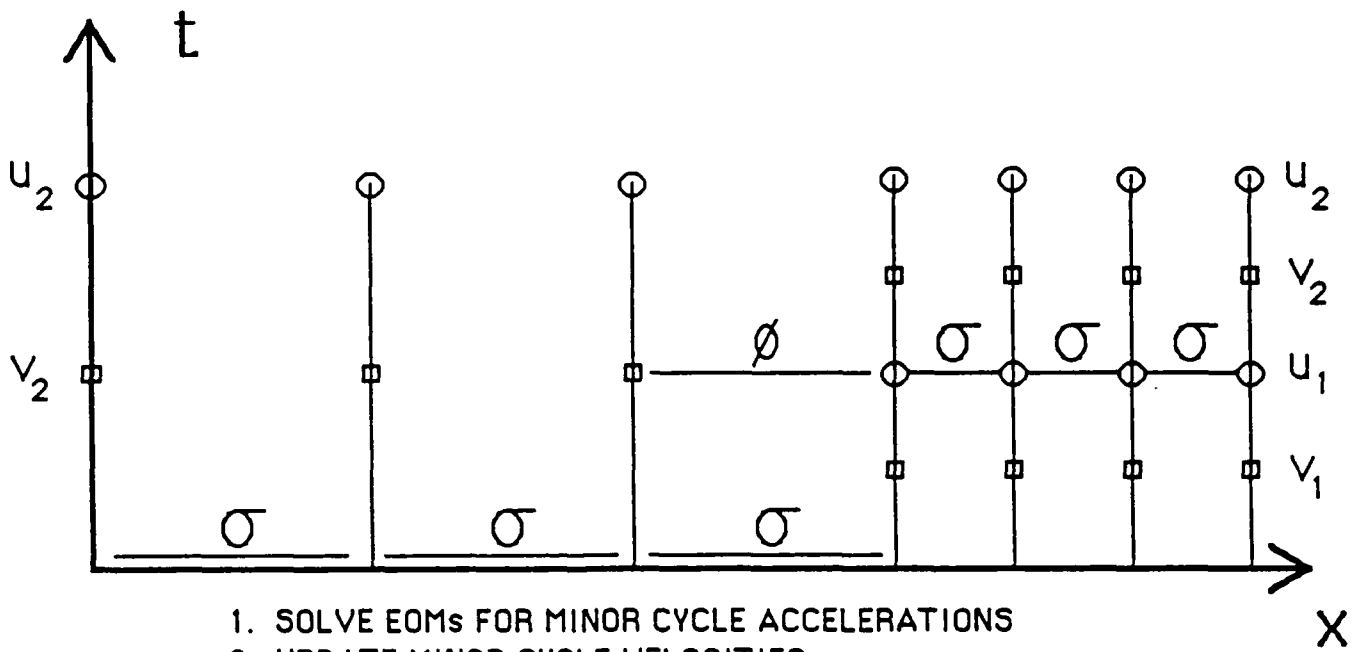
1. SOLVE EOMs FOR MINOR CYCLE ACCELERATIONS
2. UPDATE MINOR CYCLE VELOCITIES
3. UPDATE MINOR CYCLE DISPLACEMENTS
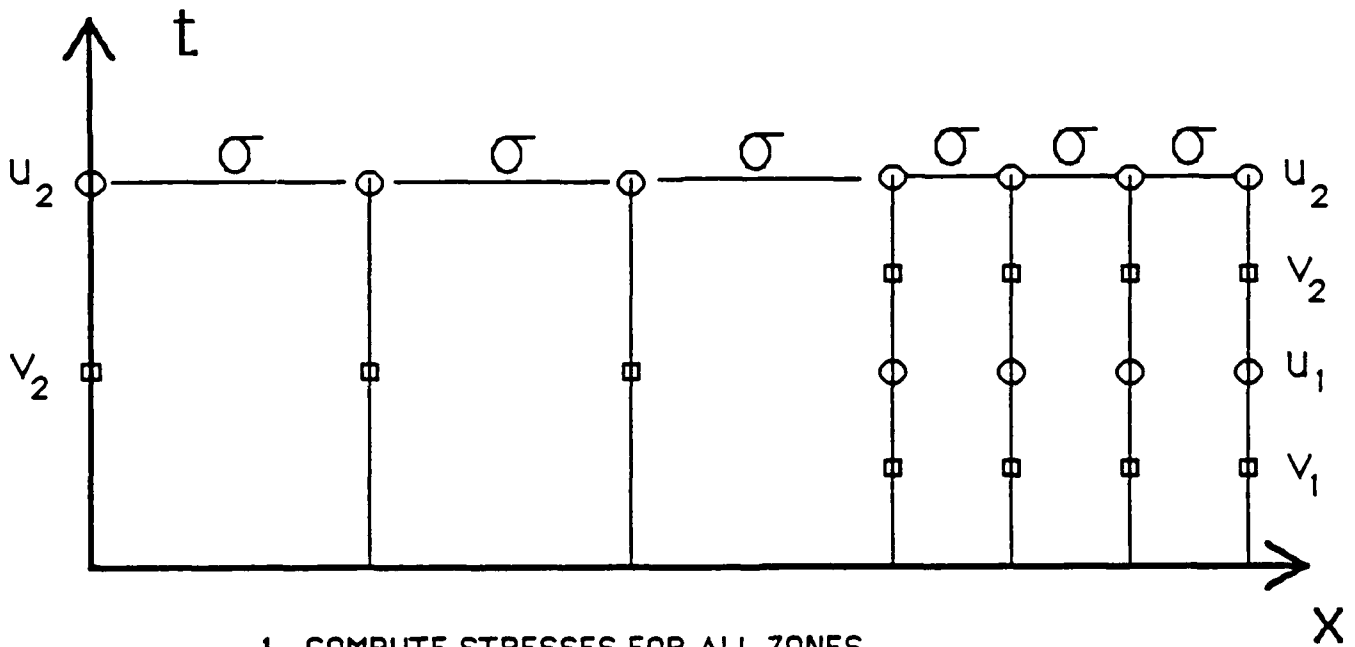
1. COMPUTE STRESSES FOR ALL ZONES

Figure 9. Timing diagrams for "free" element partition algorithm.
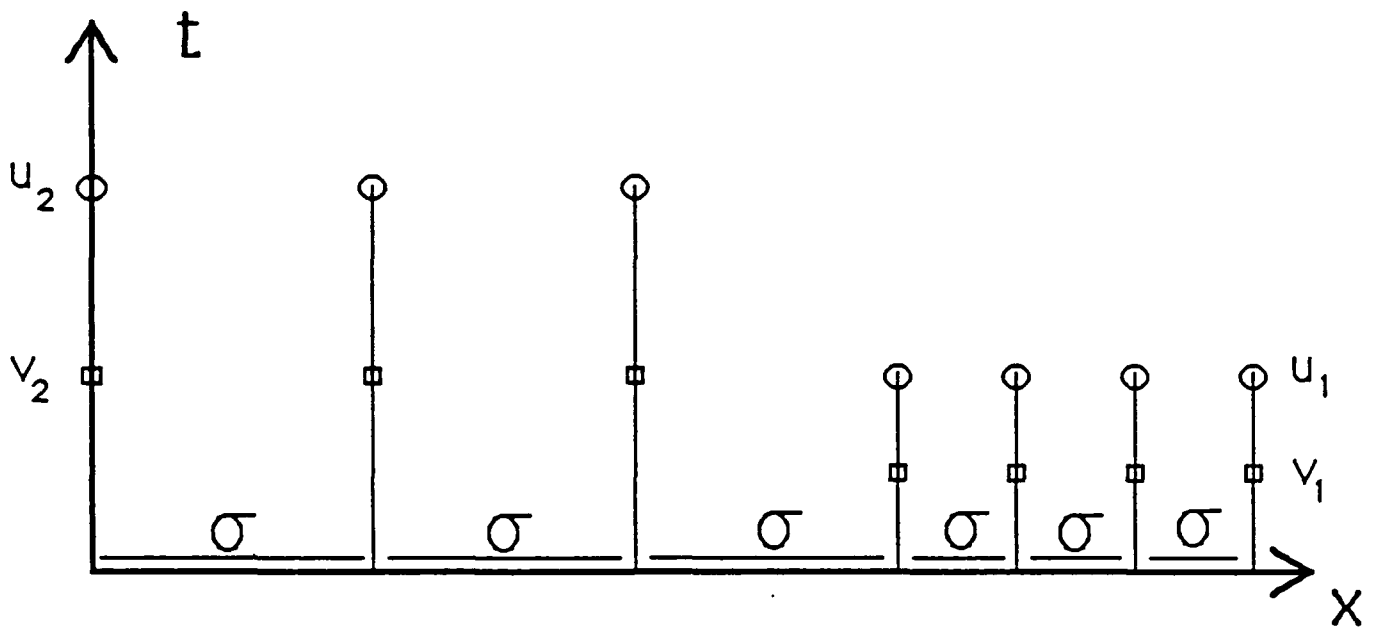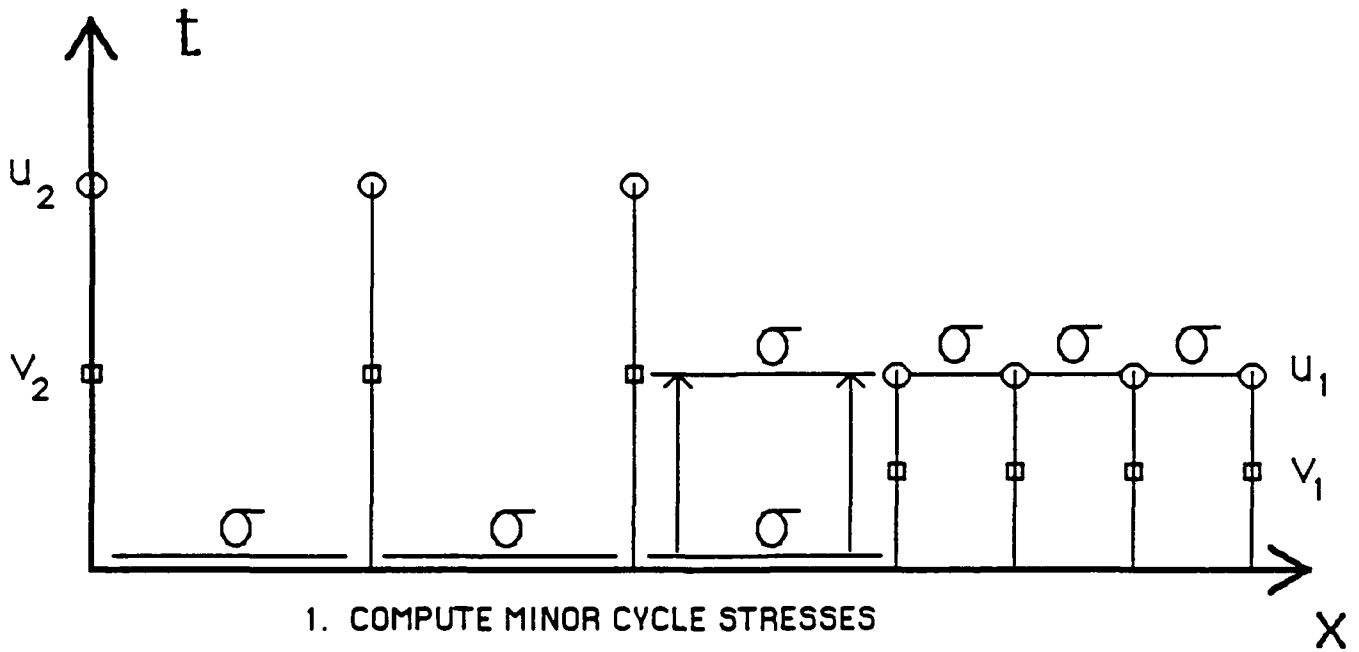
Figure 10. Timing diagrams for constant stress element partition algorithm.

31

1. SOLVE EOMs FOR MINOR CYCLE ACCELERATIONS
2. UPDATE MINOR CYCLE VELOCITIES
3. UPDATE MINOR CYCLE DISPLACEMENTS

1. COMPUTE STRESSES FOR ALL ZONES

Figure 11. Timing diagrams for constant stress element partition algorithm.

32
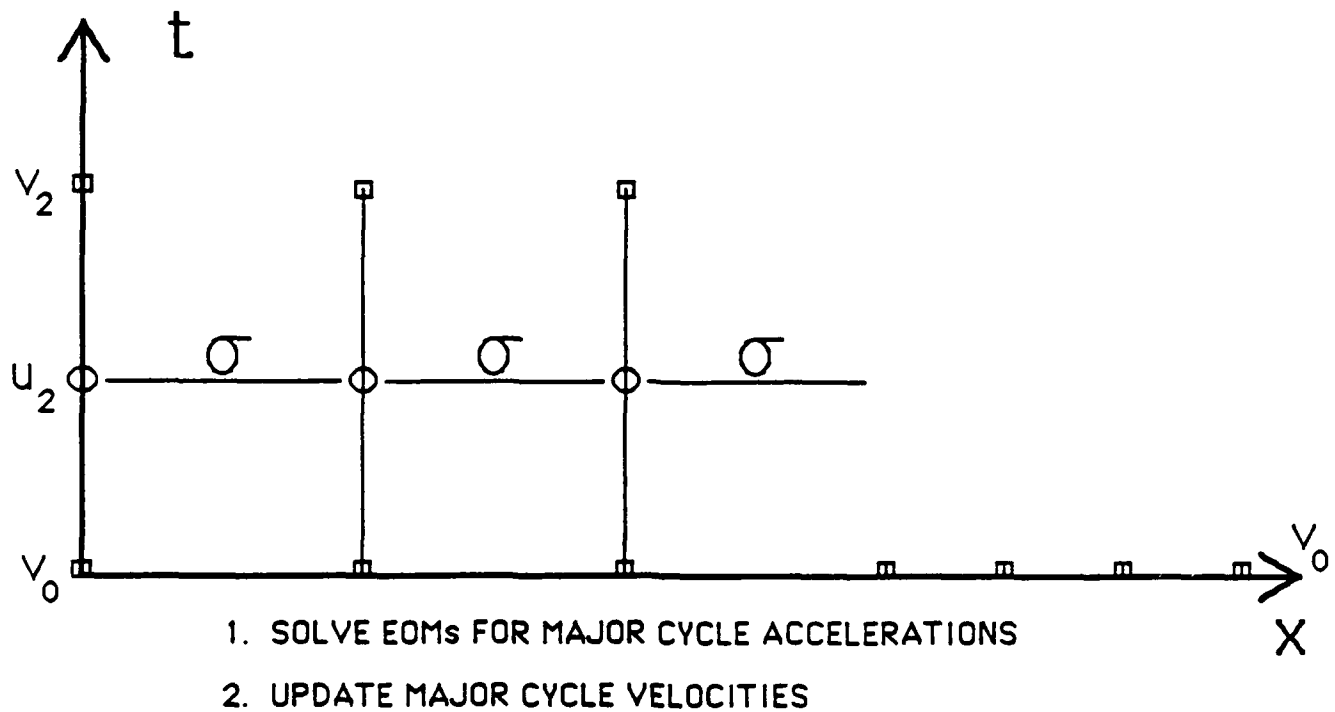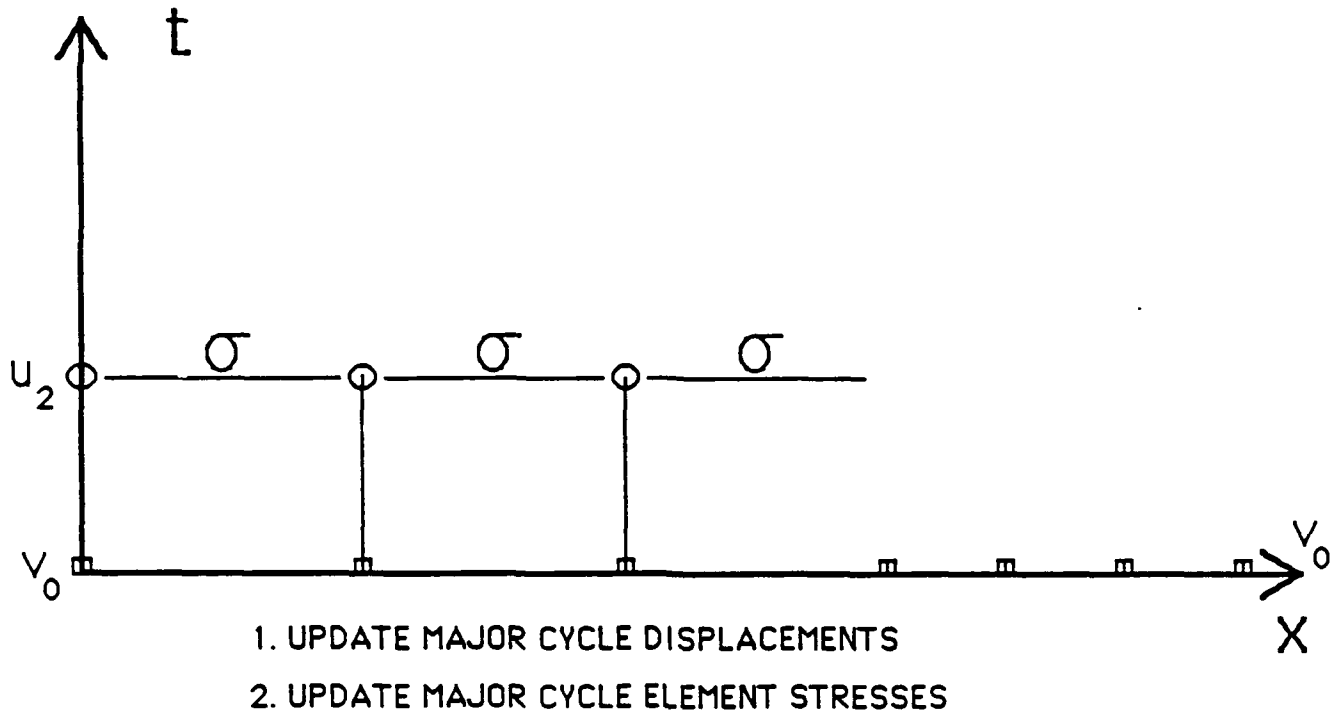
Figure 12. Timing diagrams for TRANAL element partition algorithm.

33

1. UPDATE MINOR CYCLE DISPLACEMENTS
2. UPDATE MINOR CYCLE ELEMENT STRESSES

1. SOLVE EOMs FOR MINOR CYCLE ACCELERATIONS
2. UPDATE MINOR CYCLE VELOCITIES
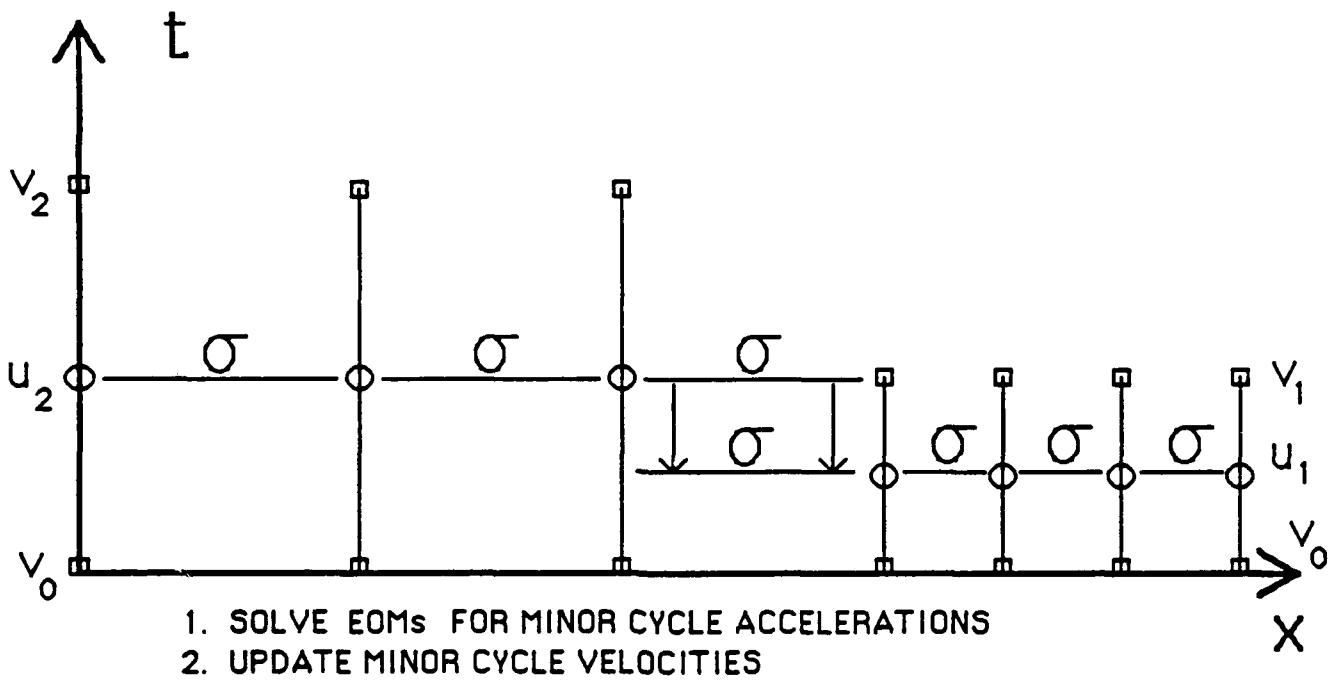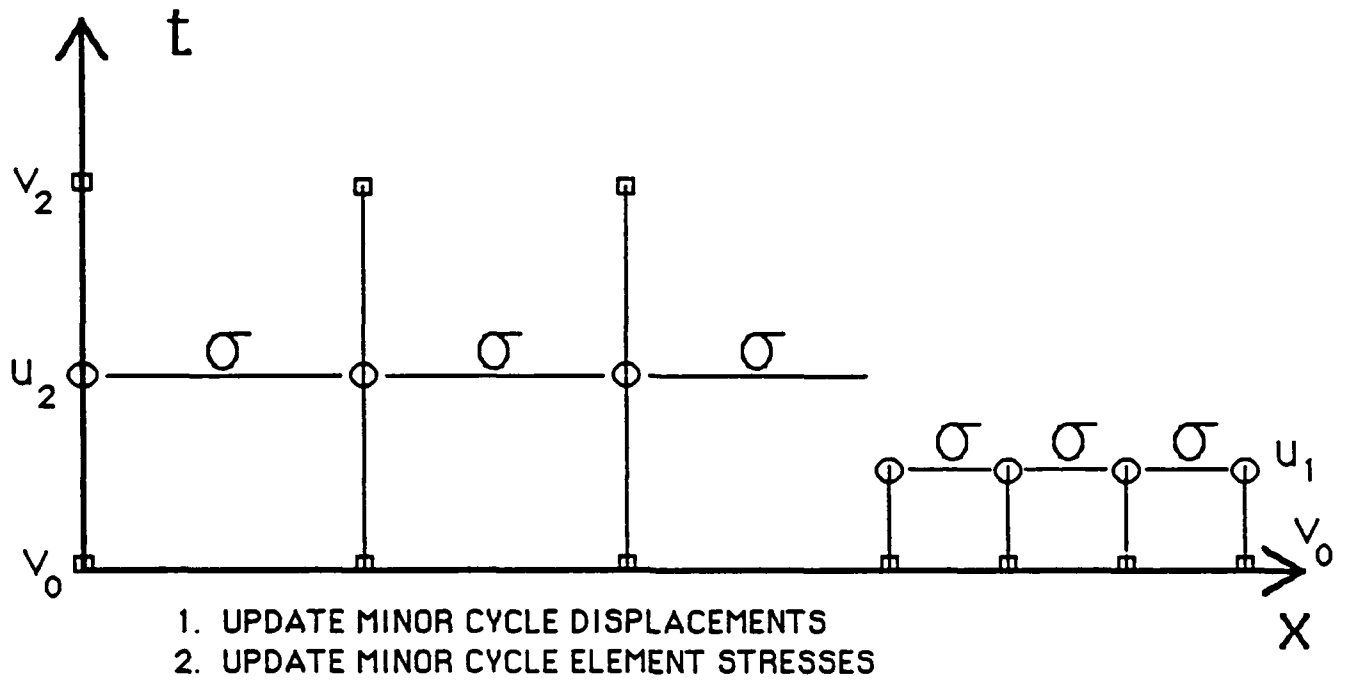
NOTE: Updated major cycle element stresses used in EOMs

Figure 13. Timing diagrams for TRANAL element partition algorithm.

34

1. UPDATE MINOR CYCLE DISPLACEMENTS
2. UPDATE MINOR CYCLE ELEMENT STRESSES

1. SOLVE EOMs FOR MINOR CYCLE ACCELERATIONS
2. UPDATE MINOR CYCLE VELOCITIES
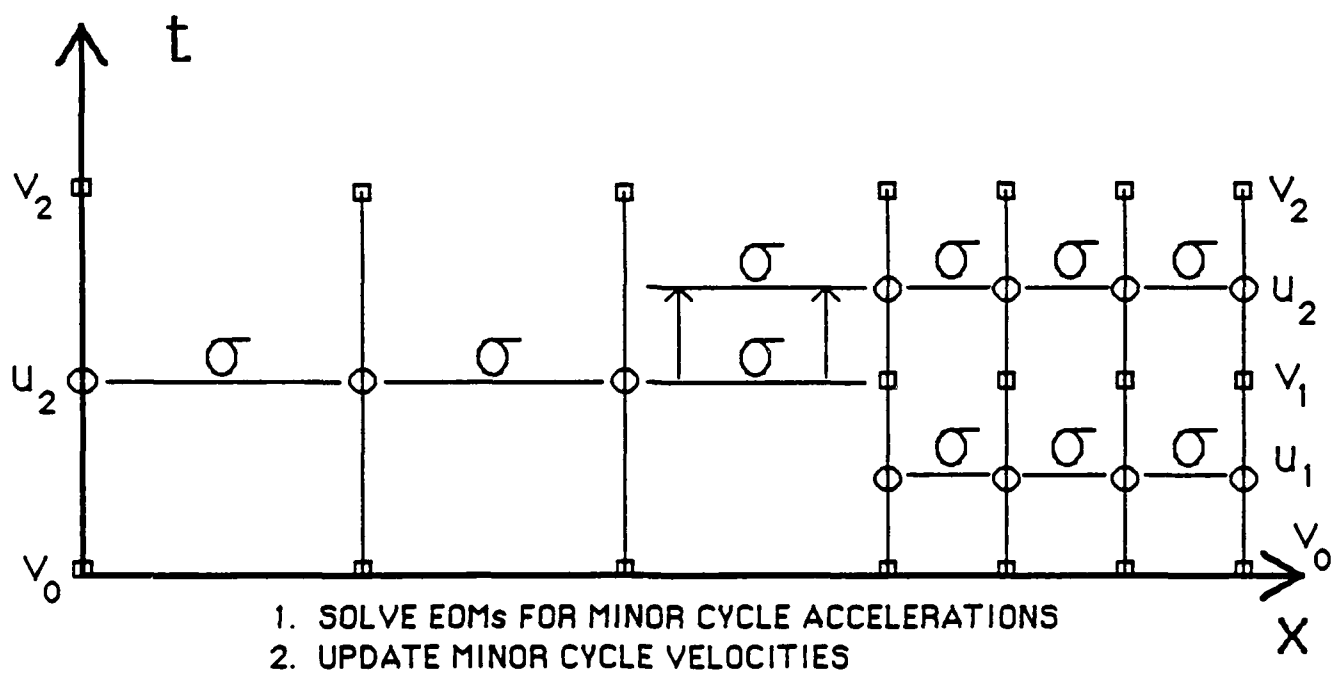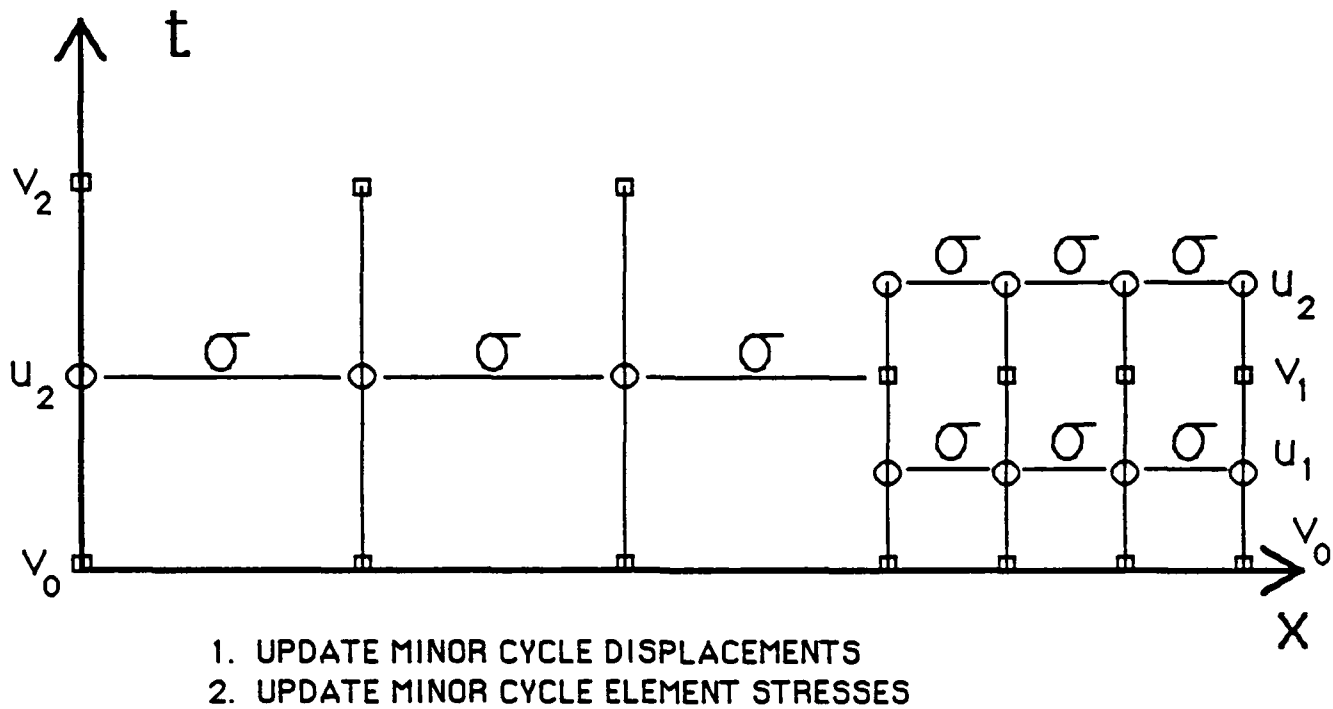
NOTE: Updated major cycle element stresses used
in EOMs

Figure 14. Timing diagrams for TRANAL element partition algorithm.

35
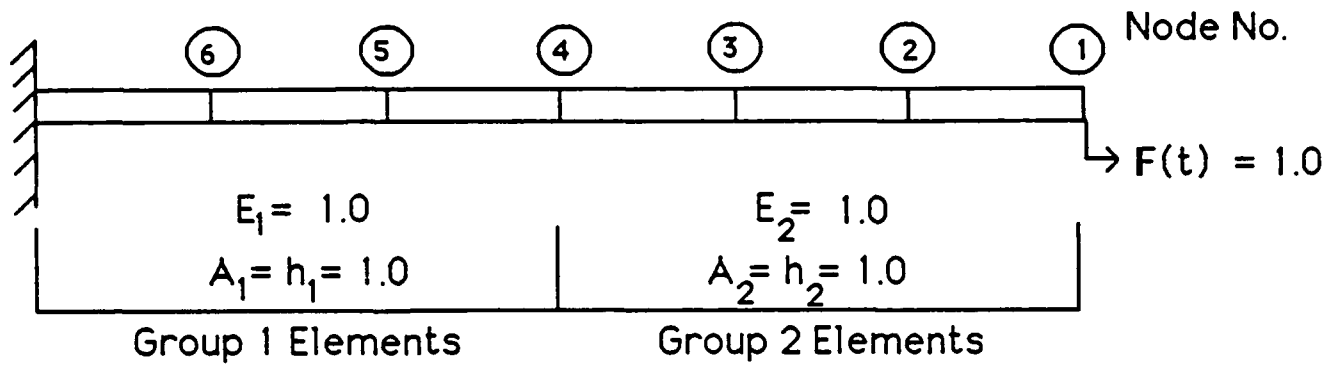
SUBCYCLING PROBLEM NO. 1
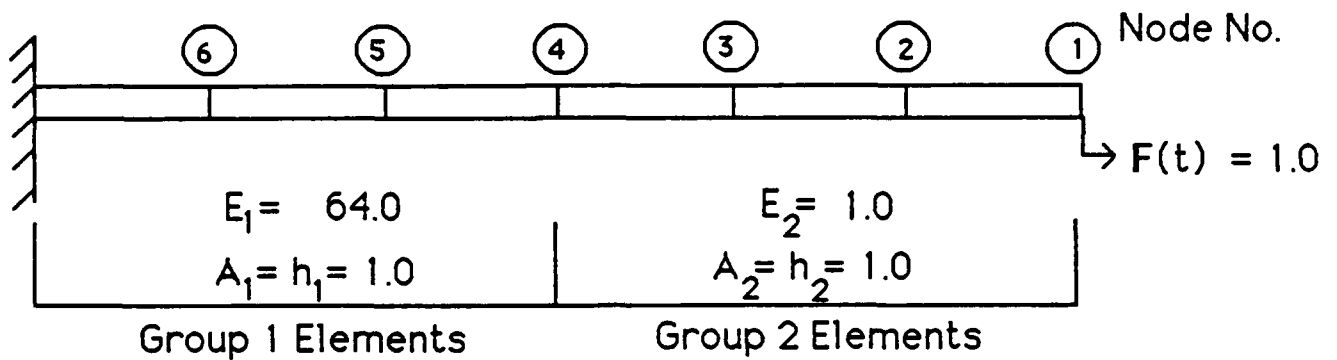
SUBCYCLING PROBLEM NO. 2
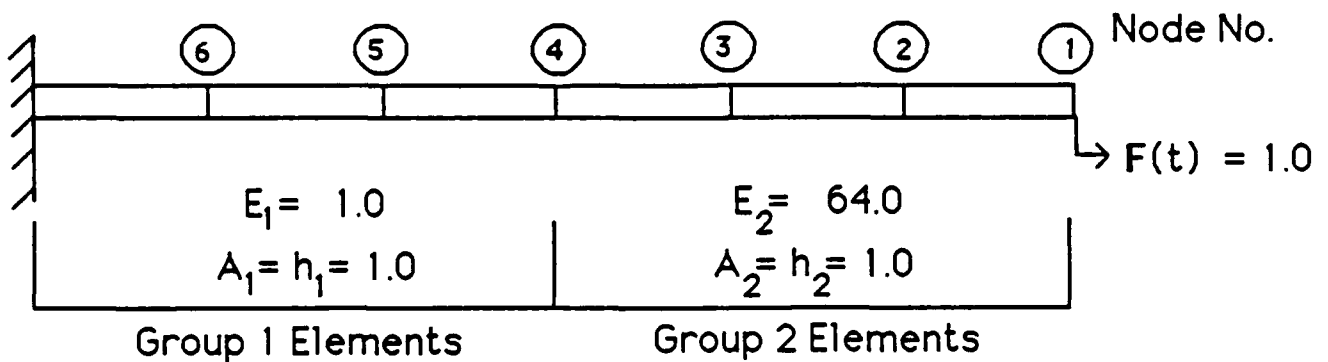
SUBCYCLING PROBLEM NO. 3

Figure 15. Three one-dimensional test problems.
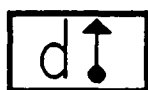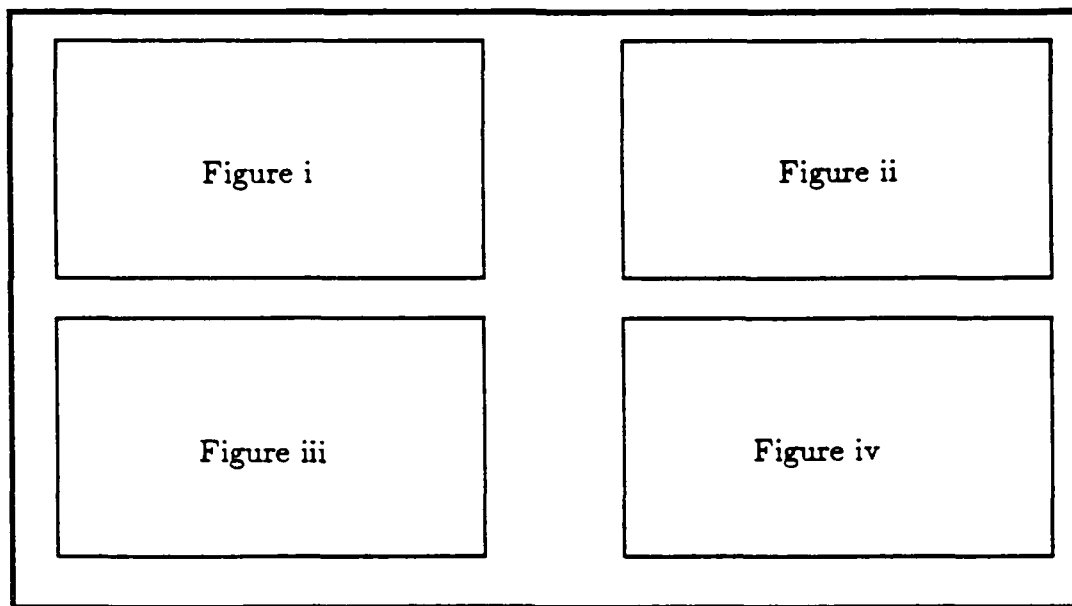
$\boxed{d\,\updownarrow}$	$\equiv$	Constant Displacement Nodal Partition Algorithm
$\boxed{d\,\updownarrow}$	$\equiv$	Linear Nodal Interpolation Algorithm
$\boxed{d\,\updownarrow}$	$\equiv$	Extrapolated Nodal Partition Algorithm
$\boxed{\sigma = 0}$	$\equiv$	"Free" Element Partition Algorithm
$\boxed{\sigma\,\updownarrow}$	$\equiv$	Constant Stress Element Partition Algorithm
$\boxed{\sigma\,\updownarrow}$	$\equiv$	TRANAL Element Partition Algorithm

CURVE LEGEND

$\bigcirc$ = node 1
$\square$ = node 2
$\triangle$ = node 3
$\Diamond$ = node 4
$\triangledown$ = node 5
$\bigcirc$ = node 6

Figure 16. Results legend for test problems 1-3.
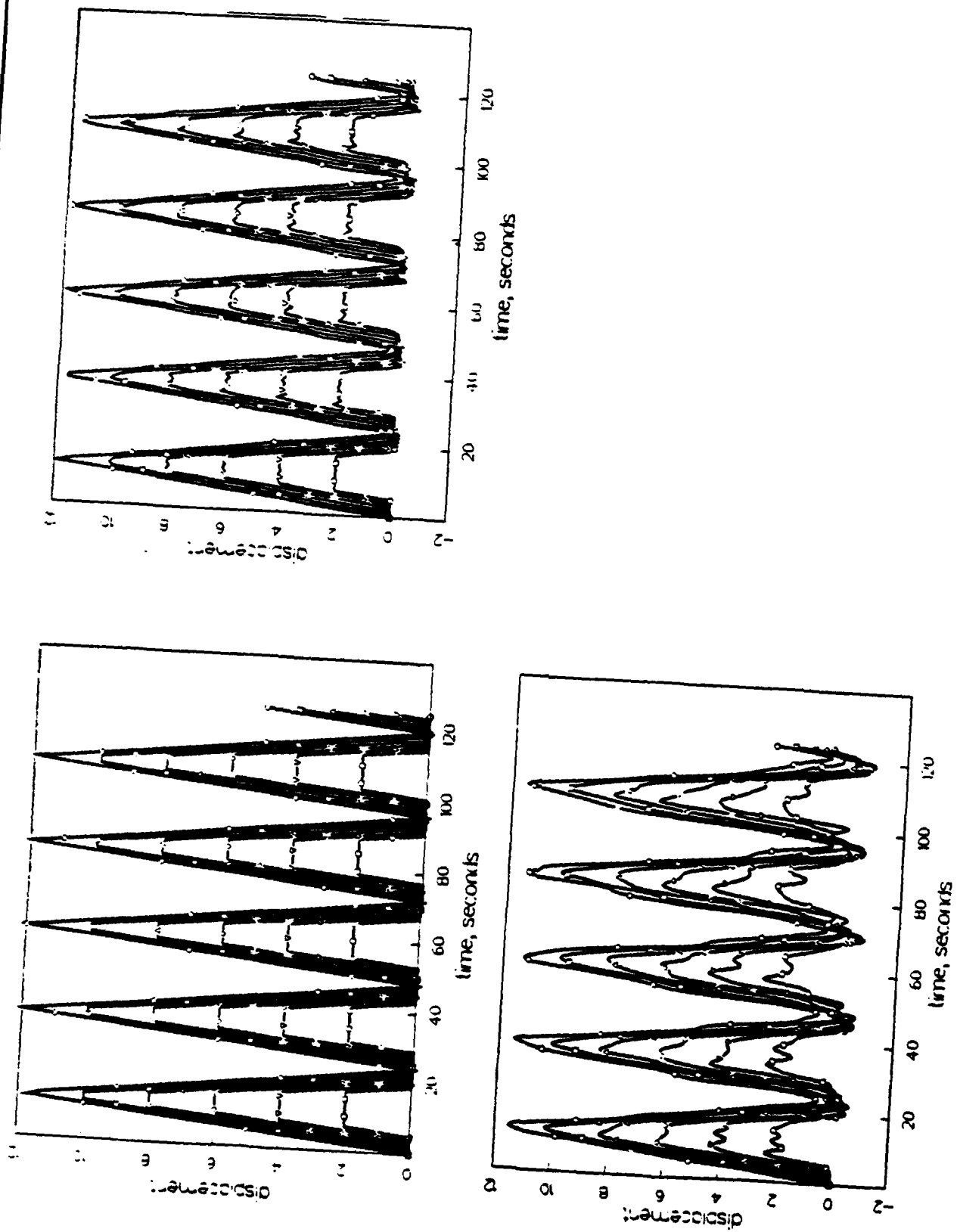
Figure 17a. Problem 1 — comparison of central difference algorithm solutions.

38
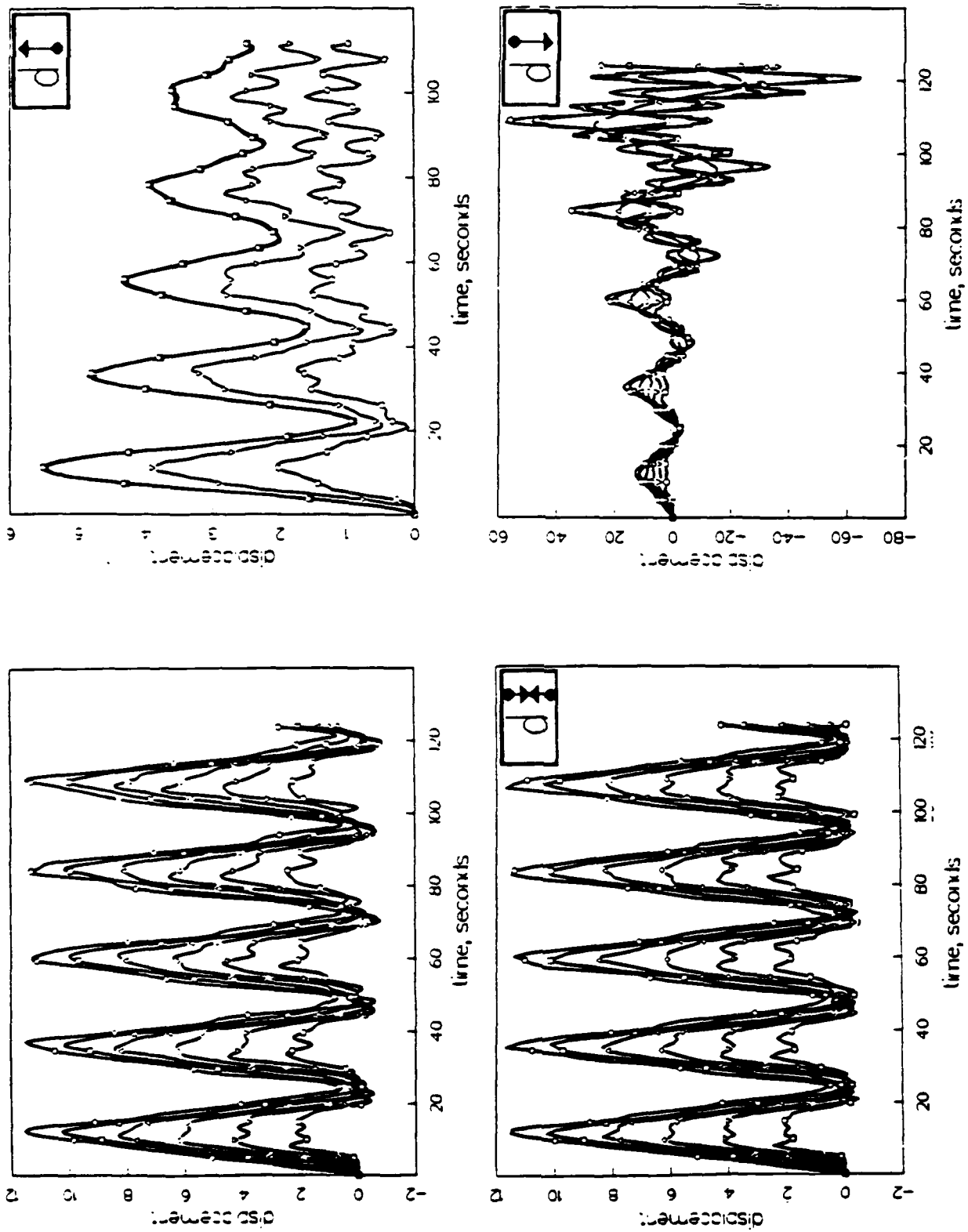
Figure 17b. Problem 1 — comparison of nodal partition algorithm solutions.
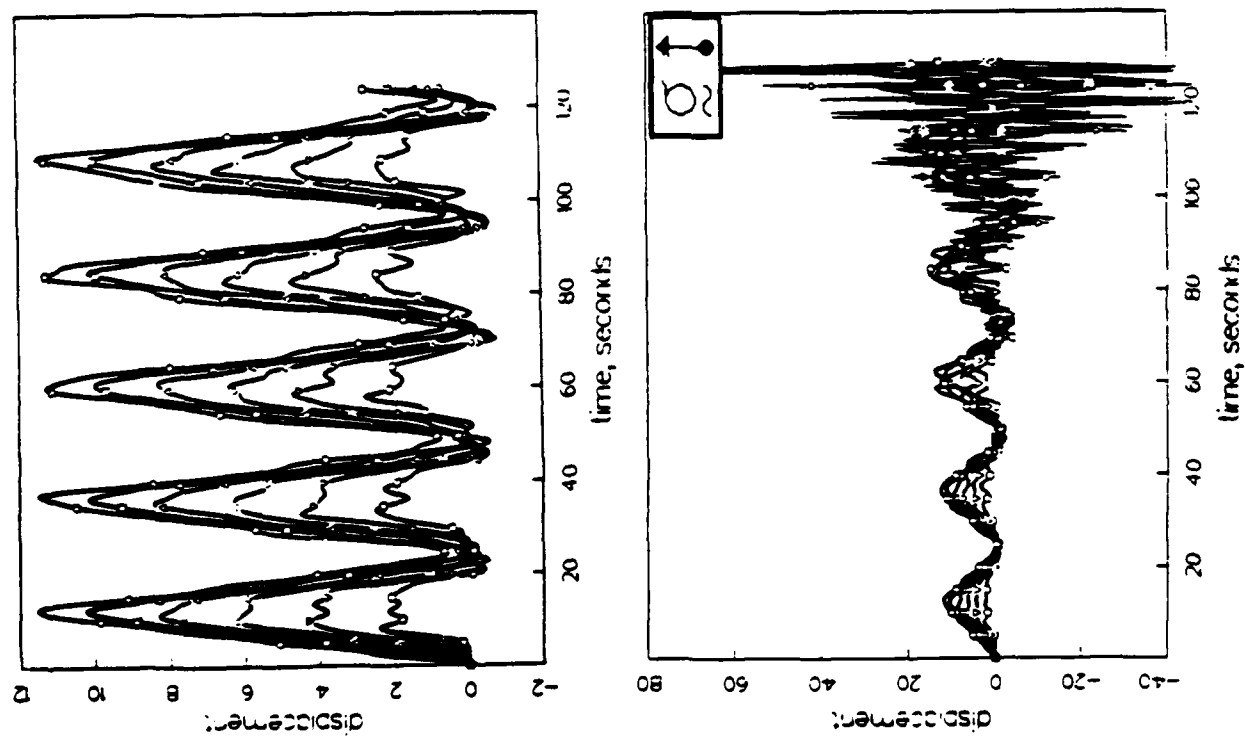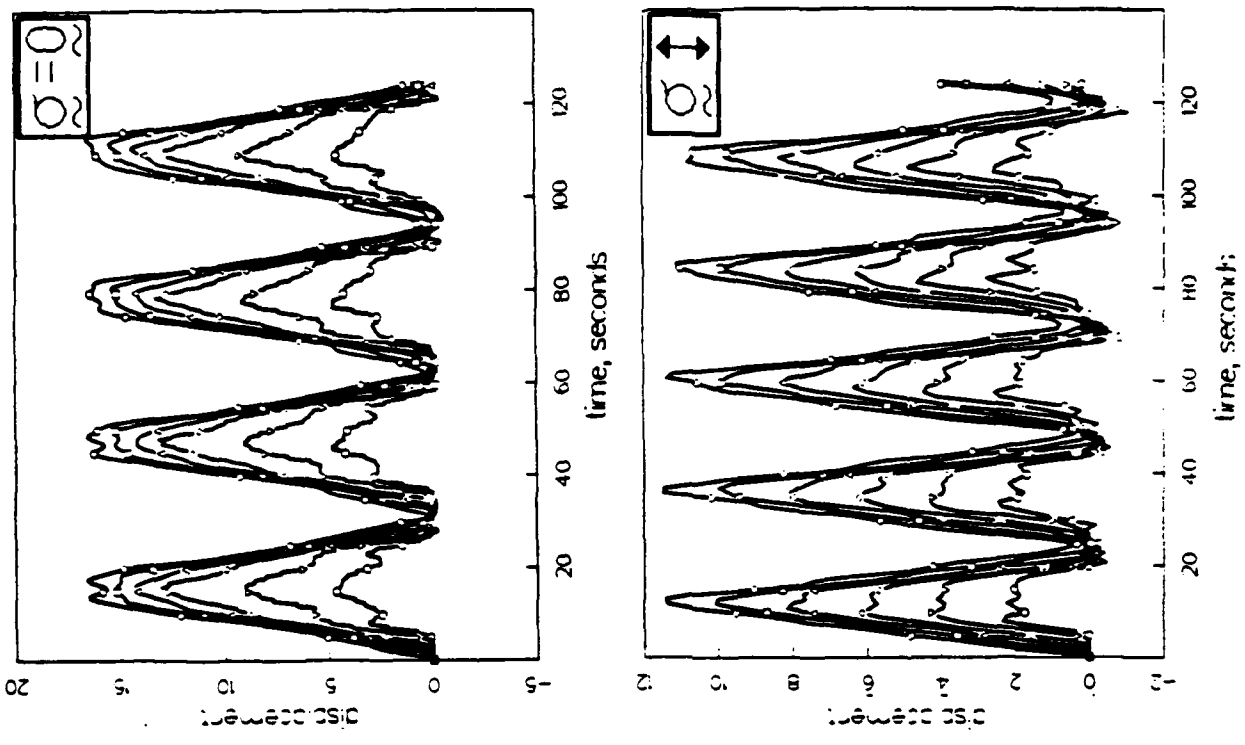
Figure 17c. Problem 1 — comparison of element partition algorithm solutions.
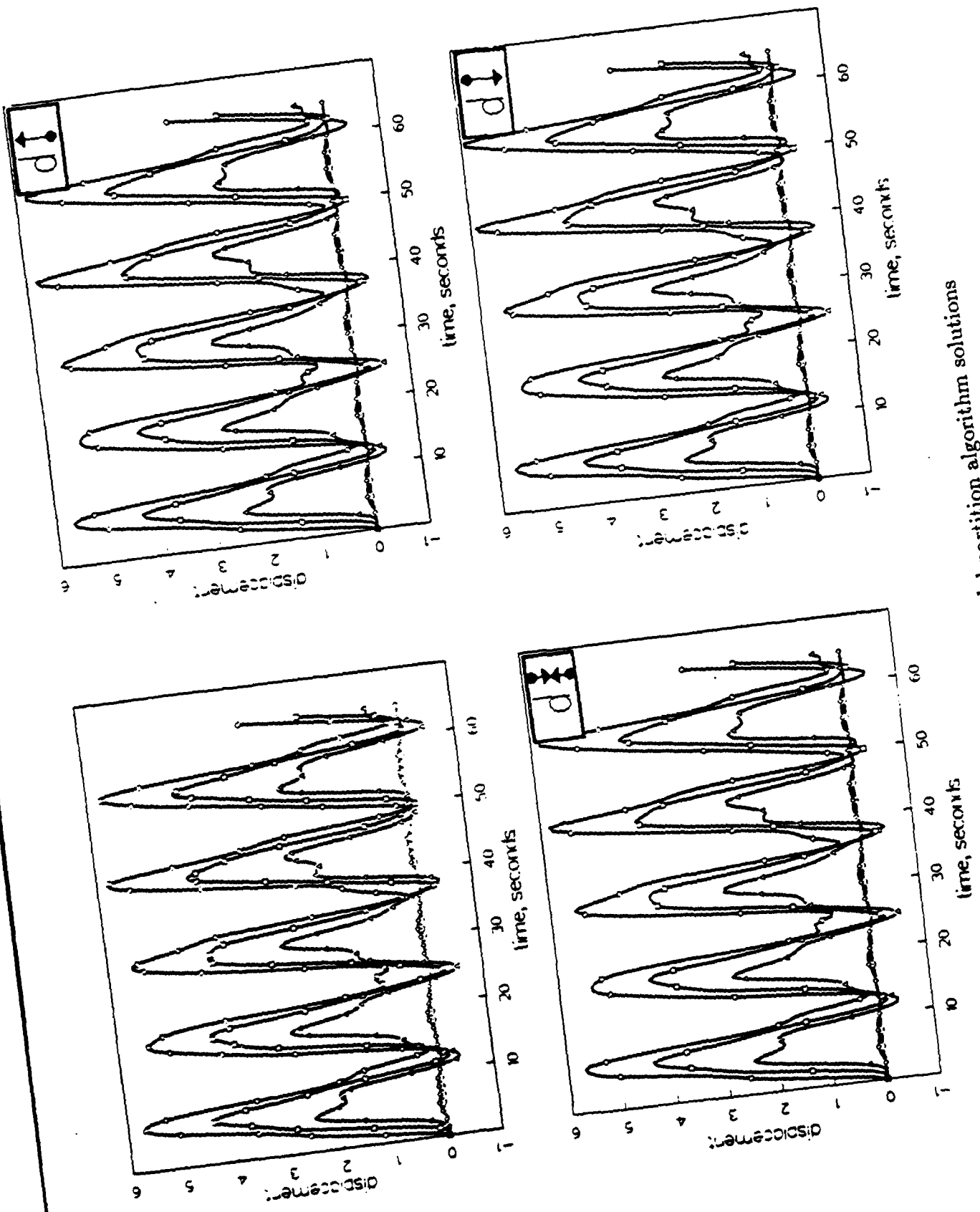
Figure 18a. Problem 2 — comparison of nodal partition algorithm solutions

$m = 2, \Delta t_c = 1.0.$

41
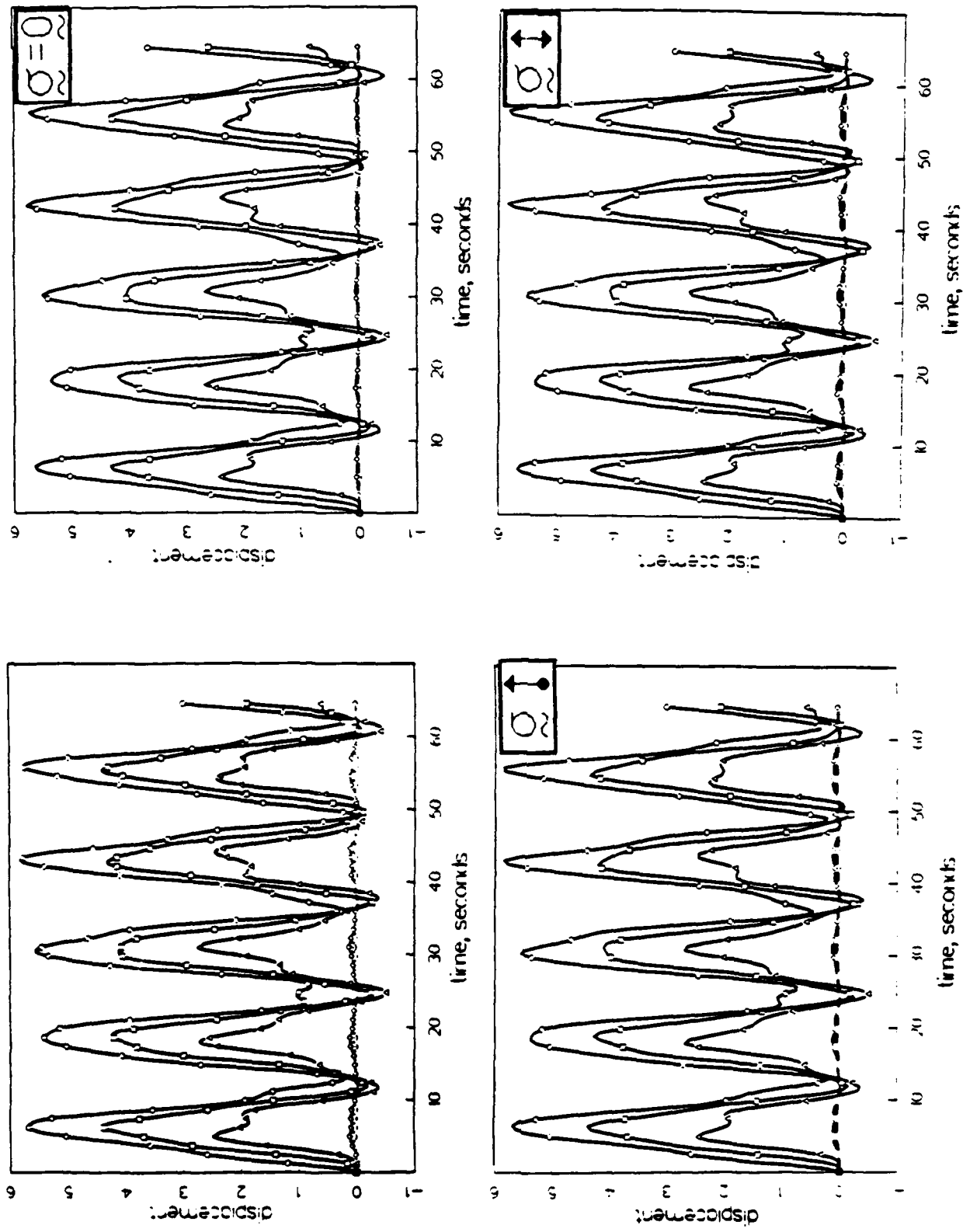
Figure 18b. Problem 2 — comparison of element partition algorithm solutions

$— m = 2, \Delta t_c = 1.0.$

42
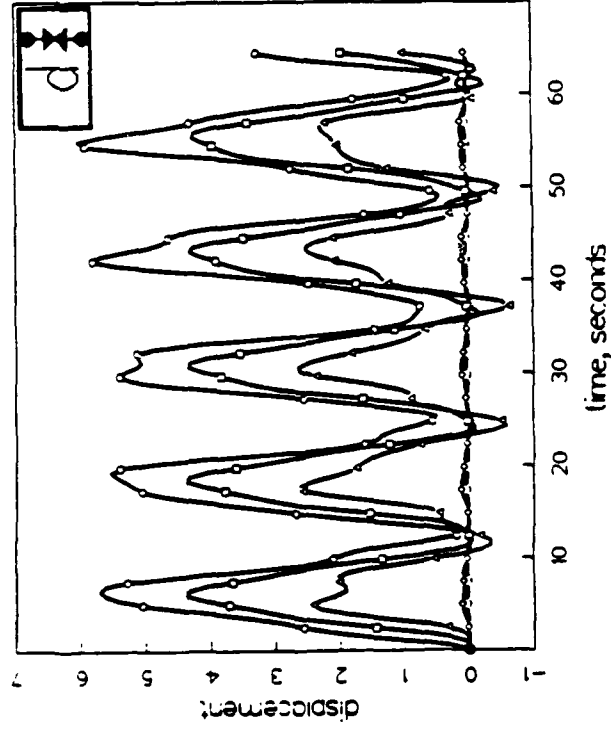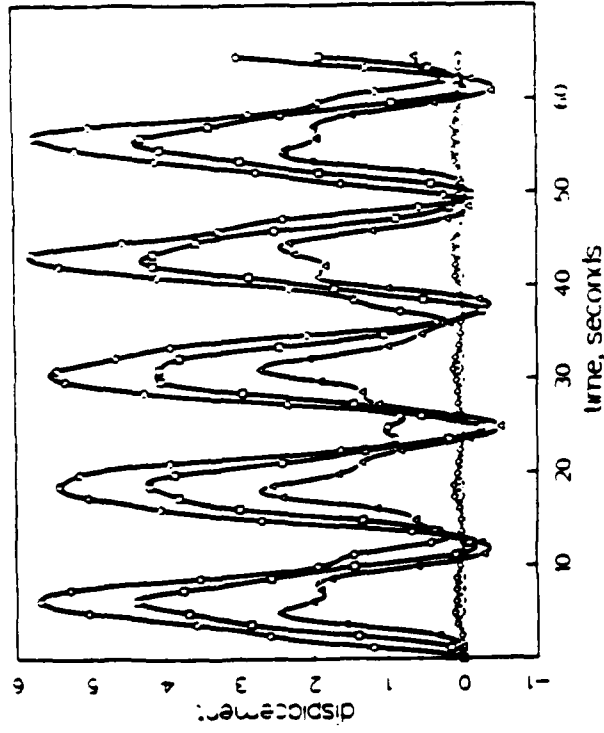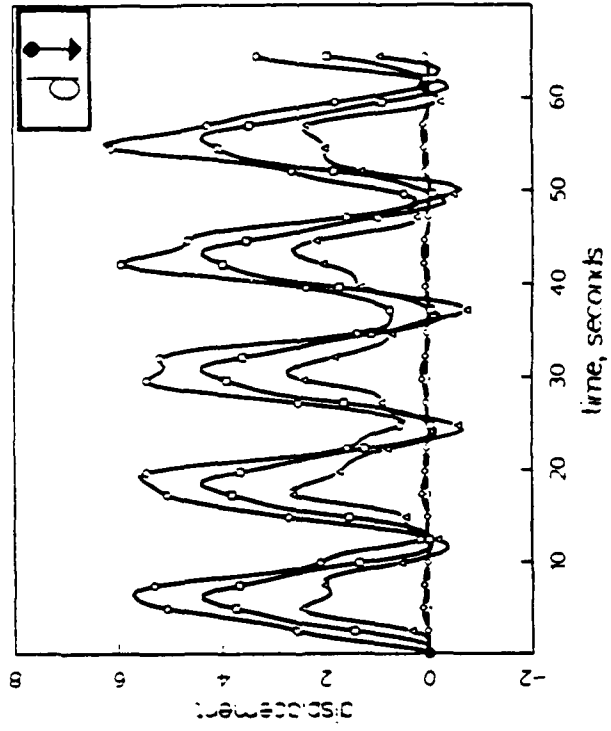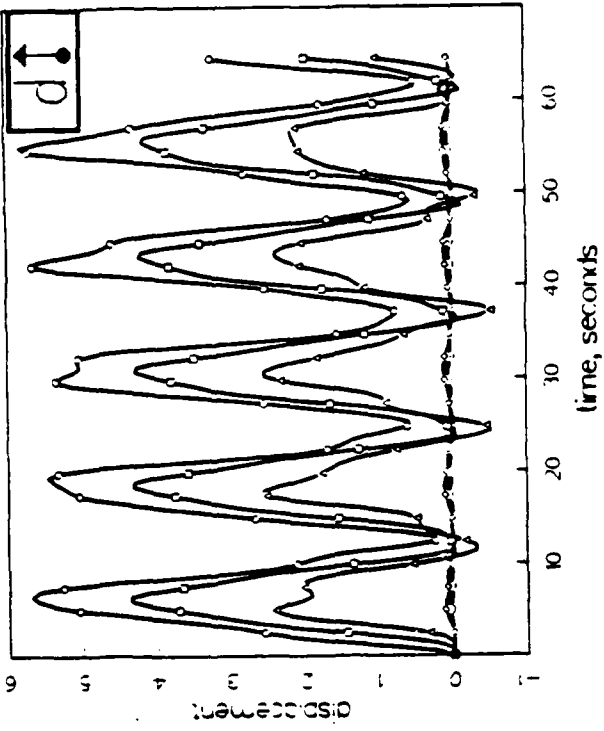
Figure 18c. Problem 2 — comparison of nodal partition algorithm solutions
— $m = 4, \Delta t_c = 1.0$.

43
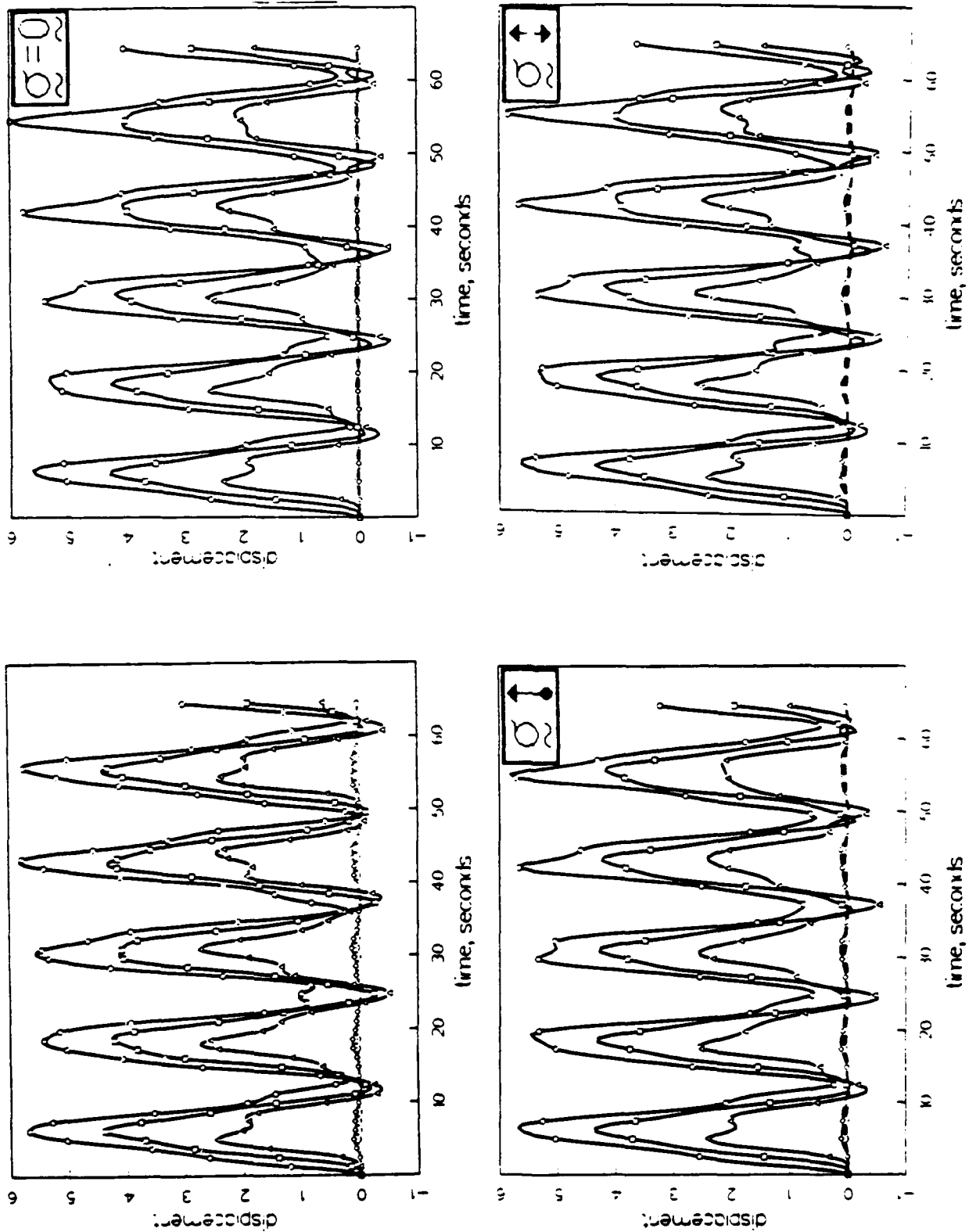
Figure 18d. Problem 2 — comparison of element partition algorithm solutions
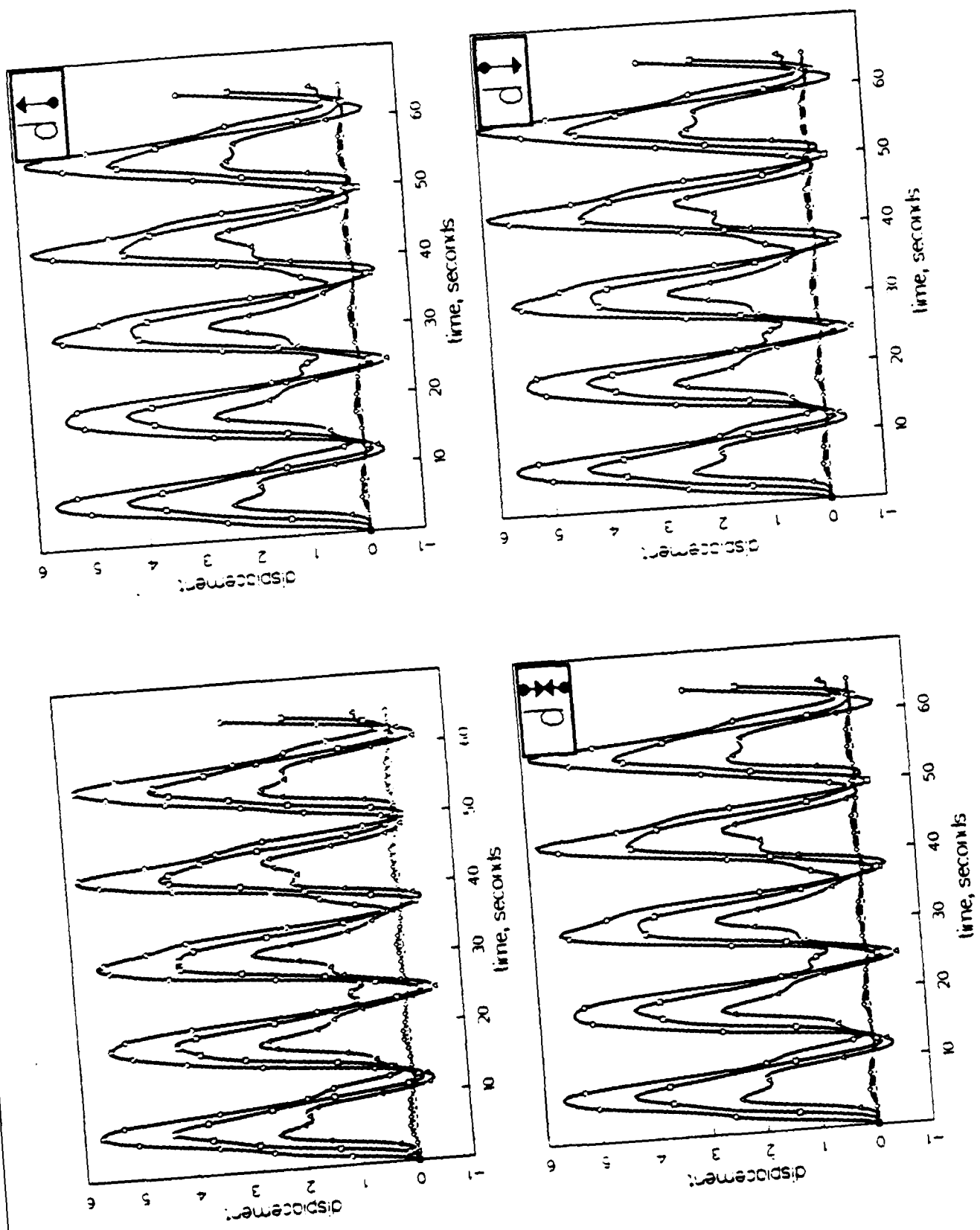
$-\!-\ m = 4, \Delta t_c = 1.0.$

Figure 18e. Problem 2 — comparison of nodal partition algorithm solutions
— $m = 4, \Delta t_c = 1/2$.

45
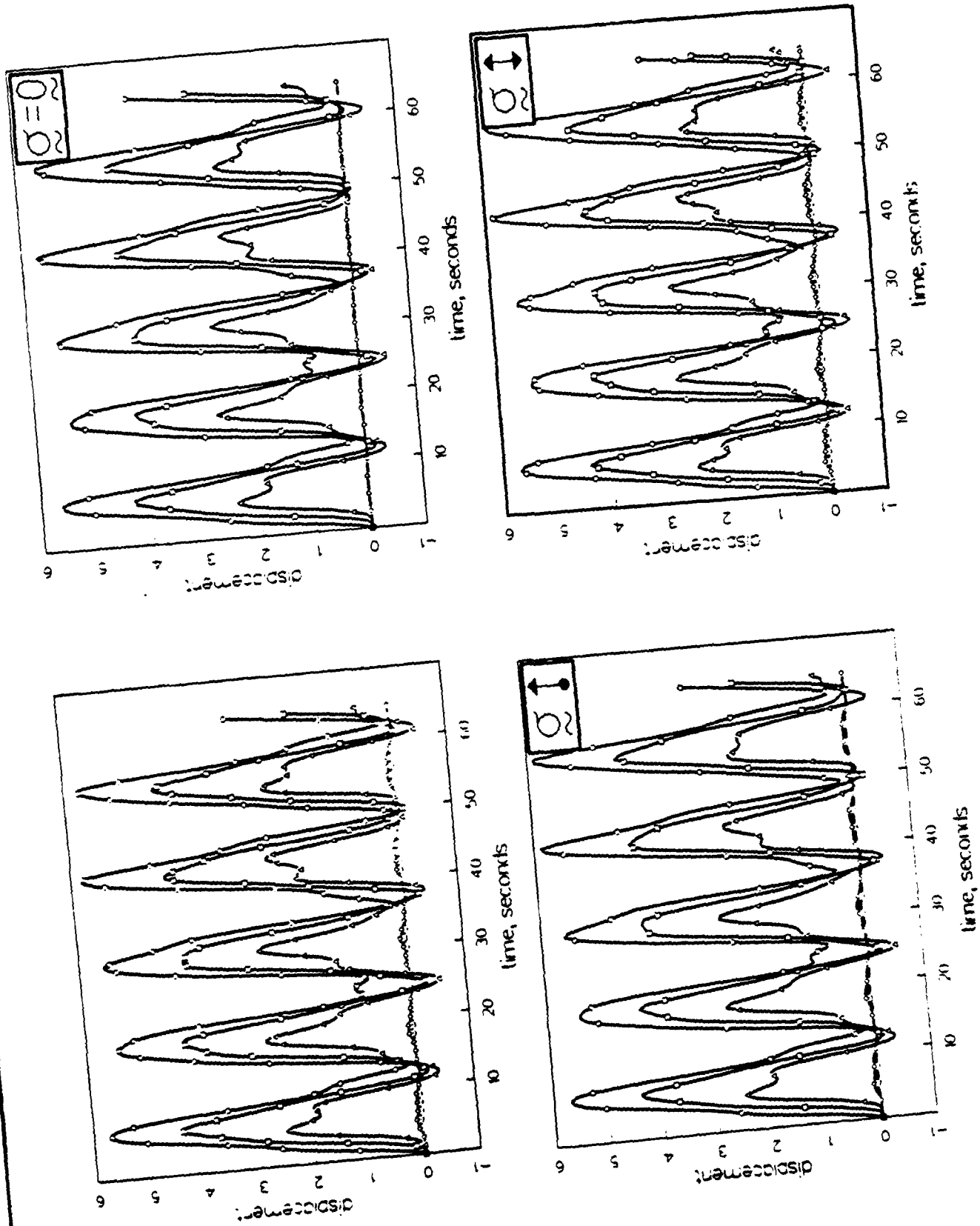
Figure 18f. Problem 2 — comparison of element partition algorithm solutions

$n = 4, \Delta t_c = 1/2$.
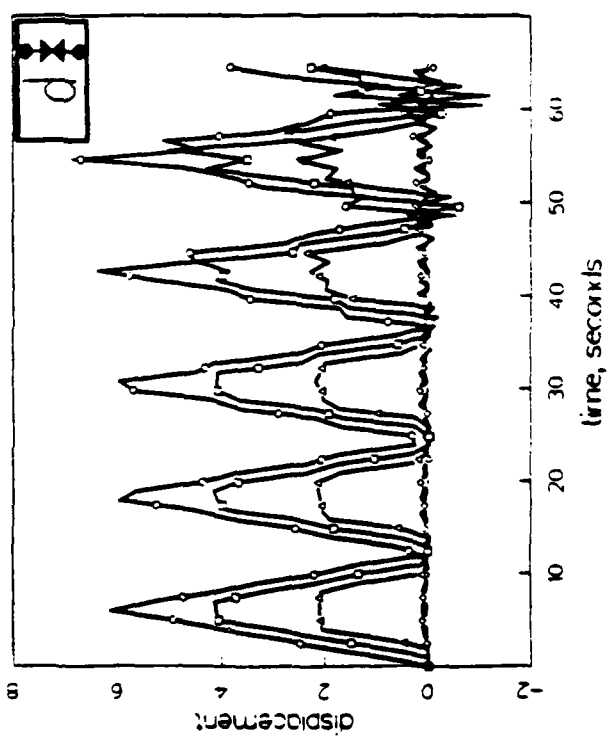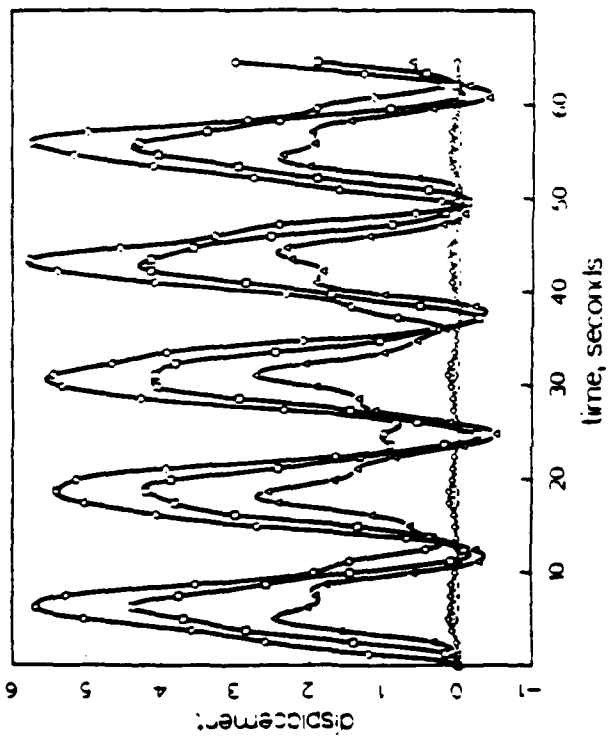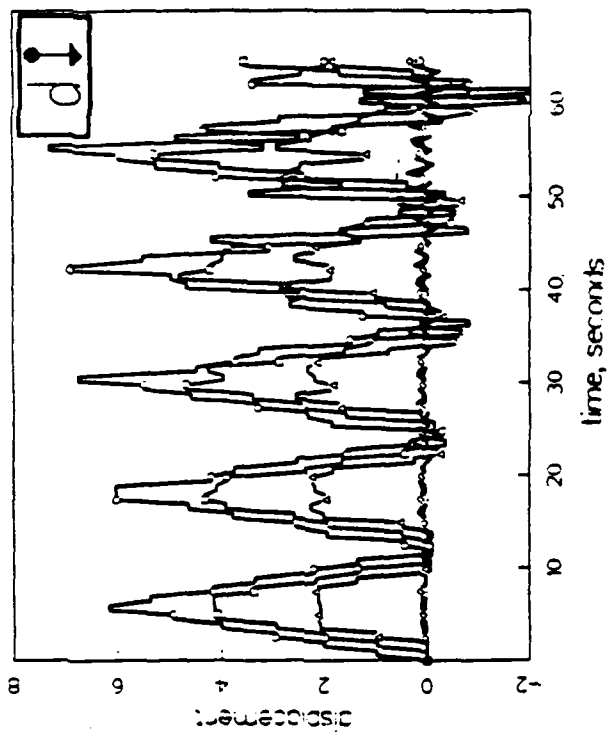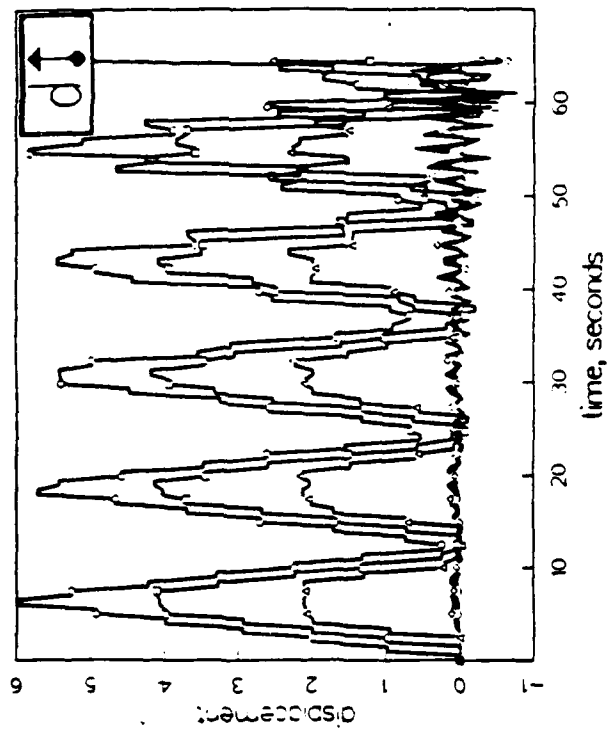
Figure 18g. Problem 2 — comparison of nodal partition algorithm solutions

— $m = 8, \Delta t_c = 1.0$.

47
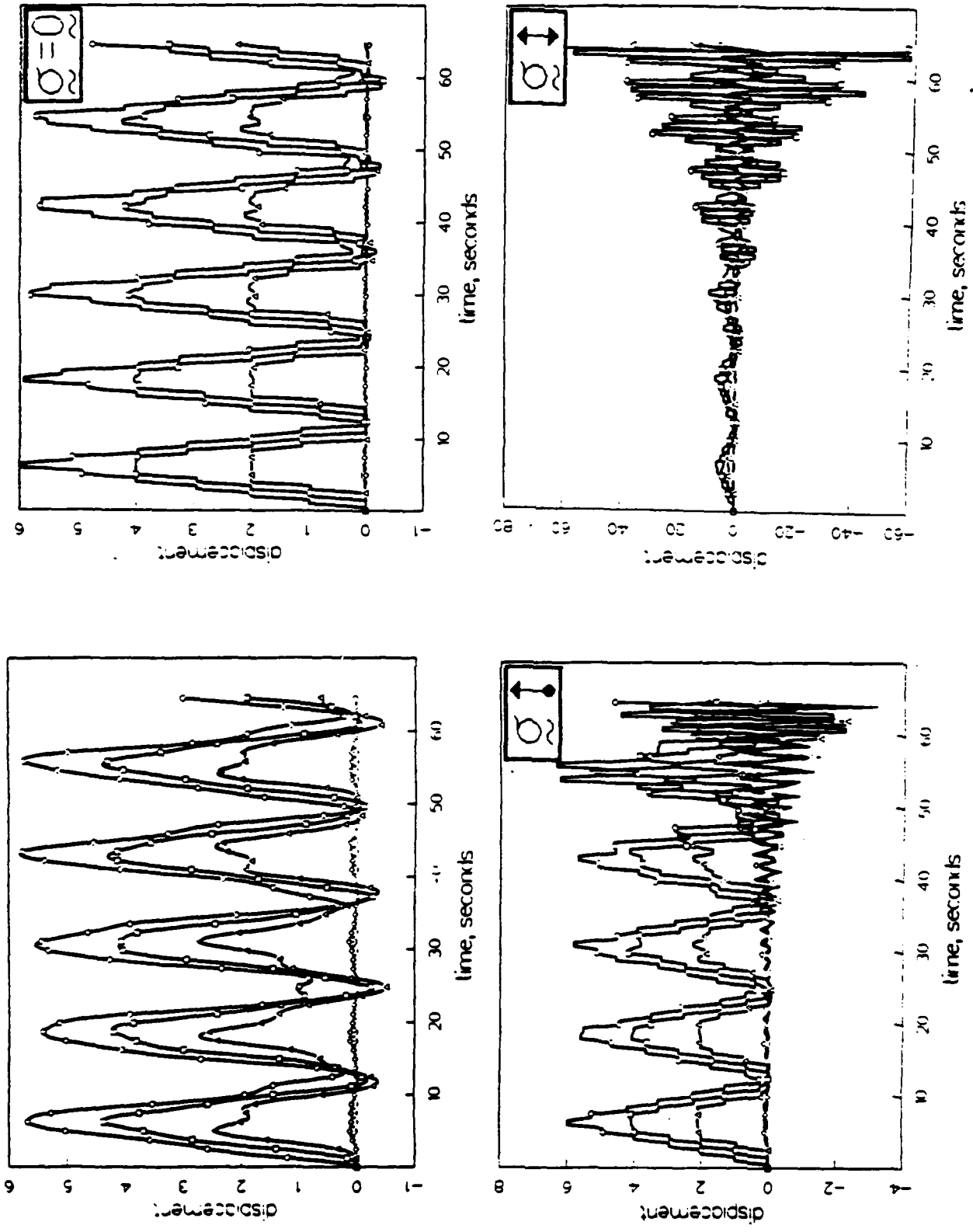
Figure 18h. Problem 2 — comparison of element partition algorithm solutions

— $m = 8, \Delta t_c = 1.0$.

48
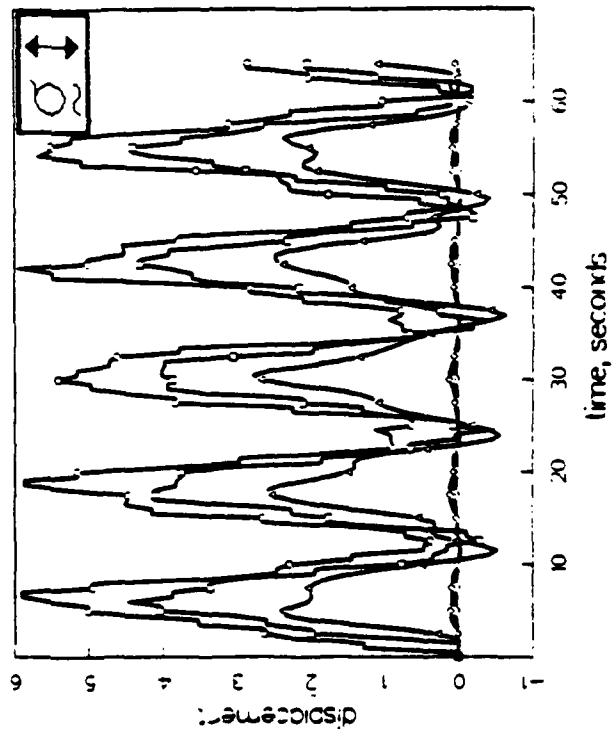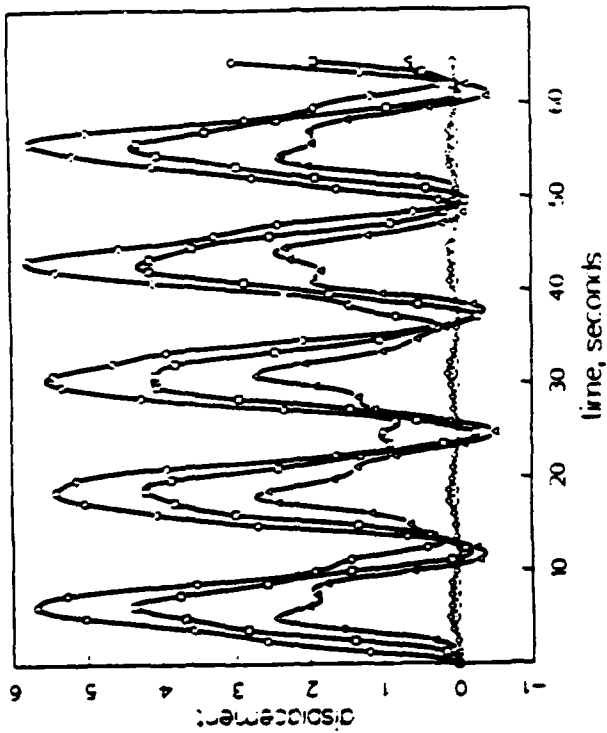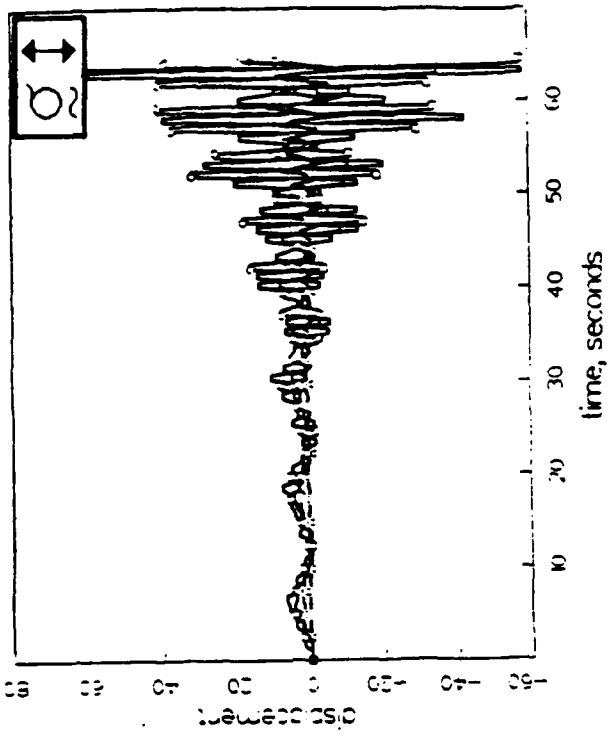
Figure 18i. Problem 2 — comparison of TRANAL element partition algorithm solutions
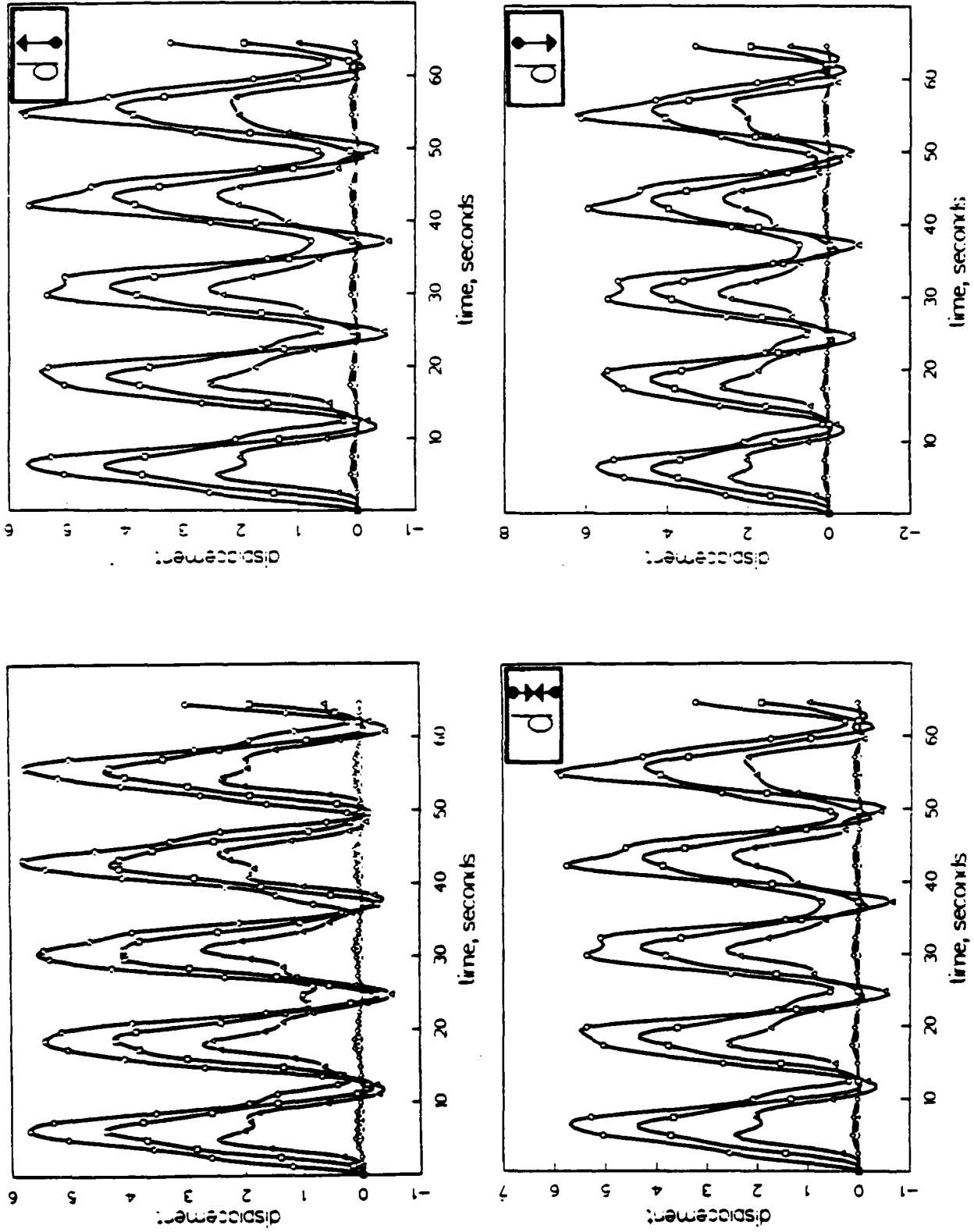
$-- m = 8, \Delta t_c = 1.0.$

Figure 18j: Problem 2 — comparison of nodal partition algorithm solutions
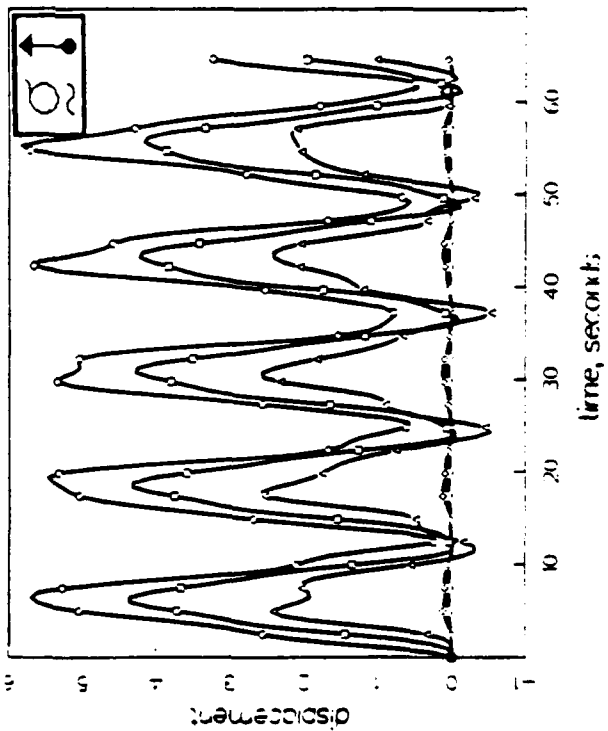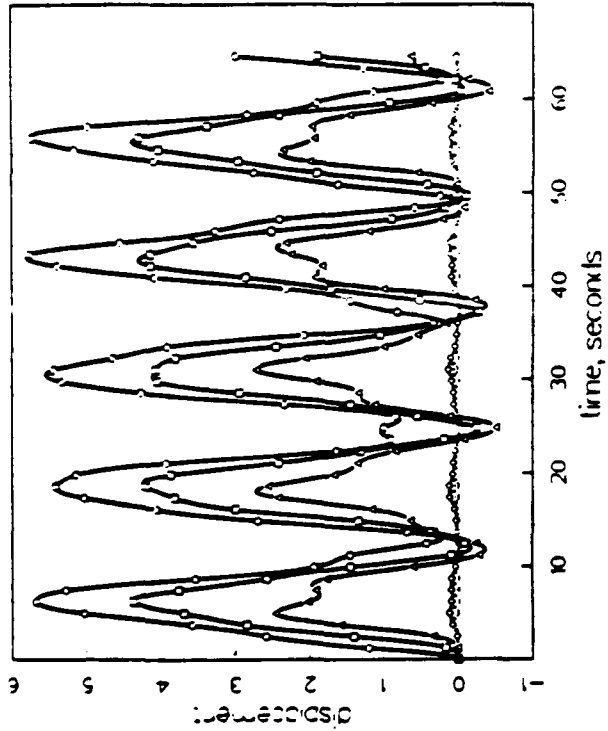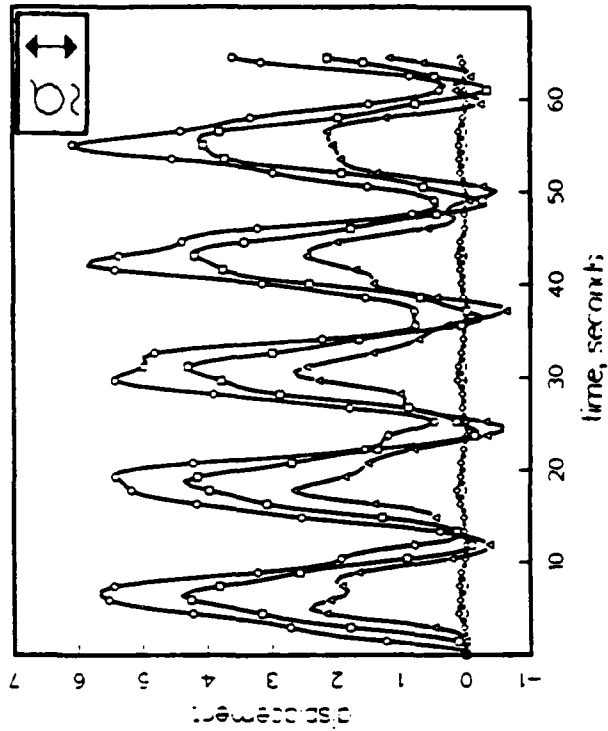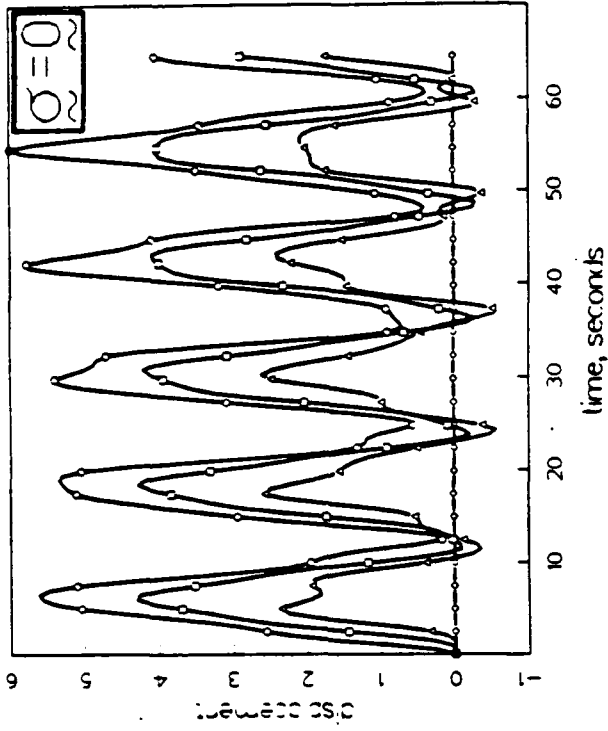
— $m = 8, \Delta t_c = 1/2$.

Figure 18k. Problem 2 — comparison of element partition algorithm solutions
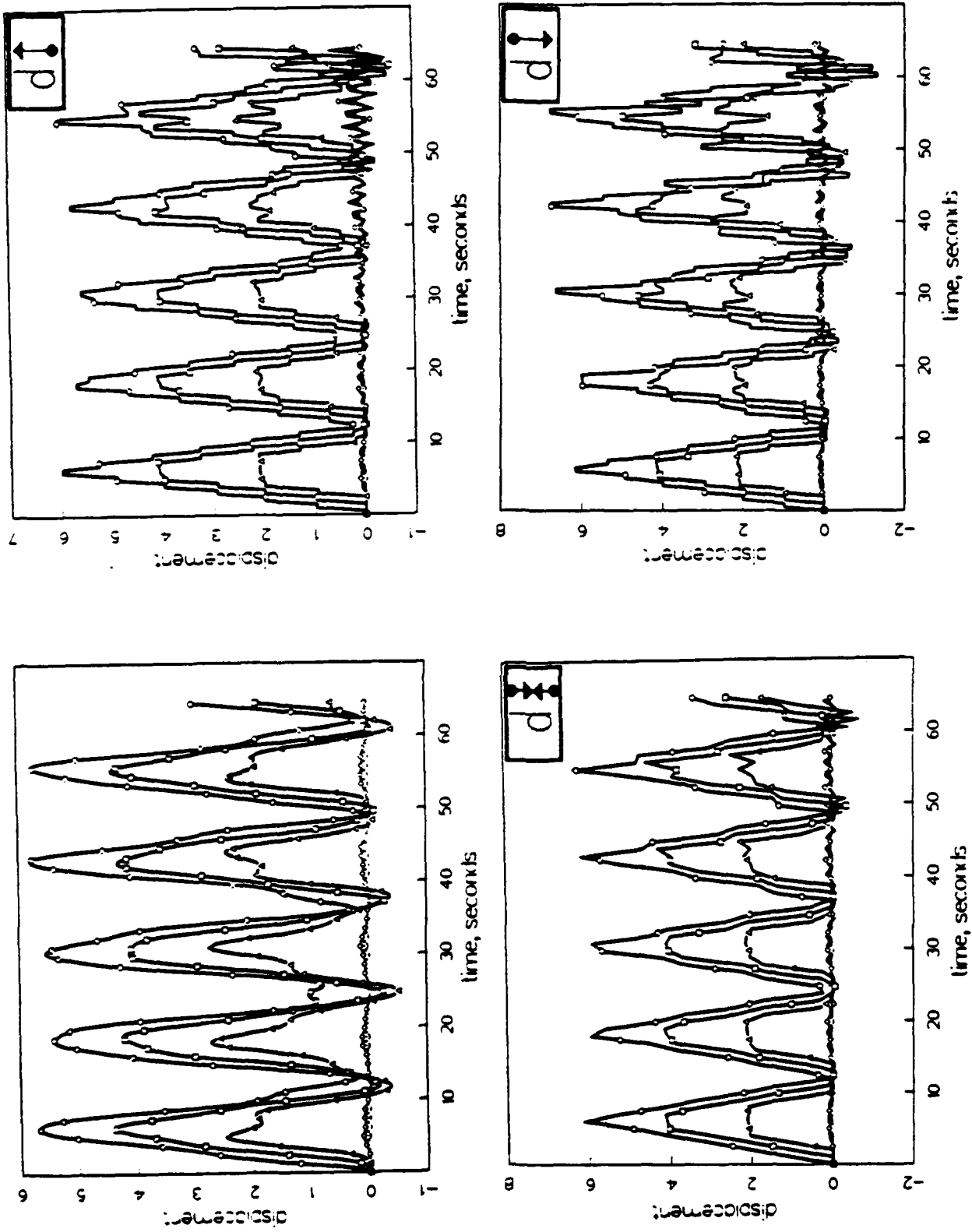
$- - m = 8, \Delta t_c = 1/2.$

51

Figure 18l. Problem 2 — comparison of nodal partition algorithm solutions
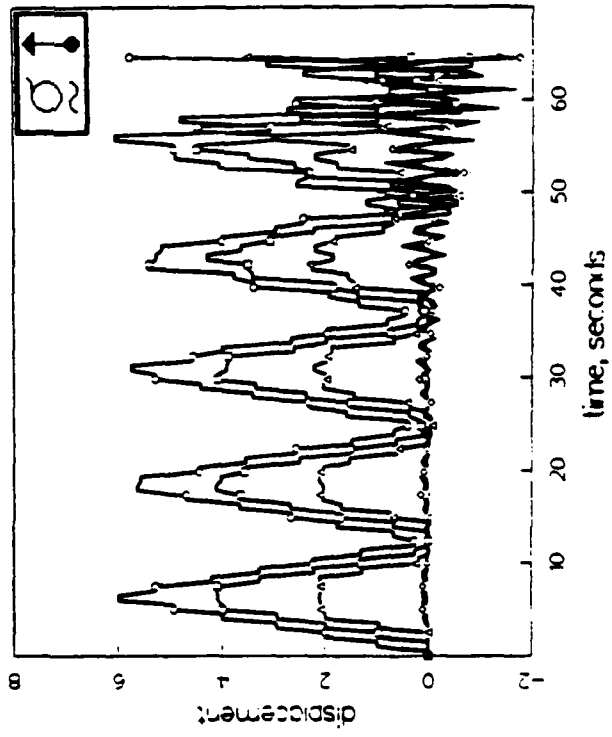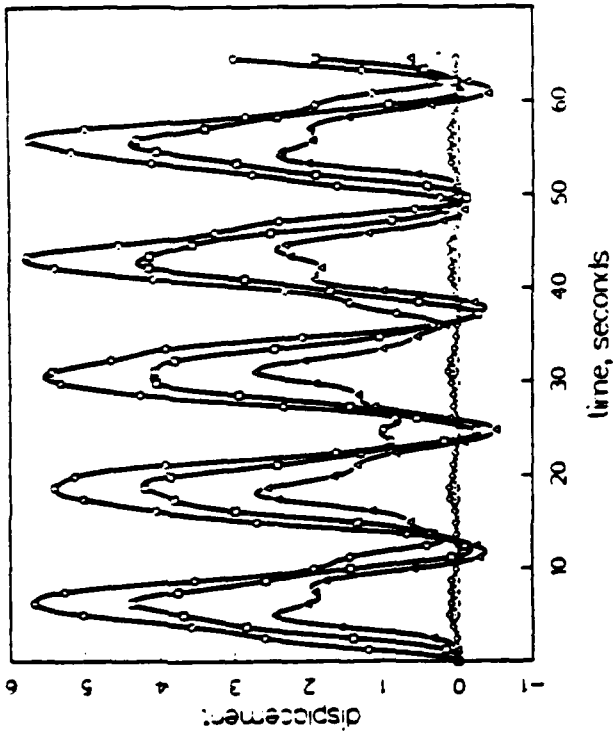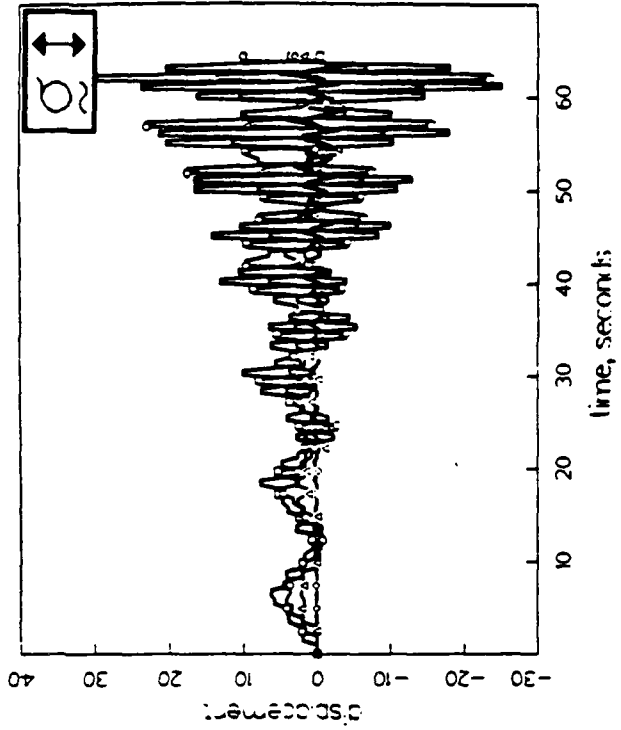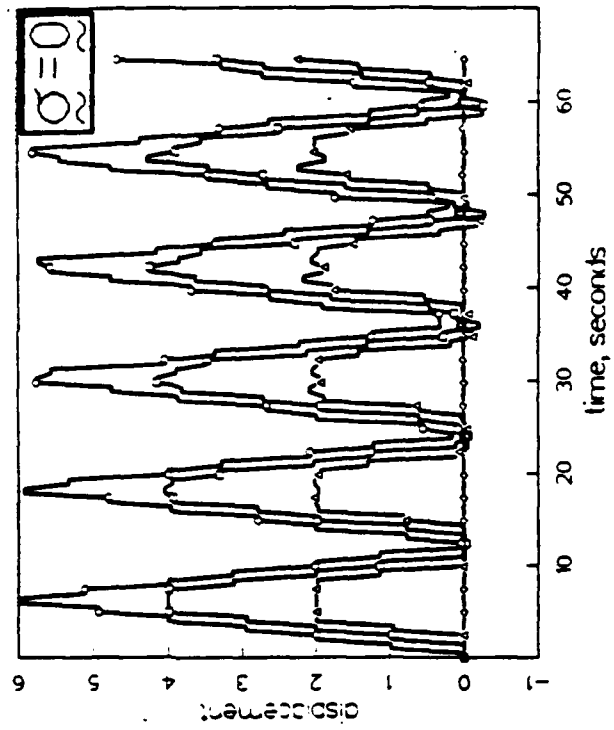
— $m = 16$, $\Delta t_c = 1/2$.

Figure 18m. Problem 2 — comparison of element partition algorithm solutions
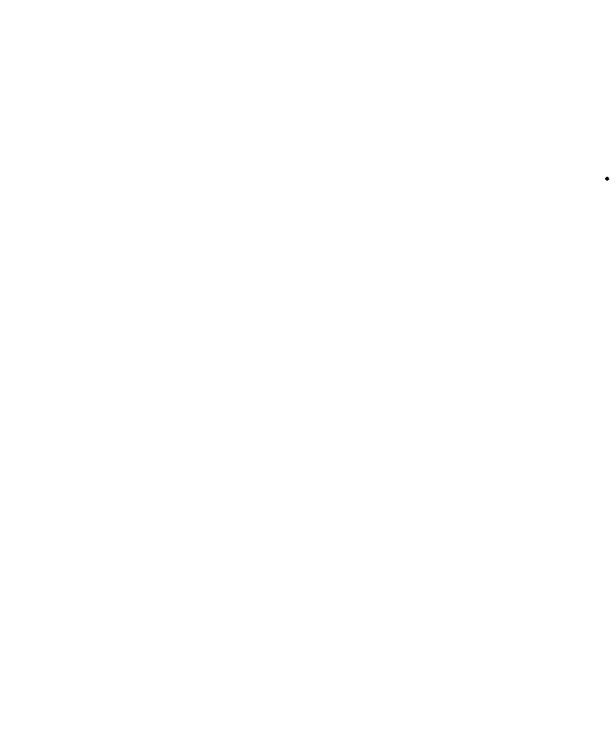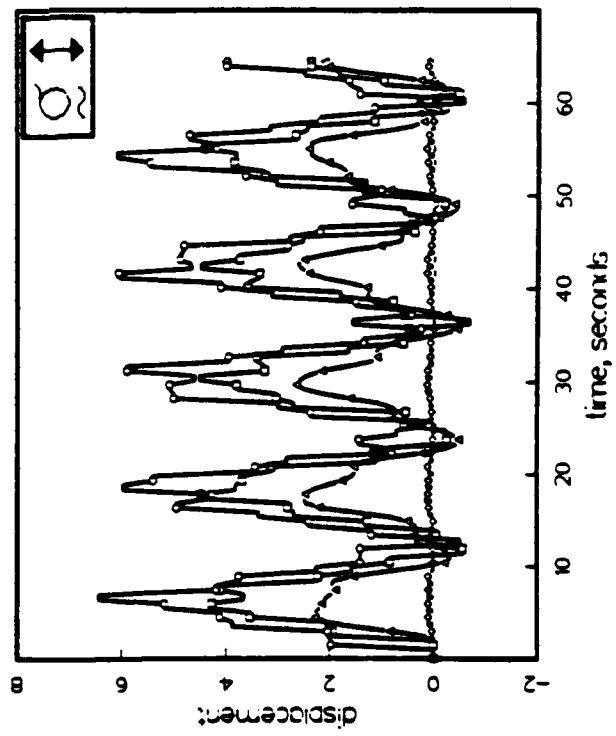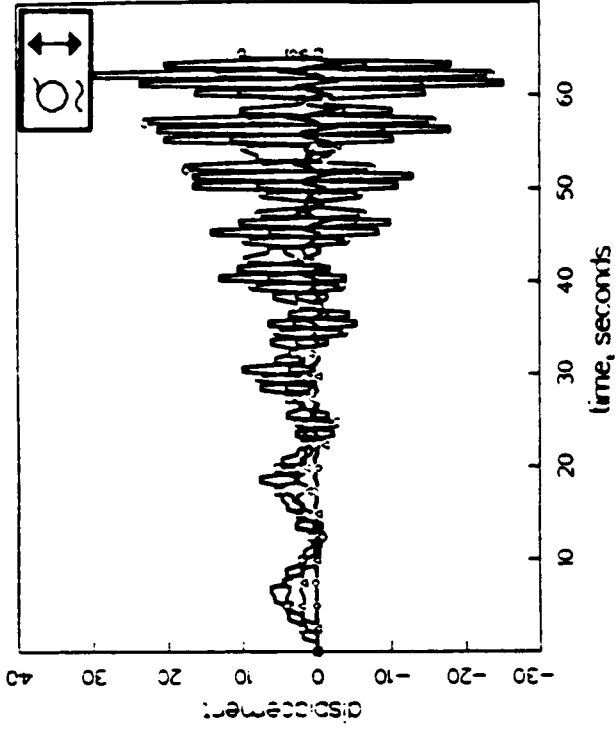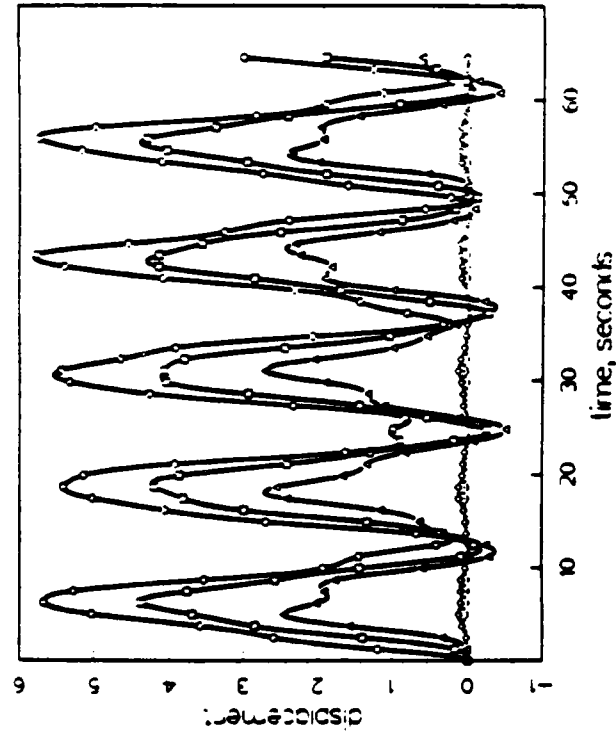
— $m = 16, \Delta t_c = 1/2.$

Figure 18n. Problem 2 — comparison of TRANAL element partition algorithm solutions

— $m = 16, \Delta t_c = 1/2$.

54
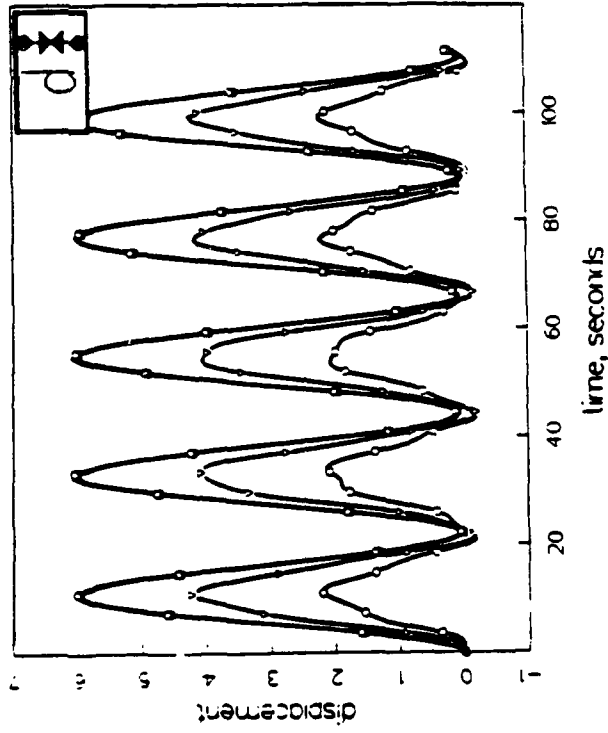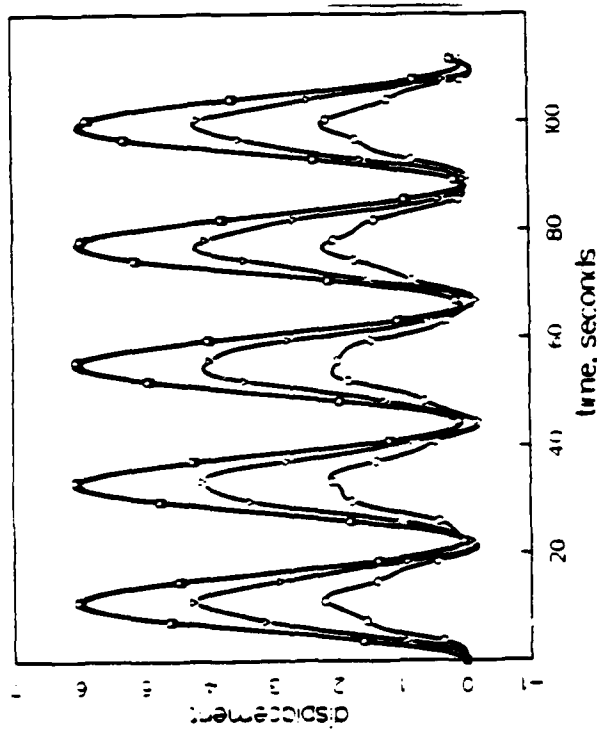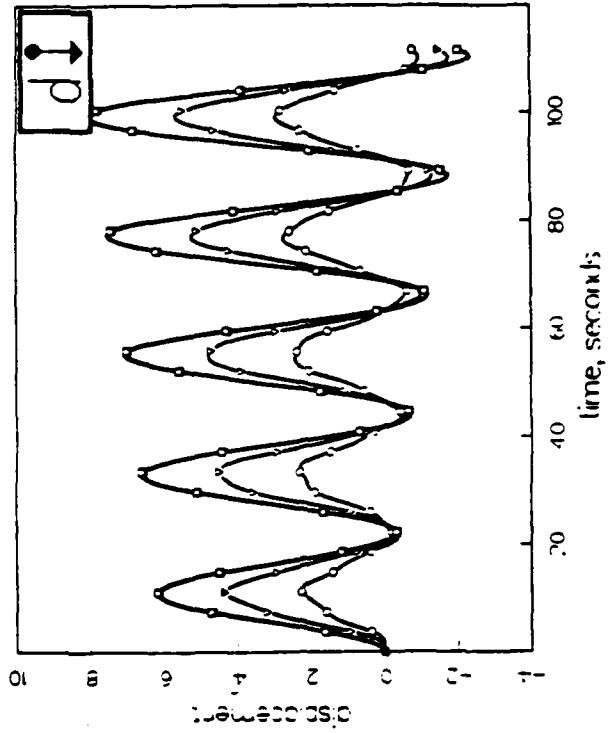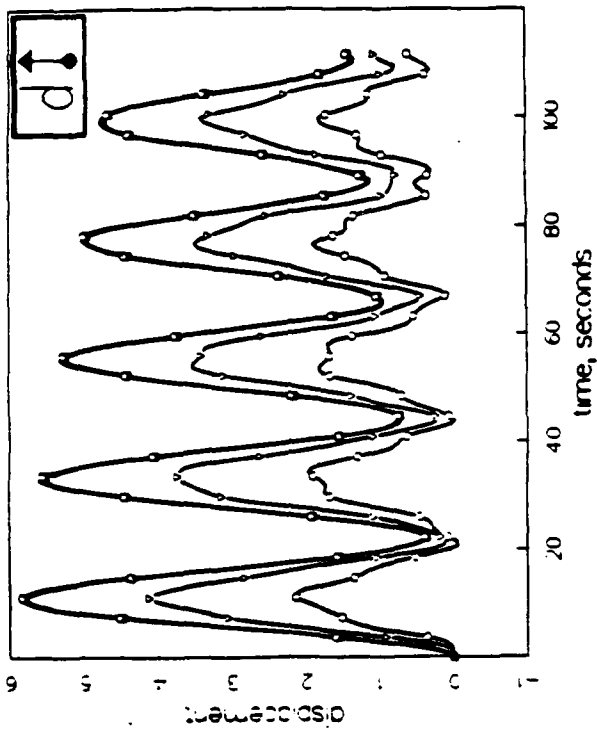
Figure 19a. Problem 3 — comparison of nodal partition algorithm solutions

— $m = 2, \Delta t_c = 1.0$.

55
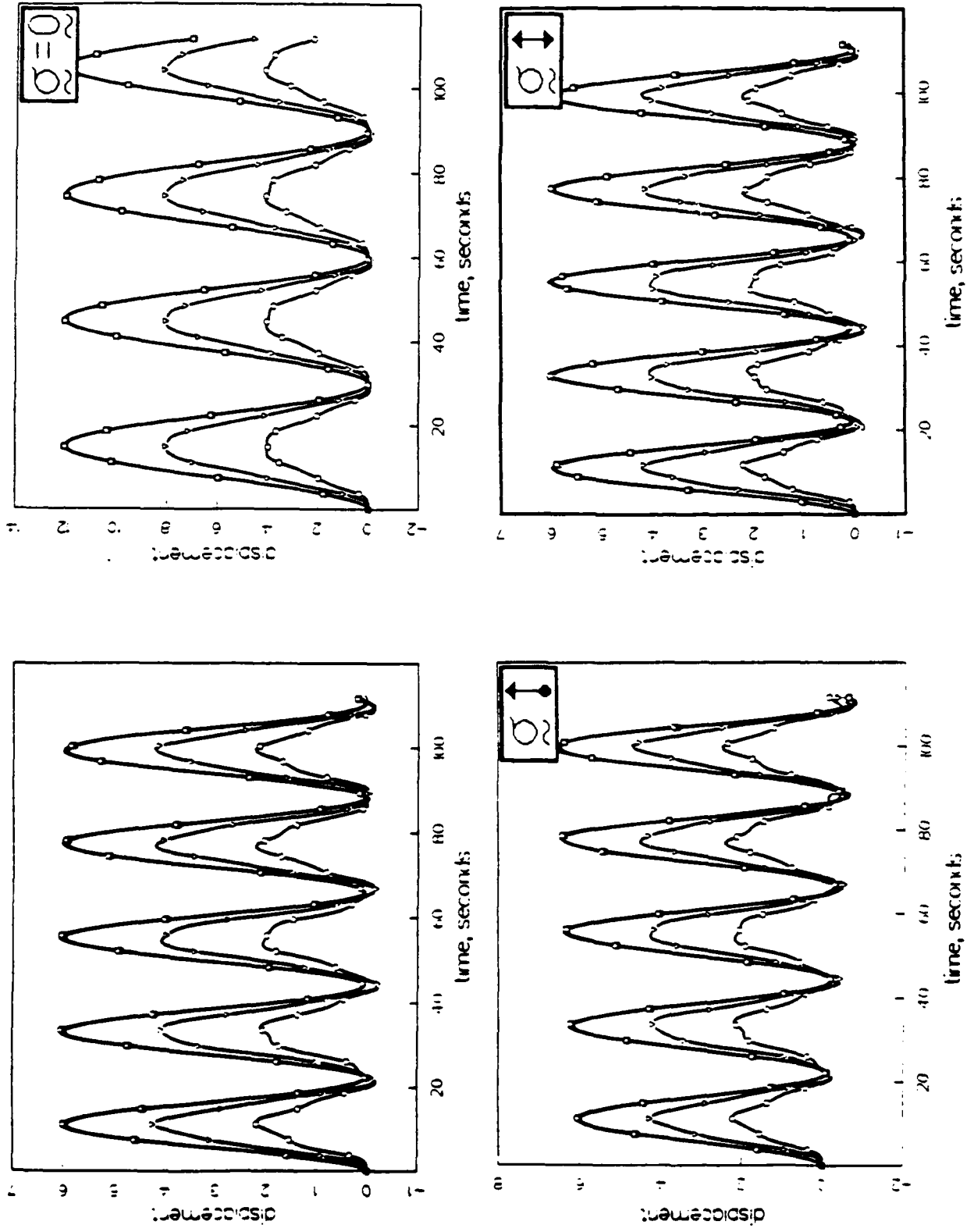
Figure 19b. Problem 3 — comparison of element partition algorithm solutions
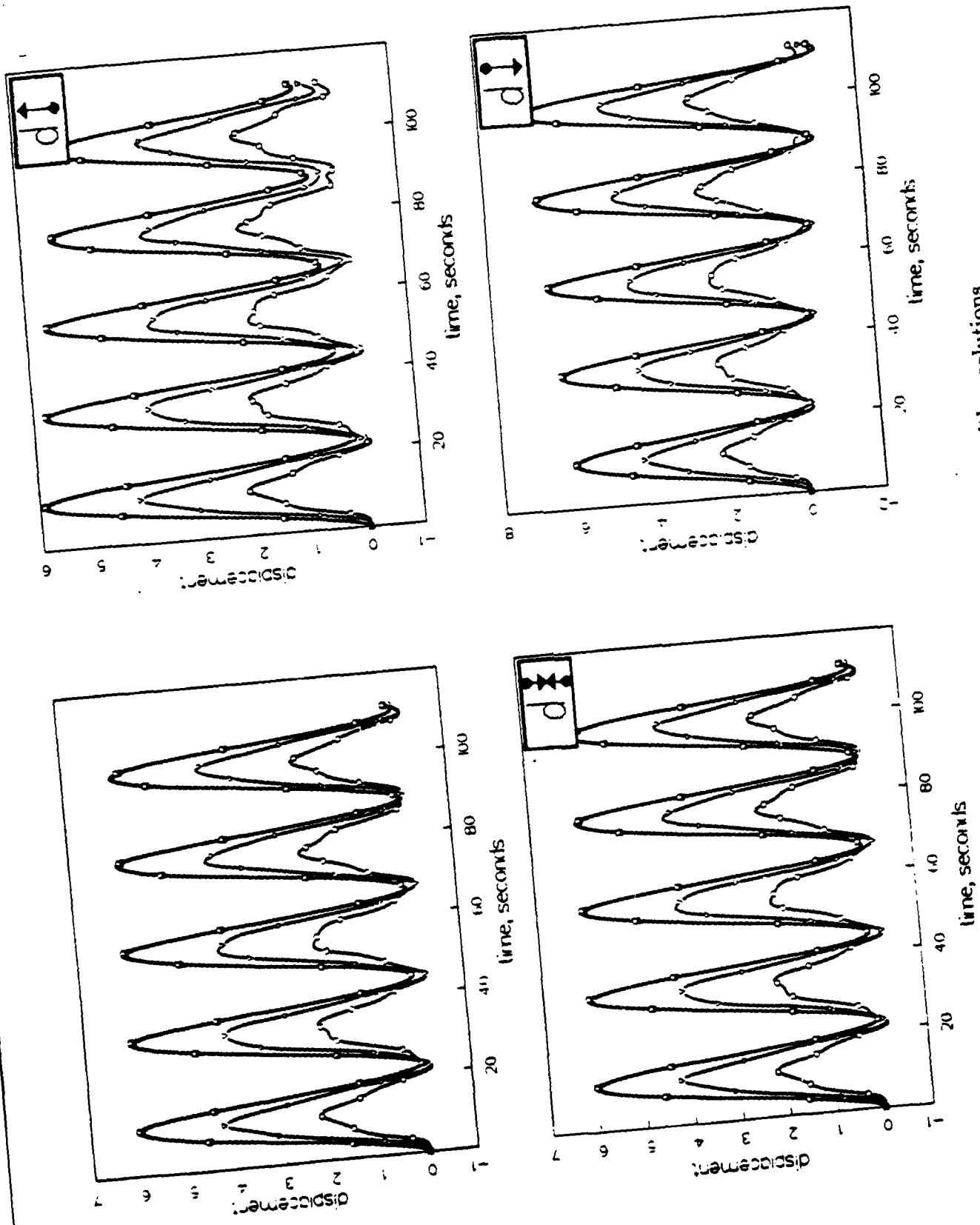
$$— m = 2, \Delta t_c = 1.0.$$

Figure 19c. Problem 3 — comparison of nodal partition algorithm solutions
— $m = 2, \Delta t_c = 1/2$.

57
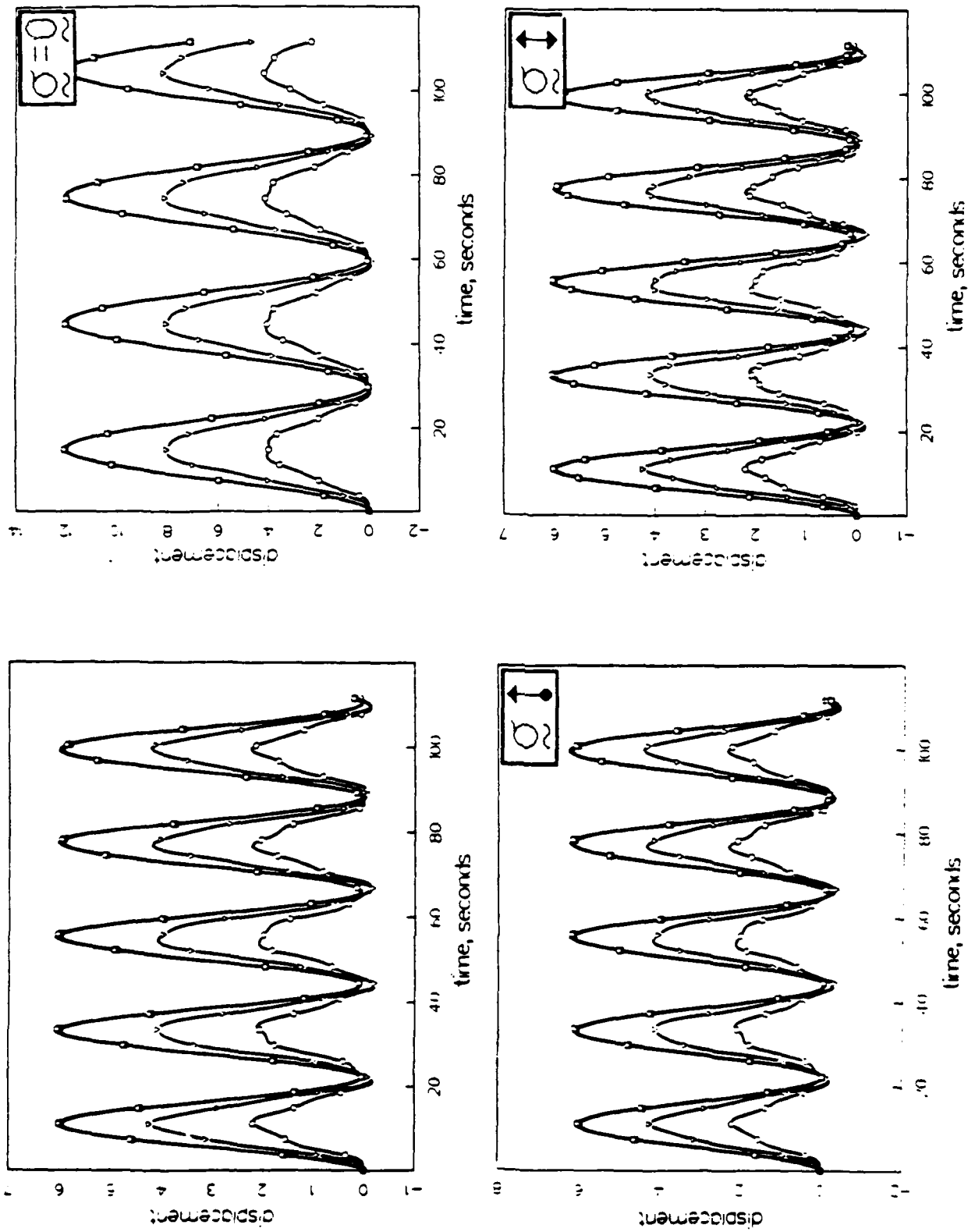
Figure 19d. Problem 3 — comparison of element partition algorithm solutions

$m = 2, \Delta t_c = 1/2.$

58
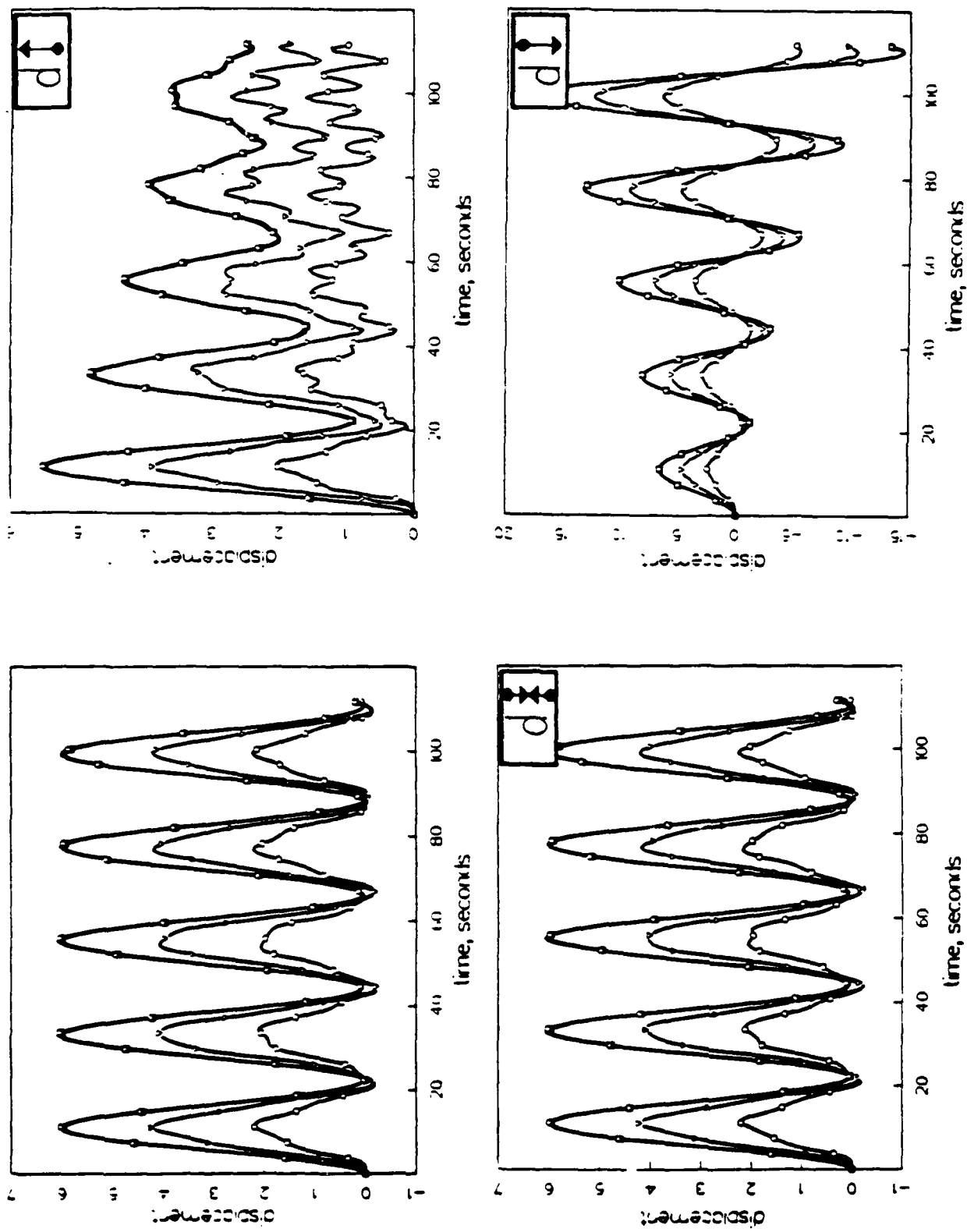
Figure 19e. Problem 3 — comparison of nodal partition algorithm solutions
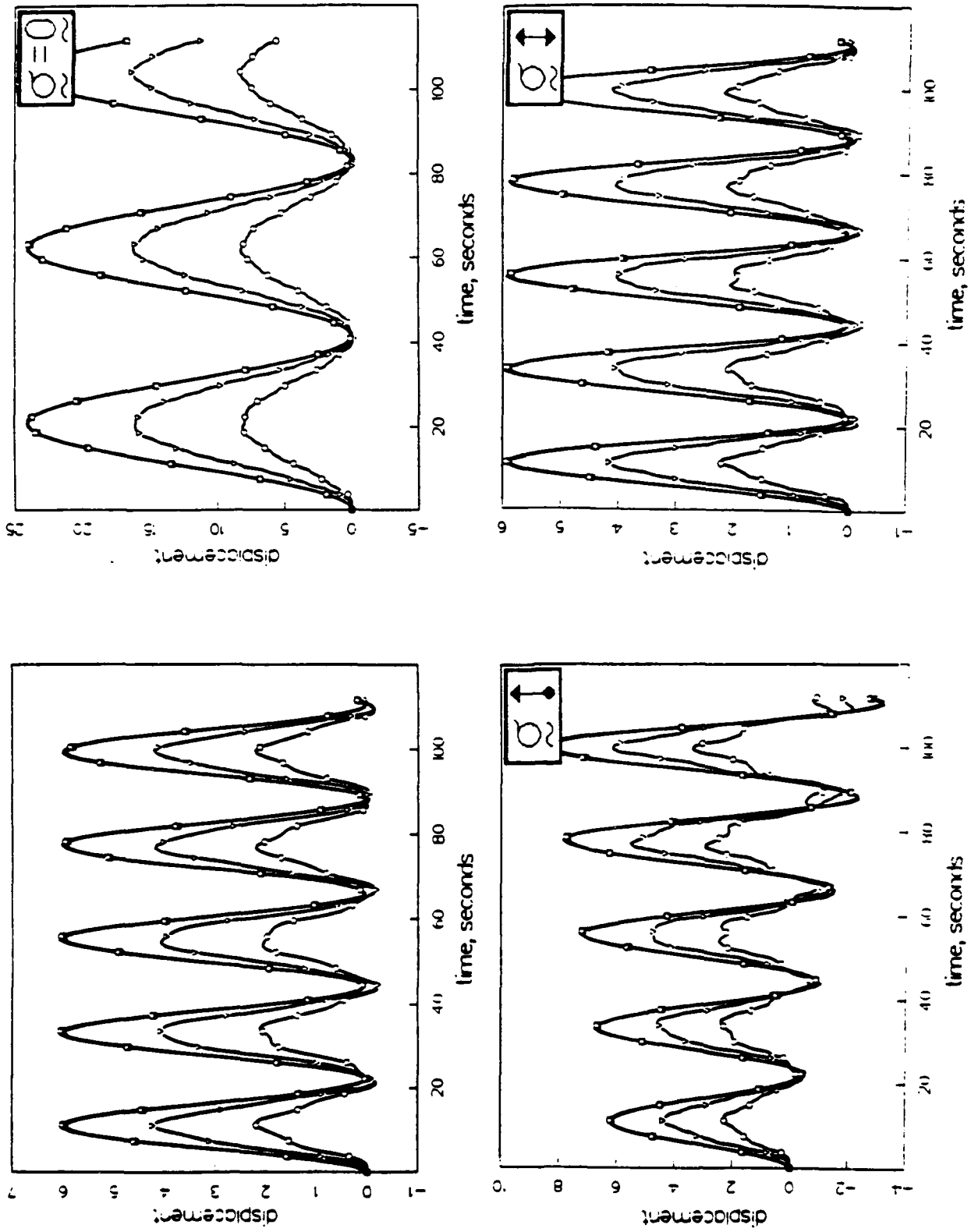
$m = 4, \Delta t_c = 1.0$.

Figure 19f. Problem 3 — comparison of element partition algorithm solutions
— $m = 4, \Delta t_c = 1.0$.
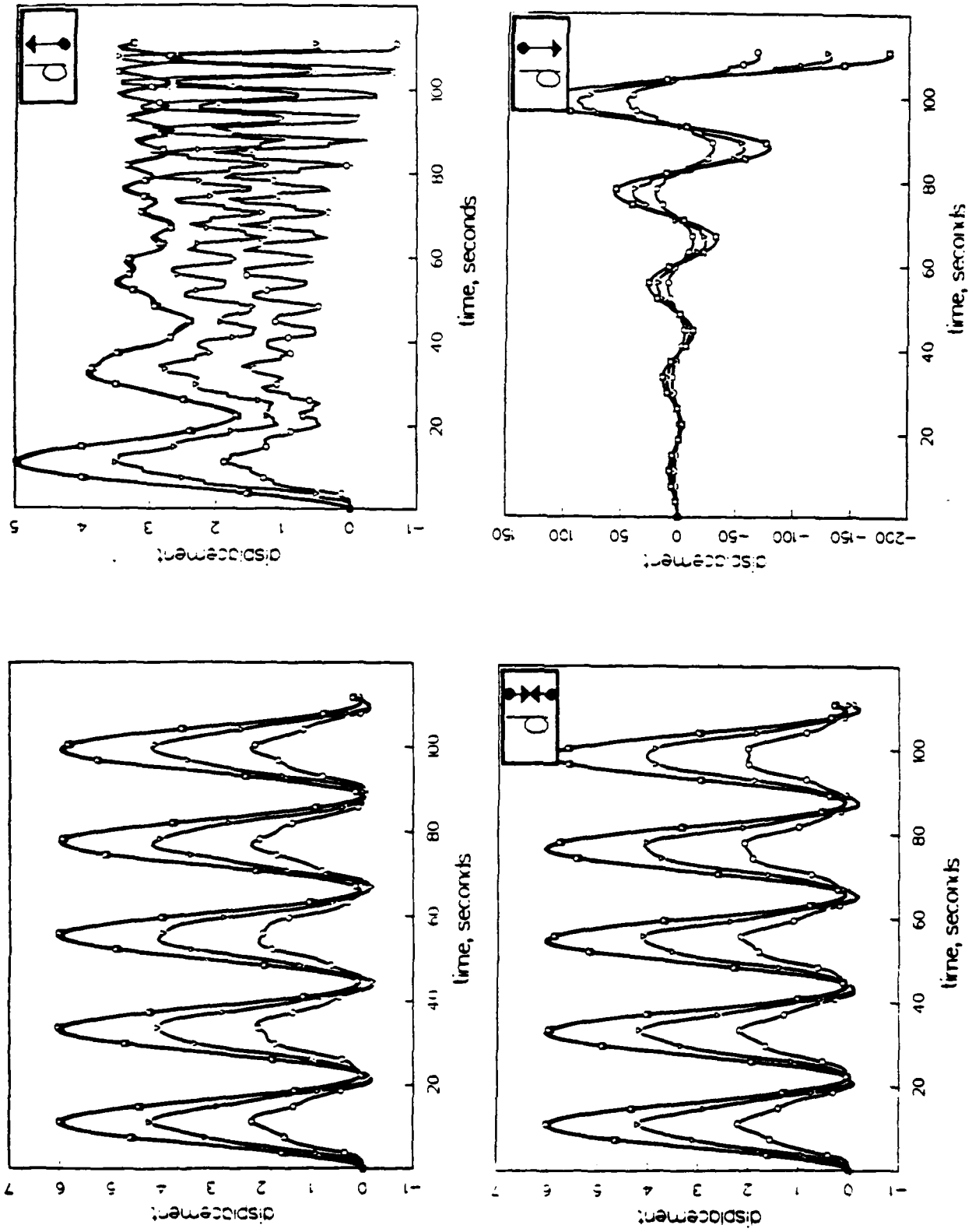
Figure 19g. Problem 3 — comparison of nodal partition algorithm solutions

— $m = 8, \Delta t_c = 1.0$.

61
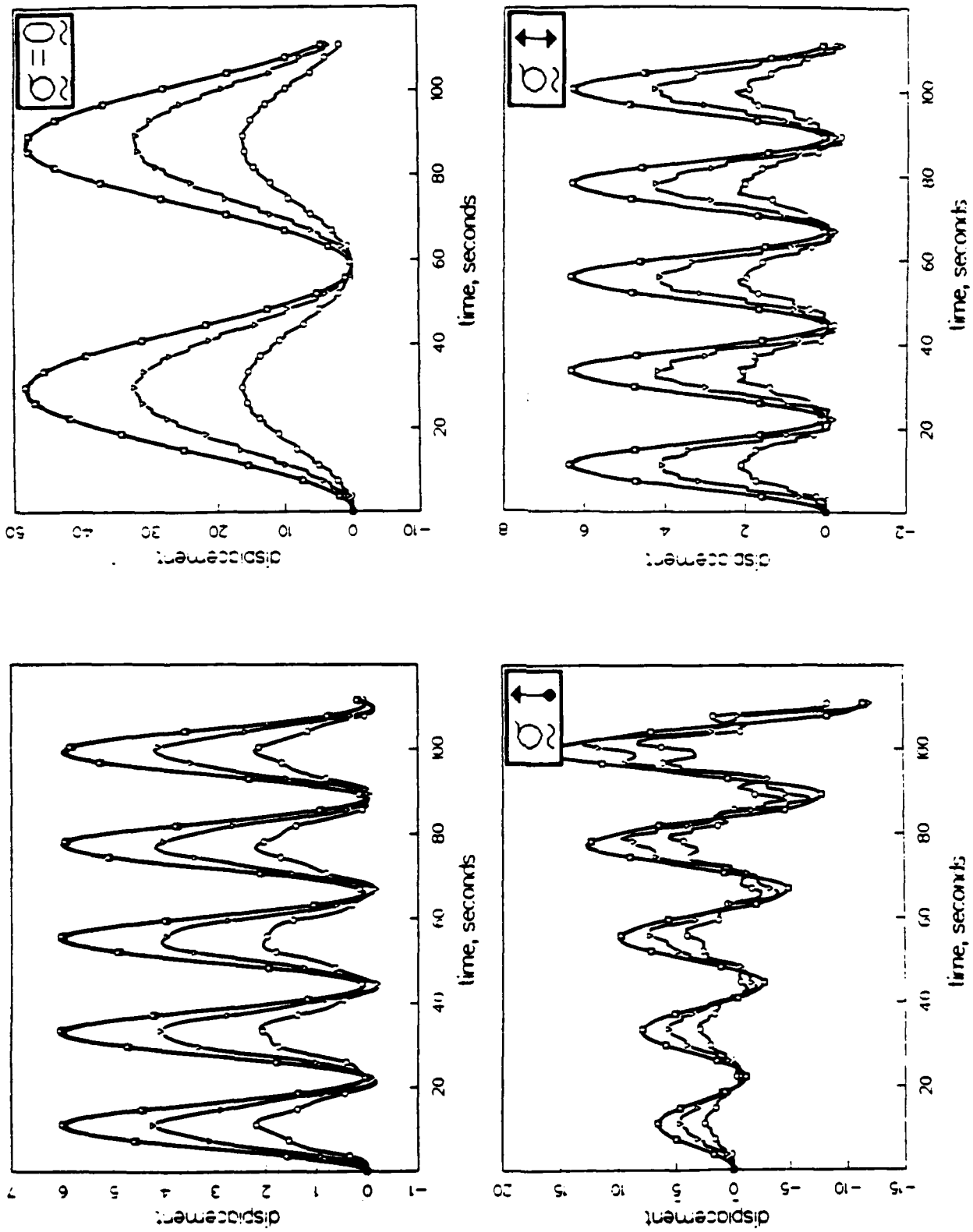
Figure 19h. Problem 3 — comparison of element partition algorithm solutions

— $m = 8, \Delta t_c = 1.0$.

Figure 20a. Test Problem 4.

CURVE LEGEND

O = node 1
□ = node 3
Δ = node 5
◇ = node 7
▽ = node 9
O = node 11
✕ = node 13

Figure 20b. Results legend for test problem 4.
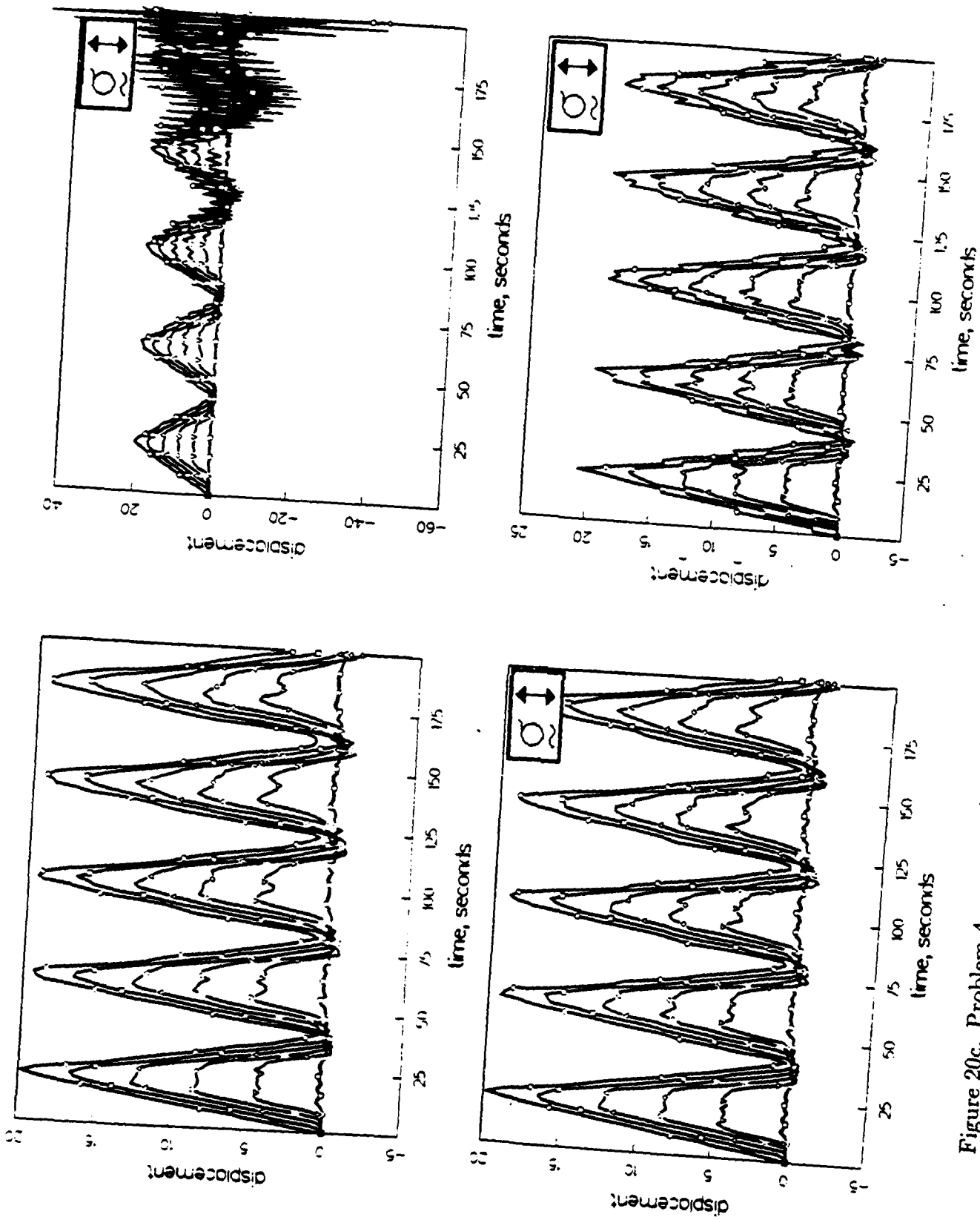
Figure 20c. Problem 4 — comparison of central difference algorithm

and TRANAL algorithm solutions — $m = 8$.
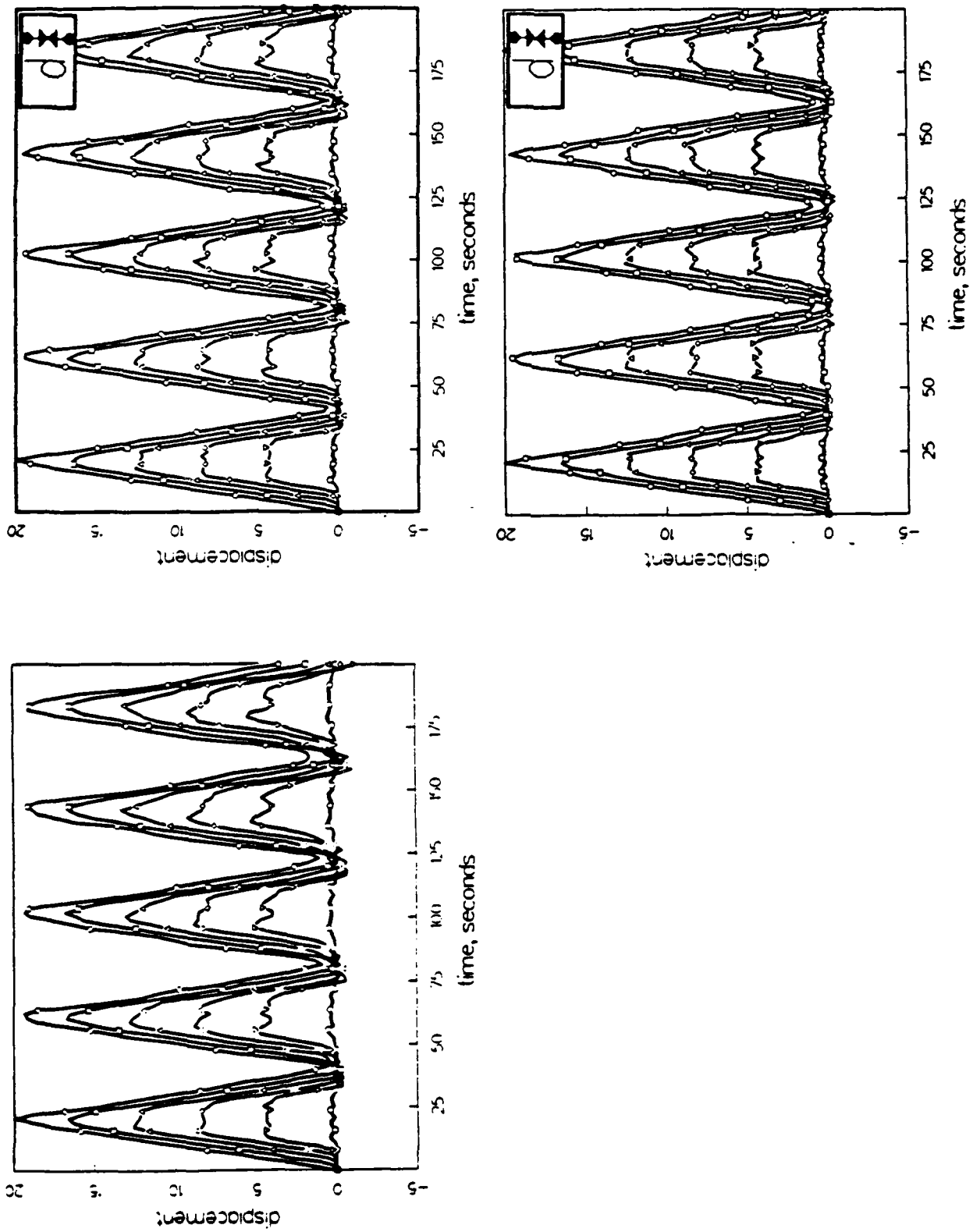
Figure 20d. Problem 4 — comparison of central difference algorithm and linear nodal interpolation algorithm solutions — $m = 8$.

DISTRIBUTION LIST

DNA-TR-88-8

DEPARTMENT OF DEFENSE

DEFENSE INTELLIGENCE AGENCY
ATTN: DB-4C
ATTN: C WIEHLE
ATTN: RTS-2B
ATTN: S HALPERSON

DEFENSE NUCLEAR AGENCY
ATTN: OPNS
4 CYS ATTN: TITL

DEFENSE NUCLEAR AGENCY
ATTN: TDTT W SUMMA

DEFENSE TECHNICAL INFORMATION CENTER
2 CYS ATTN: DTIC/FDAB

DNA PACOM LIAISON OFFICE
ATTN: DNALO

OFFICE OF THE JOINT CHIEFS OF STAFF
ATTN: NUC & CHEM DIV

DEPARTMENT OF THE ARMY

U S ARMY COLD REGION RES ENGR LAB
ATTN: LIBRARY

U S ARMY ENGINEER CTR & FT BELVOIR
ATTN: TECHNICAL LIBRARY

U S ARMY ENGR WATERWAYS EXPER STATION
ATTN: G JACKSON
ATTN: J BALSARA
ATTN: S KIGER
ATTN: TECHNICAL LIBRARY

DEPARTMENT OF THE NAVY

CARDEROCK LABORATORY
ATTN: LIBRARY

NAVAL POSTGRADUATE SCHOOL
ATTN: LIBRARY

DEPARTMENT OF THE AIR FORCE

AIR FORCE INSTITUTE OF TECHNOLOGY/EN
ATTN: C BRIDGMAN

AIR FORCE WEAPONS LABORATORY
ATTN: NTE
ATTN: R HENNY

BALLISTIC MISSILE OFFICE
ATTN: D GAGE

FOREIGN TECHNOLOGY DIVISION, AFSC
ATTN: LIBRARY

DEPARTMENT OF ENERGY

LAWRENCE LIVERMORE NATIONAL LAB
ATTN: R DONG

DEPARTMENT OF DEFENSE CONTRACTORS

AGBABIAN ASSOCIATES
ATTN: M AGBABIAN

APPLIED & THEORETICAL MECHANICS, INC
ATTN: J M CHAMPNEY

APPLIED RESEARCH ASSOCIATES, INC
ATTN: N HIGGINS

APPLIED RESEARCH ASSOCIATES, INC
ATTN: S BLOUIN

BDM CORP
ATTN: J STOCKTON

BDM CORPORATION
ATTN: LIBRARY

BOEING CO
ATTN: G R BURWELL
22CYS ATTN: R SCHMIDT

BOEING TECHNICAL & MANAGEMENT SVCS, INC
ATTN: AEROSPACE LIBRARY

CALIFORNIA RESEARCH & TECHNOLOGY, INC
ATTN: LIBRARY

CALIFORNIA RESEARCH & TECHNOLOGY, INC
ATTN: Z P LEE

H & H CONSULTANTS, INC
ATTN: J HALTIWANGER
ATTN: W HALL

KAMAN SCIENCES CORP
ATTN: D SEITZ

KAMAN SCIENCES CORPORATION
ATTN: DASIAC

KAMAN SCIENCES CORPORATION
ATTN: DASIAC

KARAGOZIAN AND CASE
ATTN: J KARAGOZIAN

LACHEL PIEPENBURG AND ASSOCIATES
ATTN: D PIEPENBURG

PACIFIC-SIERRA RESEARCH CORP
ATTN: H BRODE

R & D ASSOCIATES
ATTN: J LEWIS

STANFORD UNIVERSITY
2 CYS ATTN: G HULBURT
2 CYS ATTN: J HUGHES

TRW SPACE & DEFENSE, DEFENSE SYSTEMS
ATTN: R CRAMOND

WEIDLINGER ASSOC., CONSULTING ENGRG
ATTN: T DEEVY

WEIDLINGER ASSOC, INC
ATTN: J ISENBERG

WEIDLINGER ASSOCIATES, INC
ATTN: M BARON